



## Low-temperature plasma processing for Si photovoltaics

S.Q. Xiao <sup>a,b,\*</sup>, S. Xu <sup>a</sup>, K. Ostrikov <sup>c,d</sup>

<sup>a</sup> Plasma Sources and Applications Centre (PSAC), NIE, and Institute of Advanced Studies, Nanyang Technological University, 1 Nanyang Walk, Singapore 637616, Singapore

<sup>b</sup> Key Laboratory of Advanced Process Control for Light Industry (Ministry of Education), Department of Electronic Engineering, Jiangnan University, Wuxi 214122, China

<sup>c</sup> Plasma Nanoscience Centre Australia (PNCA), CSIRO Materials Science and Engineering, P.O. Box 218, Lindfield, New South Wales 2070, Australia

<sup>d</sup> Plasma Nanoscience, School of Physics, The University of Sydney, Sydney, New South Wales 2006, Australia



### ARTICLE INFO

#### Article history:

Available online 6 March 2014

Guiding Editor: Paul Chu

#### Keywords:

Low-temperature plasma  
Si materials and solar cells  
Plasma dissociation and deposition  
Hydrogen-surface interactions  
Plasma cleaning  
Plasma texturing  
Surface passivation  
Plasma induced p-n junction  
Plasma diagnostics

### ABSTRACT

There has been a recent rapid expansion of the range of applications of low-temperature plasma processing in Si-based photovoltaic (PV) technologies. The desire to produce Si-based PV materials at an acceptable cost with consistent performance and reproducibility has stimulated a large number of major research and research infrastructure programs, and a rapidly increasing number of publications in the field of low-temperature plasma processing for Si photovoltaics. In this article, we introduce the low-temperature plasma sources for Si photovoltaic applications and discuss the effects of low-temperature plasma dissociation and deposition on the synthesis of Si-based thin films. We also examine the relevant growth mechanisms and plasma diagnostics, Si thin-film solar cells, Si heterojunction solar cells and silicon nitride materials for antireflection and surface passivation. Special attention is paid to the low-temperature plasma interactions with Si materials including hydrogen interaction, wafer cleaning, masked or mask-free surface texturization, the direct formation of p-n junction, and removal of phosphorus silicate glass or parasitic emitters. The chemical and physical interactions in such plasmas with Si surfaces are analyzed. Several examples of the plasma processes and techniques are selected to represent a variety of applications aimed at the improvement of Si-based solar cell performance.

© 2014 Elsevier B.V. All rights reserved.

### Contents

1. Introduction . . . . .	2
1.1. General overview of Si photovoltaics . . . . .	2
1.2. Plasma technologies in Si photovoltaics . . . . .	2
1.3. Structure of the review . . . . .	3
2. Low-temperature plasma sources . . . . .	3
2.1. Capacitively coupled plasmas . . . . .	4
2.2. Inductively coupled plasmas . . . . .	4
2.3. Microwave plasmas . . . . .	4
3. Plasma dissociation and deposition for Si thin films and solar cells . . . . .	4
3.1. SiH <sub>4</sub> /H <sub>2</sub> discharges . . . . .	4
3.2. Plasma diagnostics . . . . .	6
3.2.1. Langmuir probe . . . . .	6
3.2.2. Steady-state-number density . . . . .	6
3.2.3. Mass spectroscopy . . . . .	7
3.3. Growth processes of a-Si:H and μc-Si:H . . . . .	8
3.3.1. Amorphous silicon . . . . .	8
3.3.2. Microcrystalline silicon . . . . .	8

\* Corresponding author at: Key Laboratory of Advanced Process Control for Light Industry (Ministry of Education), Department of Electronic Engineering, Jiangnan University, Wuxi 214122, China.

E-mail addresses: [larry0078@hotmail.com](mailto:larry0078@hotmail.com) (S.Q. Xiao), [shuyan.xu@nie.edu.sg](mailto:shuyan.xu@nie.edu.sg) (S. Xu), [kostya.ostrikov@csiro.au](mailto:kostya.ostrikov@csiro.au) (K. Ostrikov).

3.4.	Si thin-film solar cells . . . . .	9
3.4.1.	Micromorph tandem and triple-junction solar cells . . . . .	9
3.4.2.	VHF-CCP for high-rate deposition . . . . .	9
3.4.3.	Features of ICP and MP in high-rate deposition . . . . .	10
3.5.	HIT solar cells . . . . .	12
3.6.	SiN thin films for surface passivation . . . . .	13
4.	Plasma etching in Si-based PV applications . . . . .	13
4.1.	Hydrogen-surface interactions . . . . .	13
4.1.1.	Hydrogen insertion for c-Si passivation . . . . .	15
4.1.2.	Hydrogen adsorption for c-Si passivation . . . . .	16
4.2.	Plasma cleaning . . . . .	16
4.3.	Plasma texturing . . . . .	18
4.3.1.	One-dimensional nanostructures . . . . .	18
4.3.2.	Hybrid nanostructures . . . . .	21
4.4.	Plasma-induced p-n junction formation . . . . .	21
4.4.1.	Origin of plasma-induced p-n junction . . . . .	21
4.4.2.	Plasma-induced p-n junction solar cells . . . . .	22
4.5.	PSG removal . . . . .	23
5.	Future prospects . . . . .	24
6.	Conclusion . . . . .	25
	Acknowledgements . . . . .	26
	References . . . . .	26

## 1. Introduction

### 1.1. General overview of Si photovoltaics

Existing power systems can be considered as a prime cause for current greenhouse or global warming effects as more than 75% of the energy is produced from fossil fuel [1]. The utilization of fossil fuels, especially coal causes a major environmental impact due to the emissions of greenhouse gases such as CO<sub>2</sub>, SO<sub>x</sub> and NO<sub>x</sub> that pollute the atmosphere. Therefore, there is an urgent need for a robust and sustainable power production and distribution approach which is reliable, environment friendly and economic. In contrast to fossil fuels, photovoltaic (PV) solar energy is considered as a possible solution of the climate change or global warming problems since PV solar cells can provide electricity without producing carbon dioxide and other greenhouse gas emissions. Among feasible renewable energy sources, PV solar energy is among the most promising technologies for a sustainable future because sunlight is abundant and distributed all over the Earth. The amount of solar energy reaching the Earth within 1 h equals to the total annual energy need of all of mankind [2]. Moreover, the available energy resources are nearing exhaustion and solar energy may have to serve as the main energy source in the future.

Among the PV materials, silicon, the second most abundant element on Earth has attracted a tremendous interest in solar cell applications. This is why Si-based solar cells have been extensively studied by a large number of research groups all over the world [3–12]. In general, Si-based solar cells can be divided into two categories: the bulk silicon technology and thin-film silicon technology. At present, the bulk silicon technology dominates the PV market with a proportion of more than 85% including monocrystalline silicon (c-Si) and polycrystalline silicon (poly-Si), which reach industrial photo-conversion efficiencies of around 18.5% and 17.0%, respectively [13].

The cost of bulk silicon technology has reduced significantly as the conversion efficiency has increased drastically with the introduction and application of more sophisticated technologies. In comparison, silicon thin-film technology is always considered as the “younger cousin” of the bulk silicon technology which may potentially become the leading technology of solar energy production, although this expectation has not materialized yet. The arguments favoring the Si thin-film technology have been

based on a substantial potential for cost reduction due to thinner layer usage, cheap deposition processes, compatibility with large-area and mass production, as well as a large choice of rigid or flexible substrates (glass, metal, plastic, etc.). That is to say, thin-film silicon technology constitutes one of the most promising ways for low-cost PV solar cells and modules even though the industrial cells currently show the record conversion efficiencies of only around 13% [14,15].

### 1.2. Plasma technologies in Si photovoltaics

In the past twenty years, a number of low-temperature plasma sources and plasma facilities, such as capacitively coupled radio-frequency (rf) plasma-enhanced chemical vapor deposition (PECVD) [11,12,16–18], very high frequency (VHF) PECVD [7,9,10,19–21], microwave plasma (MP) CVD [22–26] and inductively coupled plasma (ICP) CVD [27–29] have been successfully applied for the fabrication of PV devices including bulk Si solar cells and thin-film Si solar cells. With the growing consensus that the climate change is inevitable, low-temperature plasmas are set to play a key role in the development of a cleaner and more environmentally conscious world, especially in the development of PV power as a clean, sustainable energy source [30].

For bulk Si solar cells, the plasma sources find numerous applications, e.g., the surface passivation by means of silicon nitride (SiN<sub>x</sub>:H) films [29,31–34] and the plasma etching processes for removal of phosphorus silicate glass (PSG) or parasitic emitters [27,35], for wafer cleaning [36–39] as well as masked and mask-free surface texturization [40–42]. For thin-film Si solar cells and HIT (heterojunction with intrinsic thin-layer) solar cells, however, almost all the fabrication processes including the formation of p-n junction, the interface passivation and the surface texturing for light trapping are accomplished by utilizing plasma facilities [6–12,14,16,17,19–21].

As a consequence, plasma-assisted fabrication of Si-based PV materials and complex assemblies is a topic that is continuously increasing in importance, both for fundamental research and for existing and potential industrial applications. The desire to produce Si-based PV materials with consistent performance and reproducibility and at an acceptable cost stimulates a growing number of major research and research infrastructure programs, and a rapidly increasing number of publications in the field of low-temperature plasma for Si PV devices. Therefore, large-scale

utilization of Si-based PV materials prepared using the plasma facilities has become a rapidly expanding industry.

It is the effectiveness, fast development and extensive applications of low-temperature plasma for Si-based PV devices that motivate us to write this review article, which aims to present the underlying physics, chemistry and the main characteristics of the plasma-aided fabrication approaches, methods and techniques in Si PV applications. Although we have briefly introduced the choice of low-temperature plasmas and processes as well as the most commonly used technology for the main current Si-based solar cells both in research and industry in our previous perspective article [43], the chemical and physical interactions in such plasmas containing electrons, ions, radicals and neutral species as well as the plasma interactions with Si surfaces have not been comprehensively addressed.

### 1.3. Structure of the review

In this paper, we introduce the main low-temperature plasma sources for Si PV applications and present an overview of the physical and chemical elementary processes involved in the synthesis of Si thin films and the low-temperature plasma interactions with Si materials. The most significant milestones achieved in each area of the plasma-based synthesis of PV devices are pinpointed and the main directions, opportunities and challenges for the future fundamental and applied research in this undoubtedly hot and active research area are identified. Therefore, this paper is a critical distillation of the progress in the area of low-temperature plasma applications in Si photovoltaics. This review may thus be useful to both established practitioners and junior researchers entering the field.

This article is organized as follows. Section 2 introduces three major low-temperature plasma sources that are used in the plasma processing for Si photovoltaics, namely capacitively coupled plasmas (CCPs), inductively coupled plasmas (ICPs) and microwave plasmas (MPs). Here we do not consider many other low-temperature plasma types such as DC discharges, high-pressure arc discharges, sputtering discharges, etc., because the Si-based PV applications of these plasma types are less extensive or advanced compared to the three main plasma types.

In Section 3, we first follow the synthesis of Si thin-films including hydrogenated amorphous silicon ( $\alpha$ -Si:H) and micro-crystalline silicon ( $\mu$ -c-Si:H), step-by-step, from  $\text{SiH}_4/\text{H}_2$  discharges to the prevailing growth mechanisms. The plasma diagnostic tools employed during the growth of Si-related films are also discussed. Afterwards, we present the development and status on Si thin-film solar cells and HIT solar cells commonly

prepared using low-temperature plasmas. In the final subsection, the plasma-assisted fabrication of silicon nitride layers for surface passivation and antireflection in Si-based solar cells is examined.

Section 4 provides a broad coverage of low-temperature plasma interactions with Si materials with the focus on the reactions of atomic hydrogen with Si surfaces. These reactions including hydrogen adsorption, abstraction, insertion and etching are systematically discussed and supported by some representative Si-based PV applications. Then we elaborate on the plasma cleaning of c-Si surfaces, which is necessary for fabricating high-efficiency Si-wafer based solar cells and HIT solar cells. The plasma processes for the formation of large arrays of vertically aligned nanostructures (NSs), namely the surface texturization as well as the p-to-n type conductivity conversion (PNTCC) are also analyzed. The surface texturization is used to induce light trapping in Si solar cells while the PNTCC can result in the formation of a p-n junction and thus a single-junction solar cell. The final subsection briefly discusses the PSG removal by the plasma etching.

In Section 5, we highlight some of the most important features and competitive advantages of low-temperature plasma techniques and identify major future challenges and directions of research in the field of PV solar cells. This review ends with a summary and outlook for future research and development.

## 2. Low-temperature plasma sources

A low-temperature plasma is any gas in which a significant percentage of the atoms or molecules are ionized. There are three main low-temperature plasma sources that are used in plasma processing for Si photovoltaics: capacitively coupled [CCP: typically 13.56 MHz PECVD and VHF (>40 MHz) PECVD], inductively coupled (ICP: typically 0.5 MHz and 13.56 MHz) and microwave (MW, typically 2.45 GHz) plasmas. Typical CCP, ICP, and MW plasma reactor designs are sketched in Fig. 1. Because of the very large number of the plasma configurations that are developed and used in Si PV applications, it is impossible to provide the exhaustive coverage of all them. While we discuss a specific plasma source and its effect on PV materials, wherever possible, we refer the reader to relevant publications which address the plasma discharge configuration and properties.

For plasmas to exist, ionization of neutral gas is essential. The degree of ionization of the plasma is the proportion of atoms that have lost or gained electrons, and is controlled by the discharge parameters such as electron temperature. For low-temperature plasmas used for deposition and related materials processing, the degree of ionization varies from  $\sim 10^{-6}$  to  $10^{-4}$  in typical CCP

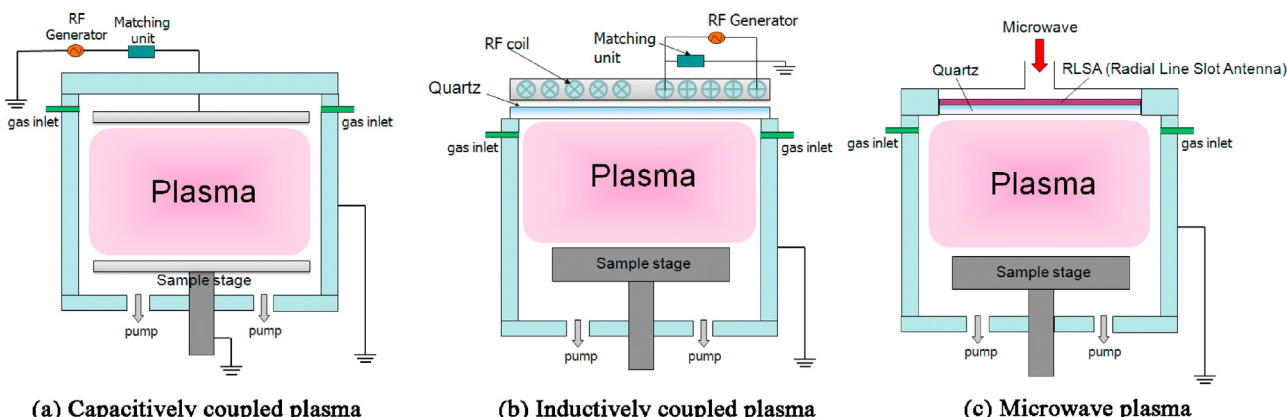


**Fig. 1.** Schematic representation of low-temperature plasma discharges used in plasma processing for Si PV: (a) capacitively and (b) inductively coupled (parallel matching unit connection) and (c) microwave plasmas.

discharges (corresponding to the electron density of  $\sim 10^9$  to  $10^{10} \text{ cm}^{-3}$ ) to as high as  $\sim 10^{-4}$  to  $10^{-2}$  in high-density ICP (corresponding to the electron density of  $\sim 10^{11}$  to  $10^{13} \text{ cm}^{-3}$ ) [44–48] or  $\sim 10^{-4}$  to  $10^{-3}$  in MP discharges (corresponding to the electron density of  $\sim 10^{11}$  to  $10^{12} \text{ cm}^{-3}$ ) [22–25].

Low-temperature plasmas with the low ionization degree are of a major interest for materials processing because electrons are so light, compared to atoms and molecules, that energy exchange between the electrons and neutral gas is very inefficient due to elastic collisions. Therefore, the electrons can be maintained at very high temperatures of several to a few tens of electron-volts while the neutral atoms remain at the ambient temperature. These energetic electrons can induce many elementary processes that would otherwise be unlikely at low temperatures, such as dissociation of precursor molecules and the creation of large quantities of free radicals. Due to the fact that electrons are more mobile than ions [49], negative electrical charges (electrons) will be lost on any object the plasma is in contact with, e.g., a chamber wall or a substrate holder. As a consequence, the plasma is normally more positive than the objects in contact and thus a sheath potential is created between the plasma and the objects across a thin plasma sheath region. Thus, all surfaces exposed to the plasma are subject to energetic ion bombardment owing to the sheath potential effect [50].

## 2.1. Capacitively coupled plasmas

In CCP, the energy is transferred through capacitive coupling. In asymmetric CCP reactors, owing to the capacitor separating the power generator from the electrode, a self-bias builds up between the plasma and the electrode, which accelerates ions (in the sheath) toward the surface [49]. When the RF power is increased to increase the plasma density, the self-bias becomes higher, so does the ion energy. In this case, the plasma density and the ion energy are coupled and cannot be changed separately. This problem could be partly alleviated by using very high frequencies (VHF). Above 40 MHz, the interdependence between the plasma density and the ion energy becomes less prominent because of the increasing electron input power fraction of the total input power with frequency [51–55]. It is necessary to note that using very high frequencies in CCP reactors with large-area electrodes ( $>30 \text{ cm}^2$ ) may lead to the plasma nonuniformities due to the evanescent field and standing wave effects [56]. Another characteristic of the CCP is that the power is coupled through the plasma sheath, meaning that the energy transfer is usually not efficient and the precursors are not easily ionized. Therefore, a relatively low electron density of  $10^9$  to  $10^{10} \text{ cm}^{-3}$  is usually observed in CCP discharges.

## 2.2. Inductively coupled plasmas

For ICP reactors, there are two types of coil configurations, namely cylindrical and planar. In the planar geometry, the electrode is a metal strip or wire wound like a spiral (or coil), as shown in Fig. 1(b). In the cylindrical geometry, it is like a helical spring, which is not shown here. For more details, the reader is referred to the monograph with the focus on the principles of plasma discharges and materials processing [49].

In ICP reactors, the energy is transferred to electrons through inductive coupling by a coil separated from the plasma by a quartz or sapphire window. The oscillating magnetic field induces an oscillating current in the plasma and, contrary to the CCP case, penetrates the bulk plasma directly with little power coupling through the sheath. Therefore, the plasma density and ion energy can be controlled separately. This allows a very efficient energy transfer and creates highly dissociated and dense plasmas [44–48]. This also results in a low sheath potential which does not depend on the plasma source power. As a result, the plasma density can be easily

increased without increasing the ion energy. Another benefit of ICP discharges is that they are relatively free of contamination because the electrodes are completely outside of the reaction chamber.

## 2.3. Microwave plasmas

Strong electric fields generated in a resonant microwave cavity can break down a low-pressure gas and sustain plasma discharges. By applying a steady axial magnetic field to the chamber of a microwave plasma discharge system, high-density plasmas can be generated and sustained even without a cavity resonance. The introduction of a steady magnetic field, in which there is a resonance between the applied frequency and the electron cyclotron frequency within the discharge, allows high-density operation without a cavity resonance. Because of the cyclotron resonance, the gyrating electrons rotate in phase with the right-hand circularly polarized wave, experiencing a steady electric field over many gyro-orbits. Thus, the strong field of the cavity resonance, acting over a short time, is replaced by a much lower field, but acting over a much longer time. The net result is to produce sufficient energy gain of the electrons to ionize the background gas. This discharge configuration is commonly named as electron cyclotron resonance (ECR) microwave plasma discharge. For the detailed design and applications of ECR plasma discharges, the reader is referred elsewhere [57].

Fig. 1(c) displays one of the possible configurations of microwave plasmas. In such configuration, the radial line slot antenna (RLSA) set on top of the chamber radiates circularly polarized uniform microwaves into the chamber through the quartz to excite the plasma. The energy is transferred through both capacitive and inductive coupling. The plasma density induced by the uniform microwave field is also fairly uniform in the radial direction of the chamber [58]. The microwaves are radiated through the dielectric plate and generate the plasma with high electron and ion densities [22–25], which in turn prevents the microwaves from penetrating into the chamber. This is why the microwave field is confined within a 1–2 cm from the dielectric plate.

Surface wave discharges can also be excited by microwave sources with the frequencies in the range of 1–10 GHz, and hence, high-density ( $>10^{11} \text{ cm}^{-3}$ ) plasmas can be sustained. There are numerous source configurations for such high-density microwave plasmas, leading to the improved densities, homogeneity, etc. We refer the interested reader to the recent colloquium article [59] and the references therein.

## 3. Plasma dissociation and deposition for Si thin films and solar cells

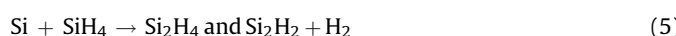
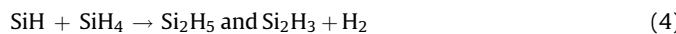
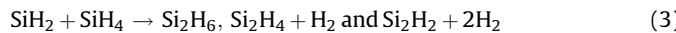
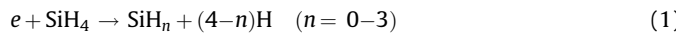
The fabrication of various thin films has perhaps been among the most extensive applications of the low-temperature plasma sources owing to the unique ability of the plasma to dissociate and activate complex gaseous molecular matter. In this section, we elaborate on two most important stages, namely the precursor dissociation and building unit deposition, for the low-temperature plasma processing of Si or Si-related thin films and solar cells. The plasma diagnostics are introduced to better understand the relevant plasma-specific effects. We also overview the development and status of Si thin-film solar cells, HIT solar cells and silicon nitride films developed by low-temperature plasma sources. The main directions, opportunities and challenges in each area are pinpointed as well.

### 3.1. $\text{SiH}_4/\text{H}_2$ discharges

The state-of-the-art growth method for a-Si:H and  $\mu$ -c-Si:H thin films is the use of  $\text{SiH}_4/\text{H}_2$  discharges generated by a variety of

low-temperature plasma sources, such as PECVD [60–62], VHF-PECVD [63–65], ICP-CVD [66–69] and MW-CVD [70,71]. Low-temperature plasmas are usually composed of multiple reactive species that continuously transform into each other and that also generate new species as a result of numerous chemical reactions in the ionized gas phase. It has been acknowledged that the plasma properties and process conditions including the substrate temperature, RF power, deposition pressure, hydrogen dilution ratio, excitation frequency, electrode configuration, etc., determine the morphological, structural, optical and electrical properties of the grown films. In order to control such plasma processing methodologies to optimize the production cost and the film properties, a thorough understanding of the physical and chemical properties of the plasma is indispensable [72,73]. It usually requires knowledge from chemistry, thermodynamics, gas transport, heat transfer and film growth kinetics. Though many groups have extensively investigated the SiH<sub>4</sub>/H<sub>2</sub> discharge [72,74–77], the knowledge of the prevailing reactions and chemical transformations leading to the production of the key radical species that act as building units of the Si-based films of interest to PV applications remains incomplete.

Since low-temperature plasmas are dominated by electron and ion interactions, it is vital to have comprehensive databases for electron-ion and atom-molecule interactions including the processes of excitation, ionization, dissociation, charge exchange, etc. In SiH<sub>4</sub> + H<sub>2</sub> discharges, electrons collide with silane molecules and as a result, H and all of the SiH<sub>n</sub> radicals, in order of typical abundance, H, SiH<sub>3</sub>, SiH<sub>2</sub>, SiH, and Si, are produced. All but SiH<sub>3</sub> are reactive with silane because SiH<sub>3</sub> has a very low reaction rate coefficient with silane [78]. The main chemical reactions that contribute to the consumption of SiH<sub>4</sub> are listed below [74]:



Specifically, electron collisions (1) with both SiH<sub>4</sub> and H<sub>2</sub> can produce a large amount of atomic hydrogen H. Atomic hydrogen is an important species because it is formed nearly in all electron impact collisions. The most abundant dissociation product, H, primarily reacts with silane (2) to yield SiH<sub>3</sub> at high silane pressures, but reaches surfaces at low silane pressures. The SiH<sub>3</sub> radicals are assumed to be responsible for the film growth [79,80]; they are usually referred to as "building units". The SiH<sub>2</sub> radicals react quickly with silane (3) and are assumed to be precursors to form higher silanes, i.e., Si<sub>n</sub>H<sub>2n+2</sub>. Some of the resultant activated Si<sub>2</sub>H<sub>6</sub><sup>\*</sup> will dissociate into Si<sub>2</sub>H<sub>4</sub> + H<sub>2</sub> or Si<sub>2</sub>H<sub>2</sub> + 2H<sub>2</sub> before being stabilized as Si<sub>2</sub>H<sub>6</sub> (stable disilane) by additional gas collisions. Disilane formation is favored at high pressures and is observed as the primary reaction product at normal operating pressures [81]. SiH is a less abundant species (4). Si<sub>2</sub>H<sub>5</sub> can also be produced by H + Si<sub>2</sub>H<sub>6</sub> reactions, and, as Si<sub>2</sub>H<sub>5</sub> reacts slowly if at all with silane, it will contribute to the film growth. It has been observed at relatively high silane pressures [82]. Despite the minor production of Si (5), some of the Si<sub>2</sub>H<sub>4</sub> species resulted from the Si + SiH<sub>4</sub> and SiH<sub>2</sub> + SiH<sub>4</sub> reactions further react with SiH<sub>4</sub> to produce a small amount of Si<sub>3</sub>H<sub>8</sub> (stable trisilane).

We have considered some of the most important electron-induced chemical reactions but what role do the ions play in

SiH<sub>4</sub> + H<sub>2</sub> discharges? Ionization of SiH<sub>4</sub>, Si<sub>2</sub>H<sub>6</sub>, and H<sub>2</sub> can produce a large number of different positive ions [78,83], as shown below. For SiH<sub>4</sub>, Si<sub>2</sub>H<sub>6</sub>, and H<sub>2</sub> these ions are SiH<sub>2</sub><sup>+</sup>, Si<sub>2</sub>H<sub>4</sub><sup>+</sup>, and H<sub>2</sub><sup>+</sup>, respectively, and are generated in the following reactions:



Clearly the ions play a critical role in establishing and maintaining the physical conditions of the plasma but they also drive much of the chemistry through ion-molecule reactions [78], e.g.



Indeed such ion-molecule reactions may produce new chemical species and dominate any neutral chemistry. It should also be noted that ions and electrons may be removed simultaneously from the plasma by (dissociative) electron recombination [84], e.g.



Modeling of the plasma chemistry can give indications on which species are important building units for the growth of Si thin films and how the plasma operating conditions can be tuned to optimize the growth process. Several plasma modeling approaches exist in the literature, such as chemical-kinetics simulations [80,85,86] and fluid models describing the chemical kinetics as well as fluid dynamics and solving the Boltzmann transport equation [78,87,88]. The interested reader is referred to a recent review [72].

In addition to the generation and reaction of radicals, the plasma-surface interactions of the neutral species have a major impact on the film properties. These interactions are commonly described by the sticking model [89,90]. In this model only the radicals react and adsorb on the surface forming a layer (or more often multilayers) while nonradical neutrals (H<sub>2</sub>, SiH<sub>4</sub>, and Si<sub>n</sub>H<sub>2n+2</sub>) are reflected into the discharge. The probability of such adsorption varies depending upon the surface material, the surface temperature and, of course, the precursor gas itself [91–93]. The plasma-surface interactions may provide a limiting factor in solar cell processing since the surface conditions may change from batch to batch throughout the manufacturing process. This obviously reduces the reproducibility achievable on the production line. One simple solution is to coat the surfaces of the reaction chamber with a known amount of material at the start of each processing cycle. Therefore, whilst the actual surface chemistry may remain unknown, by starting each cycle with the same surface conditions and running the reactor under the identical working conditions, the surface chemistry may be reproduced in each cycle leading to a greater homogeneity in the final products.

The most striking difference of low-temperature plasma CVD from thermal CVD (like hot-wire CVD) is the presence of the plasma sheath, which is a non-neutral layer of space charge separating the plasma bulk and the growth surface [50]. Because of the much higher mobility of electrons, the surface is always charged negatively with respect to the plasma bulk [49]. The resulting potential distribution sustains intense positive-ion fluxes onto the surface and impedes the fluxes of negatively charged species. The plasma-surface interactions may lead to a significant reduction of the surface diffusion activation energy through the transfer of momentum from the impinging species to the surface, a

higher surface temperature through the ion-bombardment, high growth rates through the creation of the adsorption sites via the fragmentation and rearrangement of the chemical bonds on the surface by the impinging particles, and some other effects [50,94–97].

Although the ion-bombardment effect may elevate the surface temperature and thus contribute to the film crystallization, strong ion bombardment can also result in excessive defect formation, and hence significant deterioration of the film quality. Other plasma-related effects (such as electric field- and polarization-related effects) can significantly increase the rates of dissociation of silane molecules in the gas phase, promote the fast transport of the reactive species to the growth surface, and further reduce surface diffusion activation barriers [95–99]. We refer the interested reader to the recent review with a focus on the unique plasma-specific features and physical phenomena in the organization of nanoscale solid-state systems in a broad range of elemental composition, structure, and dimensionality [100].

### 3.2. Plasma diagnostics

In order to study the fluxes of radicals and ions responsible for the film growth in  $\text{SiH}_4 + \text{H}_2$  low-temperature plasma discharges, many plasma diagnostics and modeling approaches such as optical emission spectroscopy (OES) [101–106], mass spectroscopy [105,106], laser absorption spectroscopy [107,108], UV spectroscopy [109,110] and Langmuir probe measurements of the plasma density and electron temperature [95,111,112] have been applied.

#### 3.2.1. Langmuir probe

Langmuir probe is a metal tip inserted into the plasma and biased positively or negatively to draw electron or ion currents, respectively. The probe introduced by Langmuir and analyzed by Mott-Smith and Langmuir [113] is one of the earliest and still one of the most powerful plasma diagnostic tools. Usually the probe measurements are performed in a wide range of bias voltage, providing the  $I$ - $V$  characteristic. Although the probe perturbs its local plasma surrounding, it is still possible to determine the electron temperature  $T_e$ , electron density  $n_e$ , plasma sheath potential  $V_p$  and even the electron energy distribution function (EEDF) from the measured current-voltage ( $I$ - $V$ ) characteristics of the probe. The EEDF is generally defined as the second order

derivative of the measured  $I$ - $V$  curve, and can be expressed by the following equation [49,114]:

$$g_e(V) = \frac{2m_e}{e^2 A} \left( \frac{2eV}{m_e} \right)^{1/2} \frac{d^2 I_e}{dV^2} \quad (12)$$

where  $A$  is the surface collection area of the Langmuir probe,  $e$  is the electron charge and  $m_e$  is electron mass. The electron density  $n_e$  and electron temperature  $T_e$  can be derived [49,114] from the measured EEDF by:

$$n_e = \int g_e(\varepsilon) d\varepsilon \quad (13)$$

$$T_e = \frac{2}{3n_e} \int \varepsilon g_e(\varepsilon) d\varepsilon \quad (14)$$

Both equations are also valid if a Maxwellian distribution is assumed.

One can control most of the gas-phase reaction rates and hence the balance of reactive species in the discharge via tailoring of the EEDF. Therefore, the EEDF can not only help monitor the particular process of either deposition or etching, but also help understanding the discharge process as a whole. Fig. 2 shows the experimental EEDF curves as well as the calculated  $n_e$  and  $T_e$  at various RF input power density for the inductively coupled  $\text{SiH}_4 + \text{H}_2$  discharges. One can see that the electron density increases with the input power density, reaching a maximum of  $\sim 5 \times 10^{12} \text{ cm}^{-3}$ , while the electron temperature remains at a low value ranging from 3.6 to 4.0 eV. The high electron density and relatively low electron temperature are the main merits of typical ICPs.

#### 3.2.2. Steady-state-number density

Steady-state densities of reactive species in the low-temperature plasma have been measured using various gas-phase diagnostic techniques such as OES [102], infrared-laser-absorption spectroscopy [107], and ultra-violet light-absorption spectroscopy [109]. Fig. 3 [115] shows the steady-state-number densities of chemical species including radical and ionic species in  $\text{SiH}_4$  and  $\text{SiH}_4/\text{H}_2$  plasmas used for preparing device-grade microcrystalline silicon ( $\mu\text{-Si:H}$ ) and amorphous silicon (a-Si:H). Steady-state-number densities of chemical species are determined by the balance between their generation and loss rates. Therefore, the density of short lifetime species such as  $\text{SiH}_2$ ,  $\text{SiH}$ , and  $\text{Si}$  which

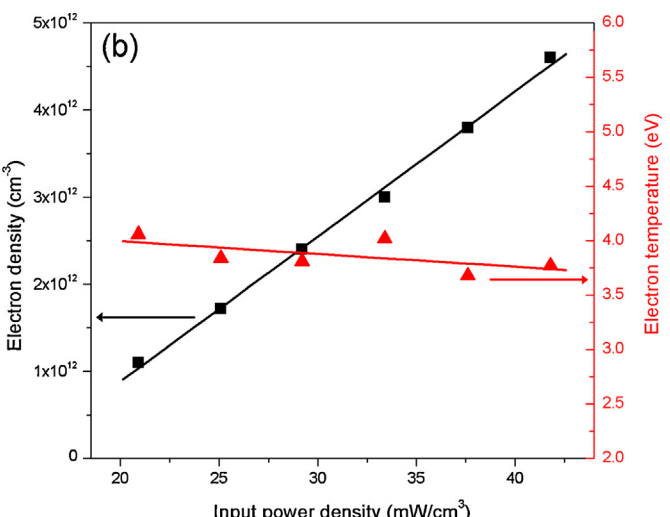
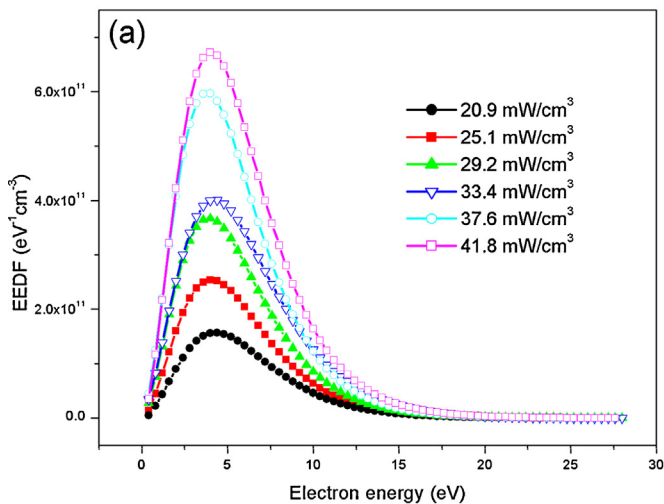


**Fig. 2.** The experimental EEDF (a) and the calculated  $n_e$  and  $T_e$  (b) of the inductively coupled  $\text{SiH}_4 + \text{H}_2$  discharges at various input power density measured at PSAC. The working pressure, flow rates of  $\text{SiH}_4$  and  $\text{H}_2$  were kept at 2 Pa, 3 sccm, and 15 sccm, respectively. The EEDF were calculated using  $I$ - $V$  measurements obtained by a single RF-compensated Langmuir probe.

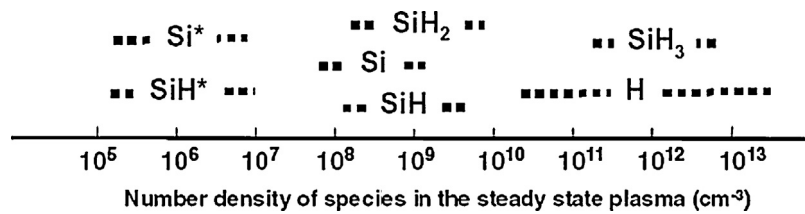


**Fig. 3.** Number density of chemical species in the steady-state low-temperature plasmas measured or predicted by various diagnostic techniques. Reproduced from Ref. [115].

are highly reactive with SiH<sub>4</sub> and H<sub>2</sub> is usually much smaller compared to that of long lifetime species (SiH<sub>3</sub>) showing no reactivity with SiH<sub>4</sub> and H<sub>2</sub> in the steady-state plasma, although the generation rates of those species are not much different. It is clearly seen in Fig. 3 that SiH<sub>3</sub> radical is a dominant chemical species both for the growth of  $\mu$ c-Si:H and a-Si:H, although the density ratio of short lifetime species to SiH<sub>3</sub> is varied when the plasma-generation conditions are changed.

Steady-state density of atomic hydrogen (H) also varies in broad limits in the plasma as shown in Fig. 3. This is mainly due to the increase in the density of atomic hydrogen with increasing the hydrogen-dilution ratio  $R$  (H<sub>2</sub>/SiH<sub>4</sub>). Given that  $\mu$ c-Si:H is formed with increasing  $R$  at constant electron density in the plasma and constant substrate (surface) temperature, it is reasonable that atomic hydrogen plays an important role in the case of  $\mu$ c-Si:H growth [116] although SiH<sub>3</sub> is the dominant film precursor both for  $\mu$ c-Si:H and a-Si:H growth [79].

### 3.2.3. Mass spectroscopy

Mass spectroscopy is a technique that can provide a great deal of information about the excited neutrals and ionized species in the low-temperature plasma. Fig. 4 presents a representative example of Quadrupole Mass Spectroscopy (QMS) spectra for (a) basic vacuum chamber, (b) SiH<sub>4</sub> + H<sub>2</sub> discharge with B<sub>2</sub>H<sub>6</sub> doped (p-type), (c) SiH<sub>4</sub> + H<sub>2</sub> discharge (intrinsic) and (d) SiH<sub>4</sub> + H<sub>2</sub> discharge with PH<sub>3</sub> doped (n-type) during the deposition of microcrystalline Si p-i-n core structure in a continuous process using a low-frequency (460 kHz), low-pressure, thermally non-equilibrium ICP deposition system [43]. The details of the plasma reactor and the setup of QMS are discussed elsewhere [69].

One can easily observe that the following peaks at 28, 29, 30, 31 and 32 amu, which correspond to Si, SiH, SiH<sub>2</sub>, SiH<sub>3</sub> and SiH<sub>4</sub>, respectively, do not change when the doping conditions change. These doping conditions are adjusted to form a graded structure including the p-layer, intrinsic (i) layer, and n-layer. It is evident

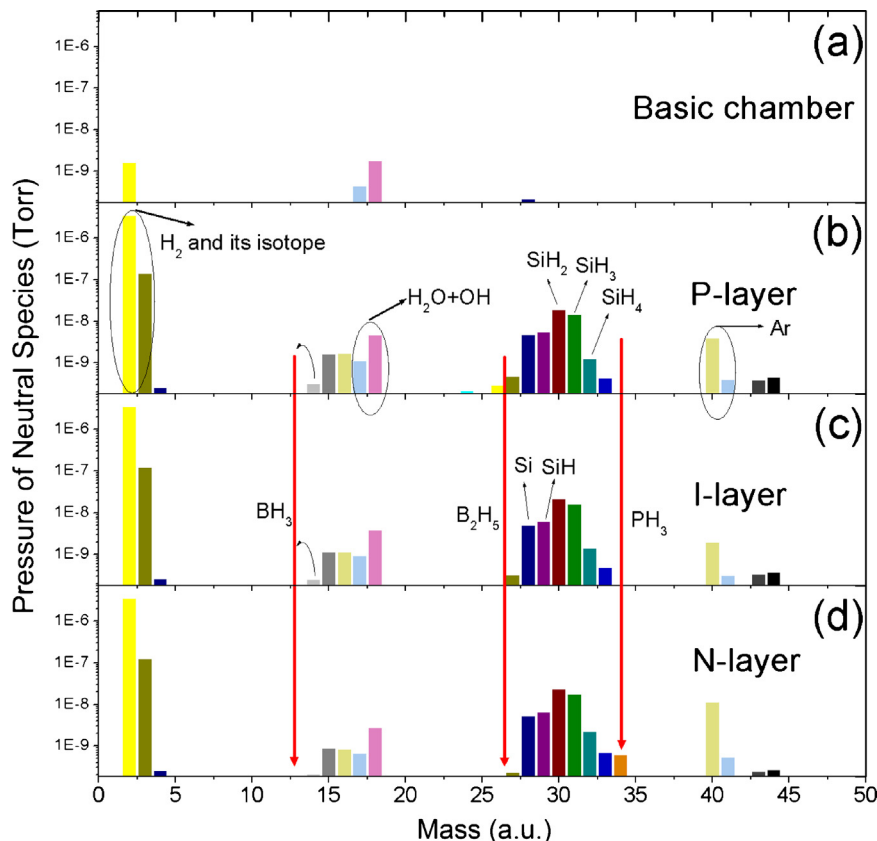


**Fig. 4.** A typical example of QMS spectra for (a) basic vacuum chamber, (b) SiH<sub>4</sub> + H<sub>2</sub> discharge with B<sub>2</sub>H<sub>6</sub> doped (p-type), (c) SiH<sub>4</sub> + H<sub>2</sub> discharge (intrinsic), and (d) SiH<sub>4</sub> + H<sub>2</sub> discharge with PH<sub>3</sub> doped (n-type) during the deposition of microcrystalline Si p-i-n core structure in a continuous process using reactive silane precursor gas diluted with hydrogen in a low-frequency (460 kHz), low-pressure, thermally non-equilibrium ICP deposition system developed at PSAC. Reproduced from Ref. [43].

that  $\text{SiH}_3$  and  $\text{SiH}_2$  are the major components while  $\text{SiH}$  and  $\text{Si}$  are the minor components in the inductively coupled plasmas of  $\text{SiH}_4 + \text{H}_2$  discharges. Moreover, the insignificant amount of  $\text{SiH}_4$  in comparison with the combined density of  $\text{SiH}_x$  radicals ( $0 \leq x \leq 3$ ) means that the silane gas precursor can be highly dissociated by the ICP discharge. The large amount of atomic hydrogen flux in the  $\text{SiH}_4 + \text{H}_2$  discharge (see Fig. 4(b)–(d)) leads to a very high surface hydrogen coverage, which increases the surface diffusion length and thus promotes the growth of microcrystalline silicon. The clear variation of  $\text{BH}_3$  (or  $\text{B}_2\text{H}_6$ ) and  $\text{PH}_3$  from Fig. 4(b)–(d) indicates the doping transition from the p-layer through the i-layer to the n-layer.

### 3.3. Growth processes of a-Si:H and $\mu\text{-c-Si:H}$

After carefully introducing the initial event for the growth of a-Si:H and  $\mu\text{-c-Si:H}$ , namely the decomposition process of source gas materials in  $\text{SiH}_4 + \text{H}_2$  low-temperature plasmas, we now explain the growth processes of a-Si:H and  $\mu\text{-c-Si:H}$  films.

#### 3.3.1. Amorphous silicon

On the basis of two experimental results [90], a surface-diffusion scheme for the a-Si:H film growth has been proposed. It has been shown in the above section that  $\text{SiH}_3$  radical is a dominant chemical species both for the growth of a-Si:H and  $\mu\text{-c-Si:H}$ . For a-Si:H growth,  $\text{SiH}_3$  radical reaching the film-growth surface starts to diffuse on the surface. During the surface diffusion,  $\text{SiH}_3$  abstracts surface-covering bonded hydrogen, forming  $\text{SiH}_4$  and thus releasing the dangling bond on the surface (growth-site formation). Another  $\text{SiH}_3$  species then diffuses toward the dangling-bond site to find the bonding site and to form a Si-Si bond (film growth) as schematically shown in Fig. 5(a).

In general, besides the adsorbed  $\text{SiH}_3$ , the remaining part of the total  $\text{SiH}_3$  flux is reflected by the surface. The adsorbed  $\text{SiH}_3$  changes its form as follows: (1)  $\text{SiH}_3$  abstracts surface-covering bonded H thus forming  $\text{SiH}_4$ ; it is also possible that two  $\text{SiH}_3$  radicals combine on the surface forming  $\text{Si}_2\text{H}_6$ , and (2) surface-diffusing  $\text{SiH}_3$  sticks to the dangling-bond site forming the Si-Si bond. Once the  $\text{SiH}_3$  building unit sticks to the dangling-bond site forming the Si-Si network, further radical incorporation is controlled by the nano- and micro-scale self-organization processes [117]. It is imperative that, depending on the surface-diffusion scheme, the a-Si:H thin films may develop through the layer-by-layer growth mechanism [118].

#### 3.3.2. Microcrystalline silicon

In order to explain specific phenomena during the formation process of  $\mu\text{-c-Si:H}$ , three models have been proposed: (1) surface-diffusion model [116], (2) etching model [119], and (3) chemical-annealing model [120].

The surface-diffusion model is sketched in Fig. 5(b). A large flux of atomic H from the plasma leads to the full surface coverage by bonded hydrogen and also generates local heating through hydrogen-exchange reactions on the film-growing surface (plasma-surface interactions). Both effects enhance the surface diffusion of  $\text{SiH}_3$  building units. As a consequence,  $\text{SiH}_3$  species adsorbed on the surface can find energetically favorable sites, leading to the formation of atomically ordered structures (the nucleus formation stage). After the formation of primary nuclei, epitaxial-like crystal growth takes place through the enhanced surface diffusion of  $\text{SiH}_3$  [116,121]. The surface-diffusion model is generally applicable to  $\mu\text{-c-Si:H}$  film growth under diverse conditions, because the increase of the surface diffusion length of building units under hydrogen dilution conditions has been confirmed experimentally [121]. It is worth emphasizing

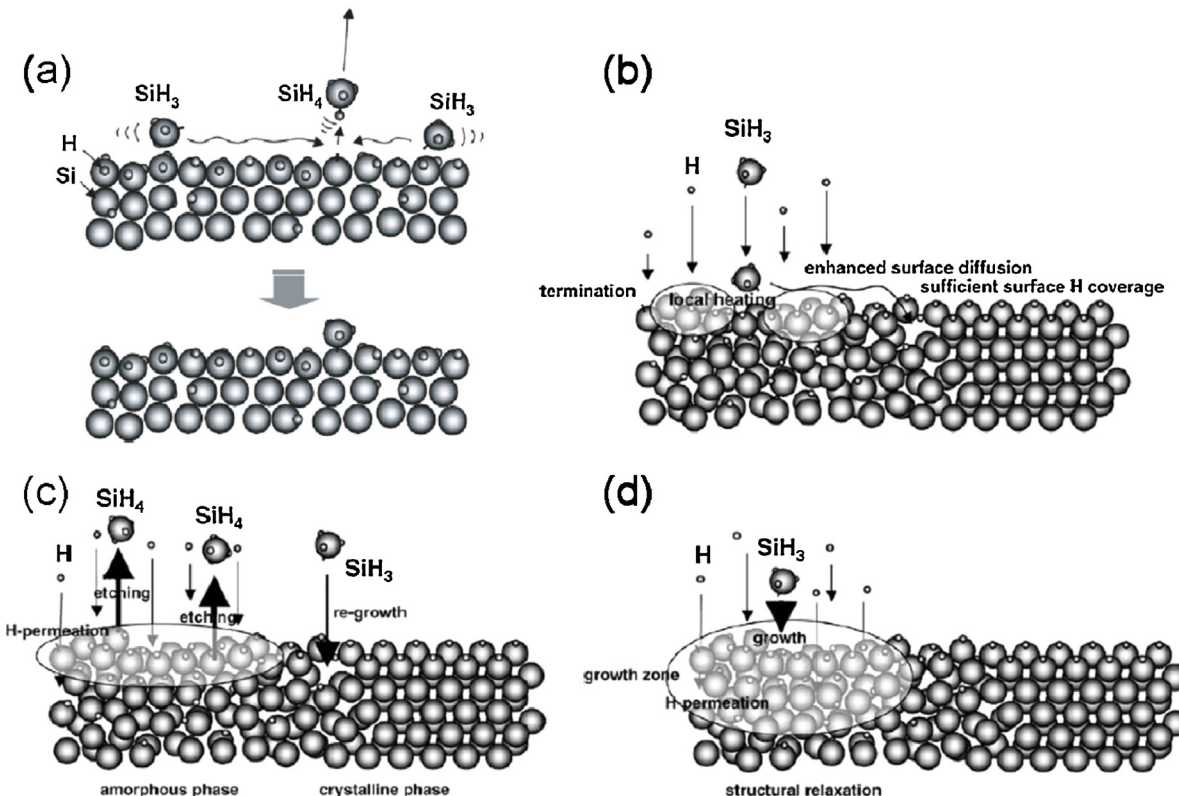


**Fig. 5.** Schematics of (a) surface-diffusion model for the surface-growth process of a-Si:H, (b) surface-diffusion model for  $\mu\text{-c-Si:H}$  growth, (c) etching model for  $\mu\text{-c-Si:H}$  formation, and (d) chemical-annealing model for  $\mu\text{-c-Si:H}$  formation. Large and small spheres represent Si and H atoms, respectively. Reproduced from Ref. [115].

that the local heating effect through the hydrogen plasma–surface interactions is considered as a major factor to enhance the surface diffusion of building units ( $\text{SiH}_3$ ) for the growth of  $\mu\text{-c-Si:H}$  films, especially under low-temperature conditions.

Etching model has been proposed based on the experimental fact that the film-growth rates are reduced with an increase of hydrogen-dilution ratio  $R$ . A concept of the etching model is shown in Fig. 5(c). Atomic H reaching the film-growing surface breaks Si–Si bonds, preferentially weak bonds involved in the amorphous network structure, leading to a removal of Si atoms weakly bonded to other Si atoms. This site is replaced with a new building unit  $\text{SiH}_3$ , creating rigid and strong Si–Si bonds, eventually giving rise to an ordered structure [119,121]. This mode can be used to explain the growth of  $\mu\text{-c-Si:H}$  films in the  $\text{SiH}_4/\text{H}_2$  glow discharges under conditions of a high hydrogen-dilution ratio and low deposition rates. The hydrogen plasma–surface interactions result in the hydrogen insertion effect, which will be discussed in Section 4.1. Two simultaneous processes that combine hydrogen insertion and surface diffusion of  $\text{SiH}_3$  radicals promote the growth of  $\mu\text{-c-Si:H}$  films. However, the experimental results showed that the removal process of weakly bonded Si atoms through hydrogen insertion is not a necessary condition for the formation of  $\mu\text{-c-Si:H}$  [121].

The chemical-annealing model has been proposed to explain the experimental fact that crystal formation is observed during the hydrogen-plasma treatment in a layer-by-layer growth by an alternating sequence of thin amorphous film growth and hydrogen-plasma treatment. Several monolayers of amorphous silicon are deposited and these layers are exposed to hydrogen atoms produced in the hydrogen plasma. These procedures are repeated alternately for several ten times to achieve the thickness sufficient for the evaluation of the film structure. However, the absence of any remarkable reduction of the film thickness during the hydrogen-plasma treatment is difficult to explain by the etching model and the chemical-annealing model has been proposed as shown in Fig. 5(d). During the hydrogen-plasma treatment, many hydrogen atoms permeate into the sub-surface area (growth zone). This leads to crystallization of the amorphous network through the formation of a flexible network without any significant removal of Si atoms provided that a sufficient amount of atomic hydrogen is incorporated into the sub-surface area [120,121]. This mode can only be used to explain the phase transition from amorphous to microcrystalline for Si:H films subjected to the post-deposition hydrogen-plasma treatment. The hydrogen plasma treatment that leads to this phase transition will be presented in Section 4.1. During the hydrogen plasma treatment, an increase in hydrogen content or a change in the film structure is usual consequences of the hydrogen plasma–surface interactions.

#### 3.4. Si thin-film solar cells

With a better understanding of the physics and chemistry of the plasma-synthesized Si thin films let us now discuss the Si thin-film solar cells fabricated using plasma-aided technologies. Si thin-film solar cells are either amorphous or microcrystalline. Perhaps the most important feature of a-Si and  $\mu\text{-c-Si}$  materials is that a wide range of temperatures (from room temperature to 400 °C) can be used for deposition. Room-temperature deposition allows the use of a variety of substrates (e.g., glass, metal, plastic), and, in particular, the possibility of using low-cost polymers such as polyethylene terephthalate (PET), which could be a significant advantage in reducing the cost of the modules.

##### 3.4.1. Micromorph tandem and triple-junction solar cells

Two recent laboratory studies of a-Si:H and  $\mu\text{-c-Si:H}$  single-junction thin-film solar cells demonstrated the record conversion efficiencies of 10.4% [122] and 10.9% [123], respectively.

The weakness of the present-day commercial a-Si:H thin-film solar modules is their relatively low photo-conversion efficiency, of the order of 6.5% [124], and also the inferior long-term stability under light exposure, caused by the Staebler–Wronski effect (SWE) [125]. A conventional way to improve the device stability is to combine a-Si:H with  $\mu\text{-c-Si:H}$  layers to form “micromorph” tandem solar cells or triple-junction solar cells. A “micromorph” tandem cell consists of a top (through which light enters first) a-Si:H cell and a bottom  $\mu\text{-c-Si:H}$  cell as shown in Fig. 6(a), while a triple-junction thin-film Si solar cell usually consists of a top a-Si:H cell and two subsequent  $\mu\text{-c-Si:H}$  cells.

As compared to amorphous silicon, microcrystalline silicon absorbs light within a broader spectral range. This difference in the range of absorption of a-Si:H and  $\mu\text{-c-Si:H}$  can be ascribed to different bandgap energy values: the bandgap of a-Si:H is 1.75 eV, while the bandgap of  $\mu\text{-c-Si:H}$  is only 1.1 eV (similar to crystalline silicon) [19,126]. Nevertheless, within its range of absorption, the absolute value of the absorption coefficient of a-Si:H (with a quasi-direct bandgap) is higher compared to  $\mu\text{-c-Si:H}$  (with an indirect bandgap). Therefore, this combination of materials takes advantage of the broader part of the solar spectrum (as compared to single-junction cells). As a result, the conversion efficiency of the tandem or triple-junction solar cells increases, e.g., up to 13.4% (initial efficiency) for mini-modules (910 mm × 455 mm), as demonstrated by Kaneka Corp. [127]. A typical performance of the “micromorph” tandem solar cells confirmed by the National Institute of Advanced Industrial Science and Technology (AIST) is shown in Fig. 6(b) [15]. The use of  $\mu\text{-c-Si:H}$  as an absorber layer in tandem or triple-junction cells has proven to be the key to achieving higher conversion efficiencies [128–131]. As of yet, the micromorph tandem or triple-junction cell configurations are among the most efficient thin-film solar cell devices, aiming for 14% stable efficiency in the short term [132].

##### 3.4.2. VHF-CCP for high-rate deposition

In view of low-cost manufacturing of plasma-synthesized silicon thin-film solar cells, high-rate deposition is targeted without any reduction of the cell's efficiency. In conventional capacitively coupled RF-PECVD (13.56 MHz) processes [133,134], however, high-rate deposition of device-grade  $\mu\text{-c-Si:H}$  or a-Si:H films has been quite difficult because of the problems discussed in Section 2.1, namely, a low dissociation efficiency of CCPs with a low electron density of  $10^9$  to  $10^{10} \text{ cm}^{-3}$  and strong ion bombardment effects even at moderate discharge powers. Bombardment of the growth surface by energetic ions accelerated in the plasma sheath often results in the excessive defect formation, and consequently, a significant deterioration of the film quality [133,134]. The solar cell performance is dominated by recombination of photocarriers, and is thus sensitive to the density of defects in the film. Therefore, how to achieve high growth rates while producing high-quality thin films becomes an important issue for the present-day plasma techniques in the field of Si-based thin-film solar cells.

As discussed in Section 2.1, this problem could be partly mitigated by using very high frequencies (VHF): in cases of above 40 MHz the interdependence between the plasma density and the ion energy becomes less pronounced. Therefore, the plasma density can be increased while the ion bombardment effect can be maintained at a low level with the increase in discharge power in order to increase the deposition rate.

In general, a typical deposition rate of ~0.5 nm/s is often achieved for the deposition of high quality a-Si:H or  $\mu\text{-c-Si:H}$  thin films using a conventional RF excitation at 13.56 MHz [17,135]. In contrast, using VHF excitation may lead to higher deposition rates of >1 nm/s and simultaneously high-quality Si thin films [136–138]. For example, Rech et al. [138] compared the deposition rate and cell efficiency of  $\mu\text{-c-Si:H}$  thin film solar cells synthesized at conventional 13.56 MHz

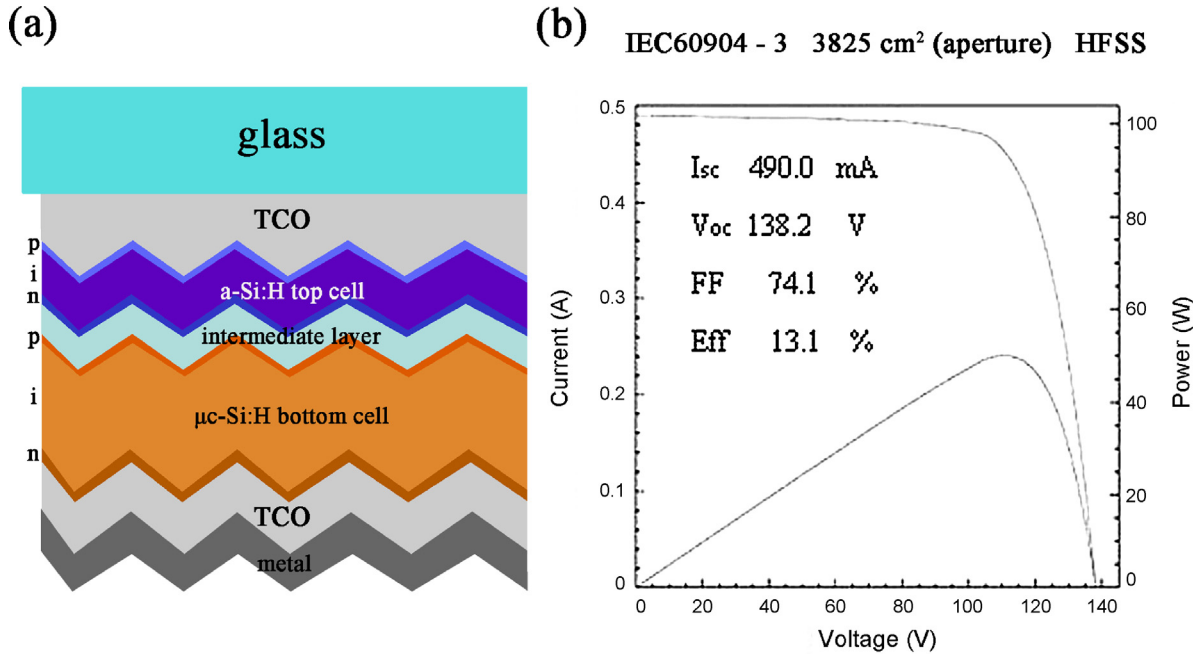


**Fig. 6.** (a) Schematic device structure of a “micromorph” tandem solar cell. (b) A typical  $I$ - $V$  characteristic of the “micromorph” tandem solar cells confirmed by AIST. Adapted from Ref. [15].

and VHF of 40.68 MHz, as shown in Fig. 7. Fig. 7(a) shows the deposition rate as a function of the discharge power for two excitation frequencies of 13.56 and 40.68 MHz. Higher deposition rates are achieved by increasing the discharge power for both frequencies. Nevertheless, the VHF approach can be used to synthesize device-grade  $\mu$ c-Si:H thin films as shown in Fig. 7(b), which presents the illuminated  $I$ - $V$  curves and the corresponding photovoltaic parameters of  $\mu$ c-Si:H solar cells developed at two excitation frequencies of 13.56 and 40.68 MHz with different deposition rates. At power densities below  $1 \text{ W/cm}^2$ , conversion efficiencies of 9.4% and 9.2% were achieved at deposition rates of 0.5 nm/s (13.56 MHz) and 1 nm/s (40.68 MHz), respectively. At higher power densities and 40.68 MHz excitation, an efficiency of 7.9% was still maintained at a high deposition rate of 2 nm/s.

#### 3.4.3. Features of ICP and MP in high-rate deposition

Record solar cell efficiencies at very high deposition rates have been reported for deposition regimes that combine plasma excitation frequencies  $>60$  MHz and relatively high deposition pressures. However, powder formation and process up-scaling toward square meter size, e.g., standing waves, “skin effect” in the electromagnetic field localization, voltage uniformity, etc., are common problems in homogeneous film growth in the VHF-regime [17,133,135]. Recently, low-pressure, thermally non-equilibrium, high-density ICPs have been demonstrated as an effective and versatile process environment to increase the deposition rate [66–69,139–142]. Kosku et al. [139] reported a remarkably high growth rate of  $\sim 6$  nm/s for device-quality  $\mu$ c-Si:H films deposited from VHF-ICPs. In the low-frequency ICP processes,

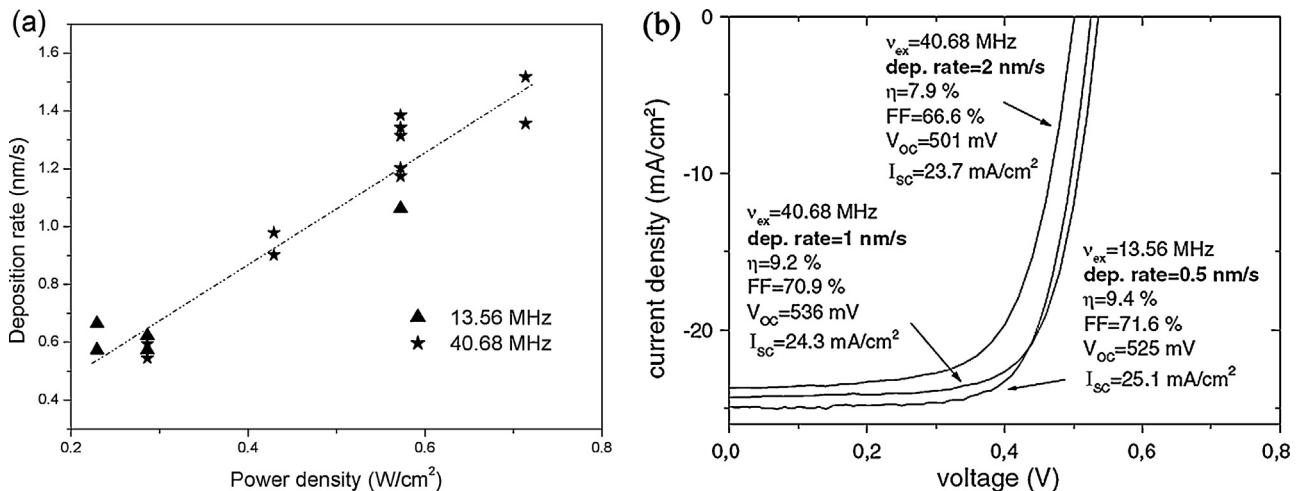


**Fig. 7.** (a) The deposition rate as a function of the discharge power for two excitation frequencies of 13.56 and 40.68 MHz. (b) Illuminated  $I$ - $V$  curves and the corresponding photovoltaic parameters of  $\mu$ c-Si:H solar cells prepared at deposition rates of 0.5, 1, and 2 nm/s for 13.56 MHz excitation frequency in the first case and 40.68 MHz in the latter two cases. The cell area is  $1 \text{ cm}^2$ .

Adapted from Ref. [138].

a very high growth rate of up to 2.4 nm/s for  $\mu$ c-Si:H films with a high crystallinity has been achieved [68].

In comparison with the conventional capacitively coupled RF plasma sources, the ICPs operating in the electromagnetic mode have several salient features: (i) high densities of the plasma species; in particular, the electron number density  $n_e$  in the pressure range of a few Pa can reach  $\sim 10^{12}$  to  $10^{13} \text{ cm}^{-3}$  and is up to two to three orders of magnitude higher compared to the CCP discharges [44–48]; (ii) low plasma sheath potentials (typically a few tens of volts) near the chamber wall or deposition substrate, which is beneficial for the reduction of ion bombardment on the deposited films; and (iii) excellent uniformity of the plasma parameters in the radical and axial directions [45,143]. This high electron number density achieved in the ICP-based process can result in large amounts of  $\text{SiH}_x$  ( $x = 1, 2, 3$ ) radicals and atomic hydrogen as a result of the intense inelastic interactions between electrons and silane molecules via the elementary processes of dissociation, excitation and ionization of the reactive silane precursor gas. A substantial amount of  $\text{SiH}_x$  ( $x = 1, 2, 3$ ) radicals on the growth surface of the film account for the achieved high growth rates [144]. On the other hand, strong fluxes of atomic hydrogen from the plasma can give rise to a higher surface coverage by bonded hydrogen, a higher etching rate to remove the disordered material, and a local heating through hydrogen interactions with the surface.

In particular, Shen et al. [145,146] have successfully applied remote-like ICPs to synthesize single-junction a-Si solar cells with the conversion efficiency of 9.6% and the improved light-soaking stability. ICPs can produce high-density plasmas to improve diffusion of the reactive radicals on substrates even at fairly low deposition temperatures because of the relatively high achievable ionization degrees. The configuration of a typical remote-like ICP system is sketched in Fig. 8(a). The growth chamber can be divided into two regions, namely the high-density plasma region and the thin-film growth region. The high-density plasma of hydrogen gas is generated and confined in the upper chamber to generate ions and electrons. At the same time, the  $\text{SiH}_4$  precursor gas is injected into the thin film growth region of the lower chamber. The  $\text{SiH}_4$  molecules interact with the plasma species and are converted into a variety of process radicals. Since these radicals are highly reactive, once they reach the substrate surface, they enable fast film deposition even at low growth temperatures. The most important characteristic of this system is the separation of high-density plasma region from the thin-film growth region. This arrangement effectively reduces the possibility of ion bombardment on the growth surface, eventually resulting in a film with a low density of defects.

Consequently, the remote-ICP a-Si:H films exhibit a lower defect density of  $\sim 3 \times 10^{15} \text{ cm}^{-3}$  compared to the typical value of  $\sim 6 \times 10^{15} \text{ cm}^{-3}$  in the VHF-PECVD a-Si:H films. The lower defect density in the ICP-produced a-Si:H films may be due to more effective hydrogen passivation of dangling bonds during the deposition [147]. Fig. 8(b) shows the light-induced degradation of conversion efficiency of a-Si:H p-i-n solar cells grown by remote-like ICP-CVD (open triangles) and VHF-PECVD (open circles). The remote-ICP a-Si solar cell shows a reduced by 11% conversion efficiency from 9.6% to 8.5% after  $10^4$  s exposure with a light irradiance of 6 Sun at 60 °C. In contrast, the VHF PECVD a-Si:H solar cell exhibits a nearly 18% decrease in PV efficiency from 8.8% to 7.2% under the same light exposure.

Light-induced degradation in a-Si:H was found to strongly depend on the amount of nano-sized voids and hydrogen content [148]. Recent experiments have shown that the SWE is accompanied by metastable structural changes of the underlying amorphous network [149]. The low defect density in the remote-ICP-produced a-Si:H layers and the good long-term stability under light soaking support the conclusion that the Si network in ICP deposited films is fairly stable and is therefore more resistant to

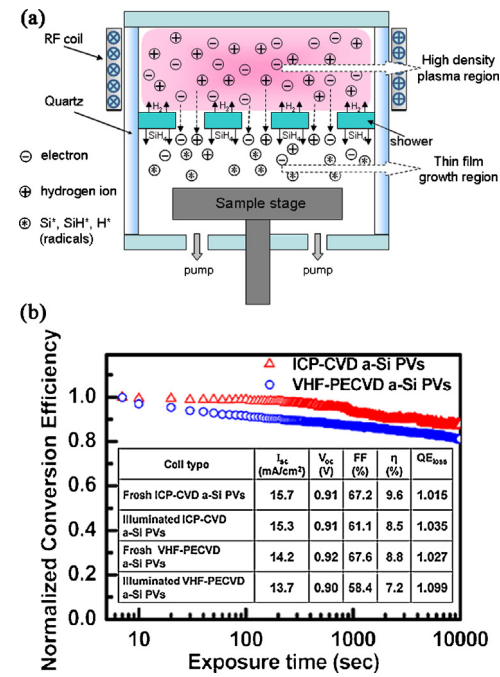


**Fig. 8.** (a) A schematic design of the remote-like ICP system. (b) Conversion efficiency of a-Si:H p-i-n solar cells grown by remote-like ICP-CVD (open triangles) and VHF-PECVD (open circles) as a function of exposure time with a light irradiance of 6 Sun at 60 °C. The insert table shows the key parameters of the above solar cells, including short-circuit current ( $I_{sc}$ ), open-circuit voltage ( $V_{oc}$ ), fill factor (FF), photo-conversion efficiency ( $\eta$ ), and loss in quantum efficiency (QE<sub>loss</sub>). Reproduced from Ref. [145].

prolonged light exposure. The stability of ICP-produced a-Si solar cell is in part due to the mild ion bombardment and relatively high ionization degree of the plasma. However, such remote-ICP configuration usually features a low deposition rate of  $\sim 0.3 \text{ nm/s}$ . Therefore, further investigation is needed to simultaneously achieve high deposition rates and a good photo-conversion performance using the high-density plasmas.

High-density, low-temperature microwave plasmas have also been developed to improve the deposition rates of amorphous and microcrystalline Si [22–25]. The use of microwaves for the plasma generation offers some advantages over the RF or VHF excited plasmas for the deposition of silicon films [22–25]. Microwaves can produce high-density plasmas, which enable high-speed deposition without the associated difficulties in scaling up process chambers such as VHF equipment where standing waves are generated. However, the  $\mu$ c-Si:H films prepared by the microwave plasma technique usually contain a relatively high void fraction which hardly meets the device quality requirements. This possibly originates from the high dissociation rates of  $\text{SiH}_4$  and hydrogen in the plasma, which is mostly determined by the high-energy-part of the electron energy distribution (typically above 10 eV) and the chemical reactivity of  $\text{SiH}_4$  [150–152].

Therefore, to suppress the excess dissociation of the source gas and to improve the rigidity of the produced Si network, a new precursor such as  $\text{SiH}_2\text{Cl}_2$  [22,26] was proposed in place of  $\text{SiH}_4$  for fabricating device-grade  $\mu$ c-Si thin-film solar cells with the smaller volume fraction of voids. Another method to resolve this issue is the use of remote-like plasmas as discussed above [23,70,71]. Due to the high concentration gradient between the upper high density plasma region and the lower thin film growth region, hydrogen ions and electrons diffuse downwards, thus sustaining the plasma diffusion all the way to the substrate. In the thin film growth region, the electron temperature and ion energy become considerably lower, with the typical values of 1.7–3 eV and

5.6–10 eV, respectively [70]. A very high deposition rate of up to 6 nm/s [71] has been reported by using remote ECR microwave plasmas thanks to its high electron density arising due to the effective electron confinement in a magnetic field [153].

From the above consideration, VHF-PECVD is still the most suitable technique for the high-deposition-rate synthesis of efficient Si thin-film solar cells. The remote-ICP is suitable for the synthesis of high-quality a-Si:H films with a lower defect density which results in thin-film solar cells with better light-soaking stability. To end this subsection, we stress that there is certainly a need for further investigations on how to simultaneously achieve high deposition rates and device-quality thin films for both high-density inductively coupled and microwave plasmas.

### 3.5. HIT solar cells

Apart from the synthesis of Si thin film solar cell, the plasma deposited a-Si:H or  $\mu$ c-Si:H films can also be utilized to fabricate HIT solar cells [154–160]. Among high-efficiency PV devices, HIT solar cells stand out for their high performance and strong potential for the low production cost. Passivation of the c-Si wafer surfaces is achieved with very thin intrinsic hydrogenated amorphous silicon layers, deposited by PECVD or similar methods. The emitter and back surface field (BSF) of the cell are formed with doped a-Si:H or  $\mu$ c-Si:H layers. Fig. 9(a) shows a schematic structure of a commercial HIT cell. Conversion efficiencies of 22.8% and open-circuit voltages up to 743 mV (see Fig. 9(b)) on thin wafers have been demonstrated [154]. A record conversion efficiency of 24.7% has recently been achieved at the research level, using HIT solar cells with 98  $\mu$ m thickness [161].

HIT solar cells have attracted an increasing attention because: (1) their structure simultaneously enables an excellent surface passivation and p-n junction, resulting in a high photo-conversion efficiency; (2) low-temperature fabrication processes ( $<200$  °C) can prevent any degradation of bulk quality that happen with high-temperature cycling processes in low-quality silicon materials such as solar-grade Czochralski Si; (3) the same process with a different impurity as the deposition process of emitter can be used to simultaneously obtain the BSF structure and a good surface passivation; and (4) the HIT cell has an improved high-temperature performance compared with conventional c-Si diffused cells, which usually exhibit poor high-temperature performance.

To achieve high open-circuit voltages and, therefore, high efficiency, the passivation of the wafer surface by thin intrinsic

a-Si:H layers has to be as effective as possible. An a-Si:H layer passivates a c-Si surface mainly by hydrogenation of the silicon dangling bonds, leading to a reduction of the interface defect density [162]. Thus, controlling the interface properties during the plasma deposition is of a major importance in achieving high-efficiency HIT solar cells. Even if the same quality a-Si:H layers are used, different cell performances would be obtained due to the plasma damage during the deposition.

Despite the energy conversion efficiencies exceeding 23%, current understanding of the physics behind HIT solar cells remains incomplete. For example, the role of the hydrogen plasma treatment and ion bombardment during the plasma deposition as well as the influence of an epitaxial layer remains a subject of debates. In a recent study [163], Lacoste et al. systematically studied these effects toward a better physical understanding of a-Si:H/c-Si HIT solar cells. The authors have demonstrated that an epitaxial layer is not necessarily detrimental to the performance of HIT solar cells as long as the interface between the materials is abrupt. However, it was also reported [164] that HIT solar cells degrade when the epitaxial Si layers are formed at the interface. The effects of hydrogen plasma strongly depend on the resistivity of the c-Si wafer, suggesting that the plasma conditions must be tuned to optimize the HIT cell efficiency according to the c-Si resistivity. More details of the hydrogen plasma interactions with c-Si surface will be provided in the following sections.

Although the ICP and MP plasma sources can also be used to synthesize device-grade a-Si:H thin films, there are very few reports on high-efficiency HIT solar cells developed by these two methods. The main reason may be attributed to the low hydrogen content in these ICP- and MP-synthesized a-Si:H films [141,165,166]. Indeed, since the key to high cell efficiency is the low carrier recombination at the a-Si:H/c-Si interfaces, the a-Si:H layers not only induce a band bending but also passivate the front surfaces of the c-Si by hydrogenation of dangling bonds [162,167]. For example, a typical low efficiency value of 9.2% was obtained in Si heterojunction solar cells with ZnO:Al/p-a-SiC:H/i-a-Si:H/c-Si/Ag structure using ICPCVD system [168]. Interestingly, the use of remote plasmas significantly increased the hydrogen content in the deposited a-Si:H layers [145,146,169], to approximately 10%, which is close to the level of a-Si:H layers synthesized by PECVD. Applying these remote-ICP a-Si:H layers to Si heterojunction solar cells, an even higher efficiency of 14.1% has recently been achieved [169]. These results suggest the potential of remote ICPs and MPs in the fabrication of high-efficiency HIT solar cells.

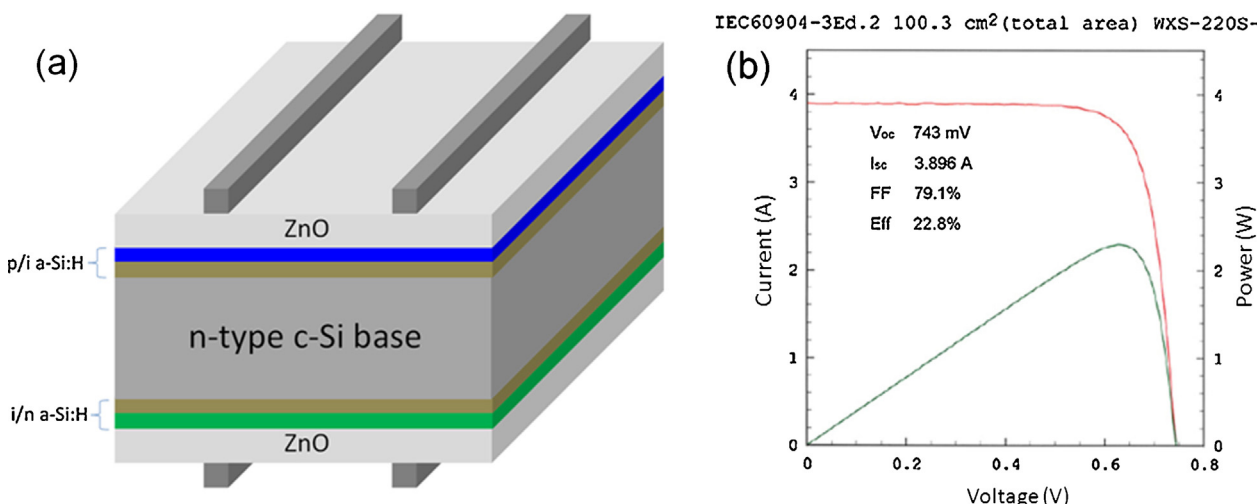


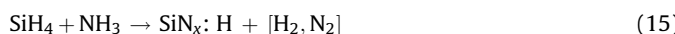
**Fig. 9.** (a) A schematic of the HIT solar cells with a symmetric structure; (b) A typical *I*-*V* characteristic of the HIT solar cells certified by the AIST. Adapted from Ref. [154].

### 3.6. SiN thin films for surface passivation

After having a detailed discussion on the plasma-aided fabrication of Si thin films and Si thin-film solar cells, we now introduce the plasma-assisted growth of thin dielectric or semiconducting layers, e.g., silicon nitride (SiN) for surface passivation and antireflection. The use of PECVD- or MWCDV-SiN deposition is becoming more and more common in the fabrication of bulk silicon solar cells. The rapid expansion of this low-temperature plasma technology is due to a substantial improvement in solar cell efficiency resulting from the deposition of SiN in combination with fire-through techniques for the metallization step.

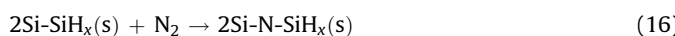
This enhancement is due to the three main reasons. First, a large amount of hydrogen originating from the process gas dissociation and incorporated in the SiN film can be driven into the solar cell during the metallization step, leading to a very effective bulk passivation for c-Si or poly-Si solar cells. An absolute efficiency improvement of 1–1.5% can be ascribed to hydrogenation of defects in the volume of the c-Si or poly-Si wafers [170,171]. The second reason is the surface passivation effect. Silicon nitride coating provides very low surface recombination rates both on phosphorus diffused regions [172] and on p-type and n-type wafers [173–176]. The third advantage is the antireflective (AR) properties of the nitride layer which significantly reduces the light reflection. SiN film deposited by PECVD or MWCDV is therefore a common method to combine bulk and surface passivation with effective anti-reflection in order to improve the solar cell electrical properties. However, the degree of this enhancement strongly depends on the deposition and annealing process parameters.

For the PV applications, SiN is usually made from a gas mixture of SiH<sub>4</sub> and NH<sub>3</sub>. Silane simultaneously acts as a silicon and hydrogen source. The ammonia, in addition to being a source of nitrogen, has a tendency to deposit SiN with a high ratio of incorporated hydrogen [177]. In SiH<sub>4</sub>/NH<sub>3</sub> discharge, electron collisions with NH<sub>3</sub> produce H, NH<sub>2</sub>, NH, and N radicals. The dissociation of NH<sub>3</sub> is quite similar to SiH<sub>4</sub>. The reactions between the nitrogen- and silicon-containing species in the plasma result in an amorphous solid deposit commonly denoted a-SiN<sub>x</sub>:H or simply SiN as shown below:



These films contain a large amount of bonded hydrogen (20–40 at %) in the form of N–H and Si–H bond groups [178,179]. Their optical properties (absorption, reflection and refractive index) depend strongly on the concentration and chemical distribution of hydrogen, silicon and nitrogen in the films, which are determined by the deposition conditions.

Recently, a concept of the plasma-atomized deposition (PAD) was adopted to synthesize SiN<sub>x</sub>:H films with high-performance surface passivation and antireflection. The PAD process is based on low-energy, high-rate production of atomic radicals in high-density inductively coupled plasmas. In this process, solid material (Si target) is first locally sputtered and then fully atomized/ionized by high-density plasmas. Silicon nitride then grows by nitrogen insertion into Si–Si bonds at low temperatures:



Multi-step reaction (16) represents the overall process, which produces Si–Si and Si–N–Si bonds.

Fig. 10(a) shows a typical X-ray photoelectron spectroscopy (XPS) survey scan pattern of the PAD-deposited SiN<sub>x</sub>:H films. The spectrum was corrected to account for any charging effects by fixing the C 1s binding energy at 285 eV. The Si 2p and Si 2s states were observed at around 102 and 152 eV, respectively. The strong

signal at about 398.1 eV stems from the N 1s state. The exact location of Si 2p shifts from the original 99.7 eV to about 102.0 eV due to the incorporation of N. In fact, as nitrogen is introduced into the Si–Si network, the homopolar Si–Si bonds are partially substituted by heteropolar Si–N bonds and the charge transfer from the Si atoms to the more electronegative N atoms leaves a positive charge on the Si atom, resulting in a shift toward higher binding energy [180]. In the present data, the Si 2p peak can be decomposed into two components as shown in the inset: the Si–Si associated peak at about 99.7 eV (green curve), and the Si–N associated peak at about 102.0 eV (red curve). In the former state, Si is in the Si<sup>0</sup> configuration of silicon. The latter state corresponds to the Si<sup>4+</sup> configuration of Si<sub>3</sub>N<sub>4</sub> [181]. The N 1s peak (open circles) located at 398.1 eV is symmetric and is assigned to the N–Si bond configuration. The calculated chemical composition *x* is 1.33 for the PAD-SiN film on the basis of the integration area under the assigned element peak and the sensitivity factor for the element concerned.

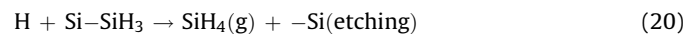
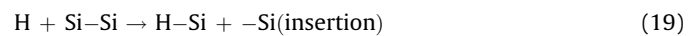
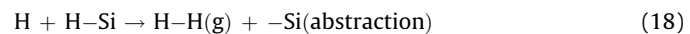
Applying this PAD technology to industrial diffusion solar cells, an energy conversion efficiency of 18.43% (see Fig. 10(b)) has recently been achieved by our group and tested at Solar Energy Research Institute of Singapore for 5 in., p-type, industrial grade silicon wafer-based solar cells. This performance is already comparable/superior to the performance of industrial solar cells passivated by standard PECVD-SiN<sub>x</sub> or microwave plasma CVD-SiN<sub>x</sub>. This process is environment-friendly and less expensive compared to the commonly used PECVD and microwave CVD processes since it only uses Si solid and N<sub>2</sub>/H<sub>2</sub> gaseous precursors. The PAD process also eliminates the use of explosive and flammable gases, such as SiH<sub>4</sub> and NH<sub>3</sub>. This new green plasma technology is promising to replace the existing standard processes and can be introduced into the established production cycles to fabricate solar cells with a higher efficiency.

## 4. Plasma etching in Si-based PV applications

### 4.1. Hydrogen–surface interactions

Hydrogen plasmas (or atoms) are well-known to modify the morphology, structure and properties of silicon materials, including crystalline silicon (c-Si) [182], a-Si:H, and μ-c-Si:H, and to also induce phase transitions [183,184]. The interaction of hydrogen plasmas with Si surfaces gives rise to a large variety of interesting phenomena [185–188], including wafer cleaning (namely native oxide and contaminant removal) [36–39,189], passivation of defects and impurities [190,191], activation of dopants [192], creation of donor-like states (e.g., the p-to-n type conductivity conversion) [193–197], surface texturization [40–42], as well as etching and hydrogen incorporation into the surface layers [37,183,184,198,199], and has thus been the subject of active research for a long time.

These phenomena are caused by the interaction of atomic hydrogen with silicon surfaces, which rearranges and removes Si atoms according to reactions of adsorption (e.g., passivation of dangling bonds, which is beneficial for HIT solar cells), abstraction, insertion of hydrogen and etching of silicon (see Fig. 11) [200]. These reactions can be schematized as follows (where the symbol –Si is for a dangling bond)



During exposure of Si surfaces to hydrogen plasmas, more than one of these reactions can occur simultaneously. Also shown in

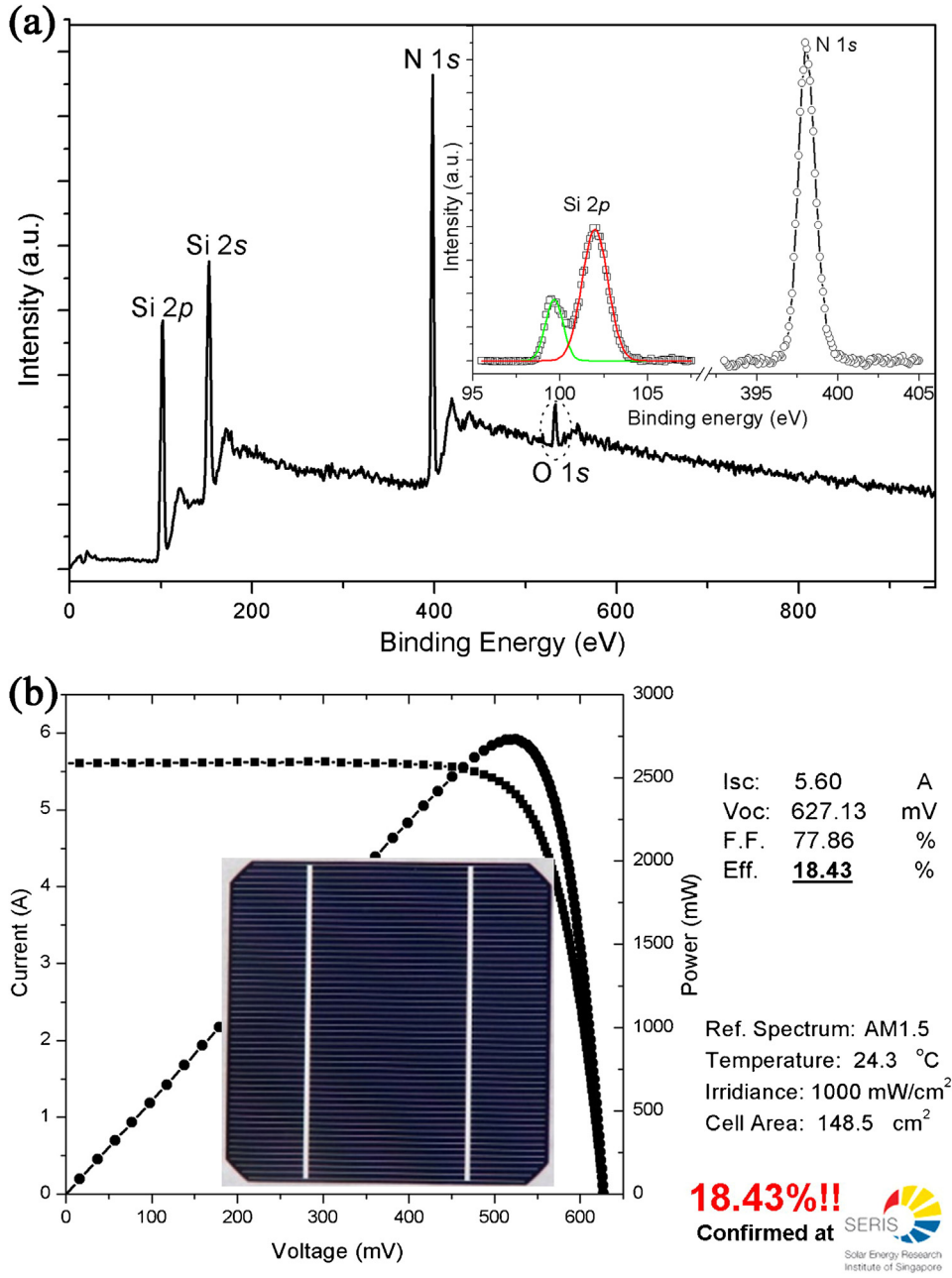


**Fig. 10.** (a) A typical XPS survey scan pattern of the PAD-deposited  $\text{SiN}_x$  film at PSAC. Inset shows the measured core structure of  $\text{Si} 2p$  (open rectangles) and  $\text{N} 1s$  (open circles) as well as the Gaussian curve fitting results for  $\text{Si} 2p$  spectrum. (b) A typical performance of the crystalline Si wafer-based solar cells passivated by PAD- $\text{SiN}$  (original unpublished results by the authors of this review).

**Fig. 11** are the reaction pathways and rate coefficients. Each reaction rate depends on the surface coverage or local concentration of the reacting species which are  $\text{Si}$ ,  $\text{H}$   $\text{Si}$ , and  $\text{SiSi}$  in reactions (17)–(19), respectively. These reactions may have different rates in the “bulk” compared to the surface, due to differences in the rate coefficient or the local concentration (coverage). The rate coefficient of reaction (17) is the “sticking probability”,  $S$ , and is generally assumed to be near unity because of the very high reactivity of hydrogen atoms. Schulze and Henzler measured  $S$  on the  $\text{Si}(1\bar{1}\bar{1}) - (7 \times 7)$  surface and obtained a value close to 1, within the 30% accuracy [201]. The rate of reaction (18) is written in **Fig. 11** assuming a reaction with monohydride species. One can write the rate of reaction (19) as  $k_l F_{\text{H}} [\text{Si}-\text{Si}]$ , where  $[\text{Si}-\text{Si}]$  represents the coverage or bulk density of strained  $\text{Si}-\text{Si}$  bonds, and  $F_{\text{H}}$  is the hydrogen atom flux. The rate coefficients  $k_l$  will be

larger for strained  $\text{Si}-\text{Si}$  bonds compared to unstrained bonds. For simplicity, we write one representative rate expression for reaction (20) as  $k_E F_{\text{H}} [\text{SiH}_3-\text{Si}]$ . If there are other surface precursors like  $\text{Si}-\text{SiH}_2$ ,  $\text{Si}-\text{SiH}$  and  $\text{Si}-\text{Si}$  to etching in addition to  $\text{Si}-\text{SiH}_3$ , a similar rate expression should be written for each of the relevant reactions. In these cases, silicon hydride species ( $\text{SiH}_n$ ,  $n = 1-3$ ) are formed instead of  $\text{SiH}_4$  in reaction (20). It is worth emphasizing that all these reactions including adsorption, abstraction, insertion and etching can take place on c- $\text{Si}$ , poly- $\text{Si}$ , a- $\text{Si:H}$  and  $\mu\text{-c-}\text{Si:H}$  surfaces.

The relative contribution of these processes depends on various factors, such as the crystallographic orientation [185], doping [202,203], and temperature [204,205] of silicon as well as on the hydrogen (plasma) exposure and coverage [203]. The kinetics of the Si surface modification stems from a competition among the

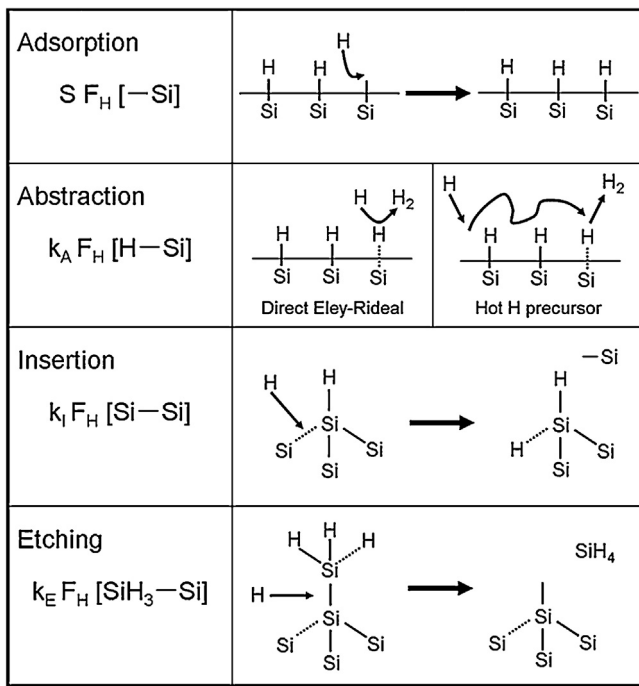


**Fig. 11.** Summary of four principal reaction pathways for the interaction of atomic hydrogen with Si surface: adsorption (sticking), abstraction, insertion, and etching. Also shown are characteristic calculation formulas for the reaction rates of each process.

Adapted from Ref. [200].

above processes and factors. Therefore, there is a strong technological and fundamental interest in the understanding and controlling the Si surface morphology and properties induced by the interaction with hydrogen plasmas. The interaction of atomic hydrogen with Si surfaces has so far been extensively studied using a variety of spectroscopic tools such as multiple internal reflection Fourier transform infrared absorption spectroscopy (MIR-FTIR) [206–208], scanning tunneling microscopy (STM) [185,209], temperature-programmed desorption (TPD) spectrometry [210,211], and mass spectrometry [212]. A comprehensive description of the work until 1995 was provided in the review by

Waltenburg and Yates [213], where the thermal reactions of hydrogen and the main group elements on silicon surfaces have been examined. The dynamics of the interaction of hydrogen with Si surfaces with a strong emphasis on hydrogen adsorption and desorption (abstraction) was reviewed by Kolasinski [214]. A subsequent report dealing with the main aspects of the interaction of hydrogen with the atomically clean crystalline silicon surfaces and submonolayer metal/silicon interfaces was presented by Oura and co-workers [186].

#### 4.1.1. Hydrogen insertion for c-Si passivation

The insertion effect of hydrogen radicals has been quantified in a recent study [157], where a major improvement in passivation was observed when  $H_2$  plasma (CCP) treatments were used during the deposition of thin intrinsic a-Si:H layers for Si heterojunction solar cells. Two deposition sequences were used to investigate the effect of  $H_2$  treatment on the passivating intrinsic layers, as shown in Fig. 12(a). The first process only involved a single step conducted in pure silane plasmas; the second process included three shorter silane plasma steps (same conditions as for the first deposition type) with an additional short  $H_2$  plasma exposure step after each silane plasma step. Infrared spectroscopy of the treated and untreated a-Si:H layers shown in Fig. 12(b) reveals significant differences in silicon–hydrogen bonding. The hydrogen content in the layer clearly increases when  $H_2$  treatment is used, since the total area under the  $SiH$  and  $SiH_2$  peaks is larger [215]. The ratio of the  $SiH_2$  peak area to the  $SiH$  peak area increases after the treatment, indicating that the treated a-Si:H matrix is more disordered and contains more voids than the untreated layer [216].

The presence of more hydrogen and more disorder result from the hydrogen insertion effect, and could be a signature that layers are close to the crystalline transition. It has indeed been shown that the hydrogen content in a-Si:H films reaches its maximum value at the transition [217], and that disorder in a-Si:H also increases close to the transition onset [218]. This increase in disorder might explain the difference in the behaviors of the wafers passivated with treated and untreated a-Si:H layers during the annealing stage (see Fig. 12(c)). We emphasize that hydrogen treatment is clearly beneficial, both before and after the annealing: the lifetimes values are nearly doubled when  $H_2$  treatment is used. This improvement can be attributed to the more effective hydrogenation at the a-Si:H/c-Si interface due to

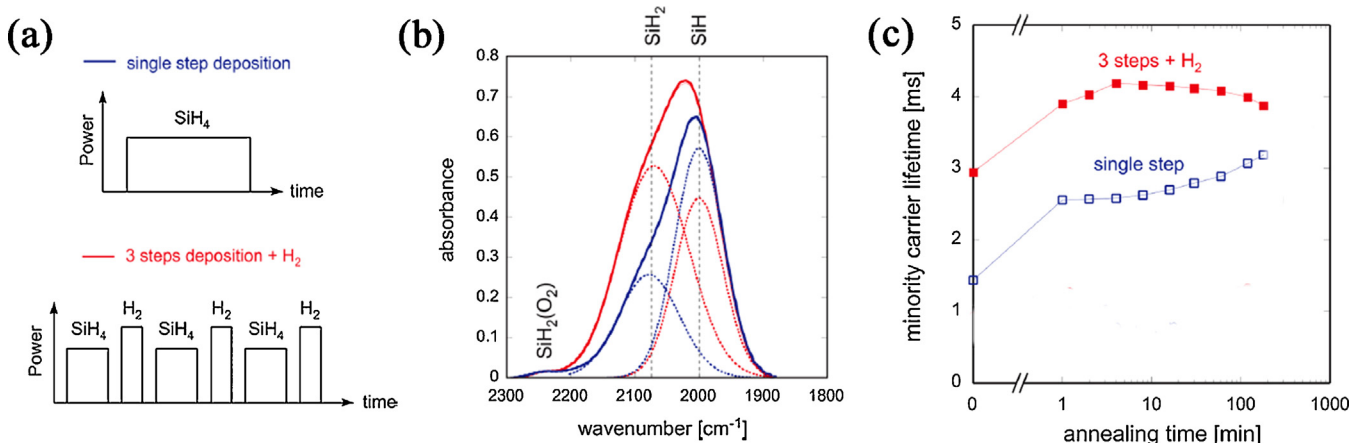


**Fig. 12.** (a) Schematic representation of the deposition sequences: single silane plasma step and deposition split into three shorter silane plasma steps, alternating with  $H_2$  plasma treatments. (b) Absorbance spectra of 15 nm thick treated (red curves) and untreated (blue curves) a-Si:H layers deposited on (1 1 1) c-Si wafers measured by Fourier transform infrared spectroscopy (FTIR). Spectra were deconvoluted with two Gaussian peaks, centered at  $2000\text{ cm}^{-1}$  (monohydride bonds, stretching mode) and at  $2080\text{ cm}^{-1}$  (higher hydrides bonds, stretching mode). The small oxide peak at  $2250\text{ cm}^{-1}$  is due to film oxidation; (c) Evolution of the minority carrier effective lifetime at an excess carrier density of  $10^{15}\text{ cm}^{-3}$  for both-side passivated (1 1 1) c-Si wafers with 15 nm intrinsic a-Si:H layers co-deposited (VHF PECVD) with the process sequences sketched in (a). Lines are guides for the eye. (For interpretation of the references to color in this figure legend, the reader is referred to the web version of the article.) Adapted from Ref. [157].

the presence of more hydrogen content in the treated a-Si:H layers. Upon annealing, both samples show a fast initial improvement in passivation, due to hydrogen reorganization at the a-Si:H/c-Si interface (migration from the bulk a-Si:H layers to the interface) [219,220].

After this large initial improvement, the lifetime obtained with the treated layers shows a rapid saturation followed by a slight decrease after roughly 10 min. In comparison, the sample passivated with untreated layers shows a continuous improvement. Schulze et al. [220] suggested that the as-deposited interface defect density is determined by the local network structure at the a-Si:H/c-Si interface, while the interface defect density after prolonged annealing is mostly determined by the bulk properties of the a-Si:H film. Therefore, this treatment-induced improvement largely dominates the eventual degradation caused by the bulk disorder if reasonable annealing times are used. Employing H<sub>2</sub> treatment, 4 cm<sup>2</sup> heterojunction (HIT) solar cells were produced with industry-compatible processes, yielding competitive open-circuit voltages up to 725 mV and aperture area efficiencies up to 21% [157].

#### 4.1.2. Hydrogen adsorption for c-Si passivation

In a more recent study [221], the authors observed a similar improved passivation effect on c-Si substrates passivated by a-Si:H films with post-deposition hydrogen plasma treatment. Combining low-temperature a-Si:H deposition and successive hydrogen plasma treatment, a high minority carrier lifetime of 11 ms and an open circuit voltage of 737 mV were achieved. The passivation improvement stems from the diffusion of hydrogen atoms to the heterointerface and subsequent dangling bond passivation. In contrast to the above example, the film disorder does not increase, though the hydrogen density of the treated a-Si:H films increases, leading to bandgap widening and void formation. This more likely reflects the hydrogen adsorption effect rather than the hydrogen insertion effect.

Fig. 13 shows data on the H bonding, band gap and mass density of the hydrogen plasma treated a-Si:H layers as functions of the substrate temperature during the hydrogen plasma treatment [221]. It is clearly visible that the overall H content increases along with the substrate temperature during the hydrogen plasma treatment, while at the same time the optical bandgap is widened, and the mass density steeply decreases. Deconvolution of the Si–H stretching mode reveals that the monohydride (SiH) mode is decreased, while the higher hydride mode (SiH<sub>2</sub>) is much increased upon the hydrogen plasma treatment. This implies that upon the hydrogen plasma treatment there is a distinct reorganization of the H bonding configuration in the a-Si:H layer, and not just an increase of total Si–H bonds. The slope of the mass density decay upon H incorporation presented in Fig. 13(d) is compatible with the formation of multi-vacancies like platelets or even (likely to be nanosized) voids in the a-Si:H film [222].

In order to demonstrate that there is no change in the disorder of the a-Si:H layers upon the hydrogen plasma treatment, the strain in the S–Si network was analyzed by deducing the Urbach energy through near-ultraviolet photoelectron spectroscopy measurements [221]. The Urbach energy remains constant upon the hydrogen plasma treatment, meaning that there is no increase in the strain of the silicon network. Therefore, the disorder in the a-Si:H film remains constant since the change of strain in the Si–Si network is related to the disorder, which is an important parameter in the metastable defect creation processes in a-Si:H [223].

In a recent study [224], it has been found that hydrogen plasmas generated in PECVD reactors exert both the adsorption and etching effects on the c-Si substrates. The adsorption of hydrogen atoms can significantly enhance the passivation quality of c-Si surfaces,

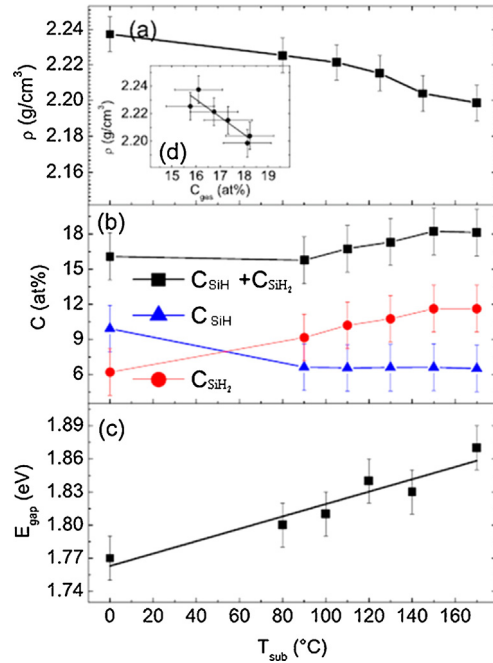


**Fig. 13.** (a) Mass density, (b) hydrogen concentration, and (c) bandgap of a-Si:H layers on c-Si substrates as functions of the substrate temperature during the hydrogen plasma treatment. In (b) black squares stand for the total volume hydrogen content, red circles for the hydrogen concentration calculated from the monohydride mode (SiH) and blue triangles for the hydrogen concentration calculated from the higher hydride mode (SiH<sub>2</sub>). (d) The mass density of the a-Si:H films is plotted versus the total H content. (For interpretation of the references to color in this figure legend, the reader is referred to the web version of the article.) Adapted from Ref. [221].

while the etching effect may degrade the passivation quality. Whether the adsorption or etching effect is dominant is strongly dependent on the processing time. The authors studied the passivation quality by optimizing the H<sub>2</sub> plasma exposure [224]. With increasing the H<sub>2</sub> treatment time, the V<sub>oc</sub> increases until 80 s and then decreases, indicating that the optimum time for hydrogen adsorption is 80 s. The excess treatment generates the defects (dangling bonds) on the Si wafer and increases the surface roughness due to the etching of the Si by H radicals. It is further found that the Si heterojunction cell performance is almost the same with and without a thin a-Si:H layer when the 80 s – long plasma treatment is used on the c-Si before the i-layer deposition.

These studies render the hydrogen plasma treatment particularly interesting for Si solar cell device applications for several reasons. First, the efficient in-diffusion of hydrogen from the plasma into the passivation layer (a-Si:H) or the c-Si wafer allow for a dramatic increase of the passivation potential on c-Si surfaces. Second, the increase of the bandgap as well as the probability of the phase transition of the hydrogen plasma-treated films open a route toward band gap engineering, which is particularly useful for Si heterojunction solar cells with the reduced parasitic absorption and the optimized band bending. Third, the hydrogen plasma-treated films can be made as stable as the untreated ones against the creation of metastable defects by employing appropriate processes.

#### 4.2. Plasma cleaning

Cleaning of Si substrate surfaces is an important step in the fabrication of high-quality Si epitaxial films [225], high-efficiency Si wafer-based solar cells as well as HIT solar cells. To achieve this aim, different wet cleaning methods have been studied. However, most of these methods are difficult to control and produce

hazardous residuals. This is why the attention has recently shifted toward dry cleaning, which is one of the most favorable methods of pre-cleaning of Si surfaces and is easier to transfer into the solar cell mass production. Hydrogen plasma cleaning is considered as an effective way of removing native oxide and hydrocarbon contaminants from the Si surface at low temperatures [226–228].

This is why a number of investigations have been carried out on the structural and chemical properties of Si surfaces treated with hydrogen plasmas. Auger electron spectroscopy (AES) [229] and FTIR studies [230,231] revealed that hydrogen plasma treatment of Si surfaces dramatically reduces the level of contaminant species such as oxygen and hydrocarbons. Reflection high-energy electron diffraction (RHEED) [229] and low-energy electron diffraction (LEED) studies [232] showed that hydrogen plasma cleaning produces Si surfaces with  $(1 \times 1)$ -,  $(2 \times 1)$ -, and  $(3 \times 1)$ -reconstructed structures, depending on the process pressure and the substrate temperature. Furthermore, residual gas analysis (RGA) experiments and atomic force microscope (AFM) studies showed that during the hydrogen plasma treatment at low substrate temperature, desorption of  $\text{SiH}_x$  fragments occurs, leading to a rough surface [232,233].

These studies suggest that hydrogen plasma treatment rearranges and removes the surface Si atoms. Moreover, transmission electron microscopy (TEM) studies revealed that during the etching of Si surfaces, hydrogen atoms diffuse into the bulk Si crystal to produce platelet defects that are predominantly oriented along  $\{1\bar{1}1\}$  crystallographic planes, and that etching of the  $\text{Si}(1\bar{0}0)$  surface preferentially occurs at portions where  $\{1\bar{1}1\}$  platelet defects intersect the surface [227,234].

Shinohara et al. [235] have used infrared absorption spectroscopy (IRAS) in the multiple internal reflection geometry to investigate the interaction of hydrogen-terminated  $\text{Si}(1\bar{0}0)$ ,  $(1\bar{1}0)$ , and  $(1\bar{1}\bar{1})$  surfaces with hydrogen plasmas at room temperature. IRAS data show that at the initial stages of H-plasma treatment, surface hydride species ( $\text{SiH}_n$ ,  $n = 1–3$ ) are removed from the surface. A long-term H-plasma treatment of  $\text{Si}(1\bar{0}0)$  and  $(1\bar{1}0)$  surfaces produces monohydride species and creates hydrogen-terminated Si vacancies in subsurface regions, i.e., near the surface. On  $\text{Si}(1\bar{1}\bar{1})$ , no hydride species are produced even after a long-term H-plasma treatment. It is suggested that monohydride is rather stable against the attack of hydrogen radicals as compared to higher hydride species such as  $\text{SiH}_2$  and  $\text{SiH}_3$ . The formation of Si vacancies depends on the crystallographic orientation of the Si surface: Si vacancies formation is more favored on  $\text{Si}(1\bar{1}0)$  than on  $\text{Si}(1\bar{0}0)$ , while Si vacancy formation on  $\text{Si}(1\bar{1}\bar{1})$  is very unlikely.

Apart from hydrogen plasmas, many other low-temperature plasma techniques such as Ar [236],  $\text{SF}_6$  [237] and  $\text{CF}_4/\text{O}_2$  [36] plasmas have also been used to clean the Si surfaces. However, for Ar plasmas, the substrate is easily damaged by the ion bombardment effect. The substrate damage is believed to be due to the heavy ion ( $\text{Ar}^+$ ) bombardment. These effects can degrade the quality of the grown layers and the interfaces between them. The ion-induced damage should be annealed dynamically at quite high temperatures ( $\sim 800$ ) to ensure defect-free epitaxy.

Hydrogen plasma cleaning, on the other hand, is known as a chemical etching by lighter hydrogen atoms and ions in comparison with heavy argon atoms and ions, and it has been used as an excellent substitute for Ar plasma cleaning. In addition to the reduced substrate damage, the silicon surface can be passivated by hydrogen as a result of the hydrogen plasma cleaning procedure. This passivation suppresses the recontamination of the cleaned surface and simultaneously reduces the recombination rates of the carriers at the interface, which is quite beneficial for the synthesis of high-quality Si epitaxial films as well as high efficiency Si wafer-based solar cells and HIT solar cells.

In comparison with hydrogen plasma,  $\text{SF}_6$  or  $\text{CF}_4/\text{O}_2$  treatment represents a good choice in the cleaning process and passivation of the textured p-type crystalline silicon surface [237,238]. Specifically, the etching of p-type float-zone silicon substrates by microwave  $\text{SF}_6$  plasmas with the subsequent deposition of an a-Si:H passivation layer in the same vacuum cycle has led to an effective surface passivation performance [237]. However, the use of  $\text{SF}_6$  or  $\text{CF}_4$  may produce toxic fluorides and therefore these plasma techniques are not entirely environment-friendly.

In a recent study [239], Moreno et al. studied the etching of the native oxide and the passivation of c-Si surfaces by the plasma in a standard RF PECVD system. They used  $\text{SF}_4$  plasmas to remove the native  $\text{SiO}_2$ . The imaginary part of the pseudo-dielectric function  $\text{Im}[\varepsilon]$  of the c-Si was monitored by in situ ellipsometry in order to optimize the etching process. In particular, the characteristic peak of c-Si located at 4.2 eV ( $E_2$ ), whose amplitude is very sensitive to the presence of native  $\text{SiO}_2$  on the c-Si surface [240,241], was monitored.

When the c-Si surface is clean, the  $E_2$  amplitude has a value close to 42. When a native  $\text{SiO}_2$  layer is present on the c-Si surface, however, the  $E_2$  amplitude decreases to around 35. Fig. 14(a) shows the evolution of the  $E_2$  peak as a function of the  $\text{SiF}_4$  plasma treatment time. As one can see the  $E_2$  amplitude reaches a maximum at around 400 s of the plasma exposure, related to the complete removal of the native  $\text{SiO}_2$  layer. A further plasma exposition leads to a reduction of the  $E_2$  amplitude associated with the roughening of the c-Si surface. The inset in Fig. 14(a) shows the  $\text{Im}[\varepsilon]$  spectra before and after 400 s of the plasma cleaning, where one can see that the  $E_2$  amplitude peaks at 4.2 eV.

In order to characterize the quality of the c-Si surface after the  $\text{SiF}_4$  plasma cleaning, the authors deposited 40 nm of intrinsic a-Si:H to passivate the c-Si surface. Various plasma treatments were performed after the native  $\text{SiO}_2$  etching and before the a-Si:H deposition. Fig. 14(b) [239] shows the effective lifetime ( $\tau_{\text{eff}}$ ) as a function of the carrier density of the samples cleaned by the

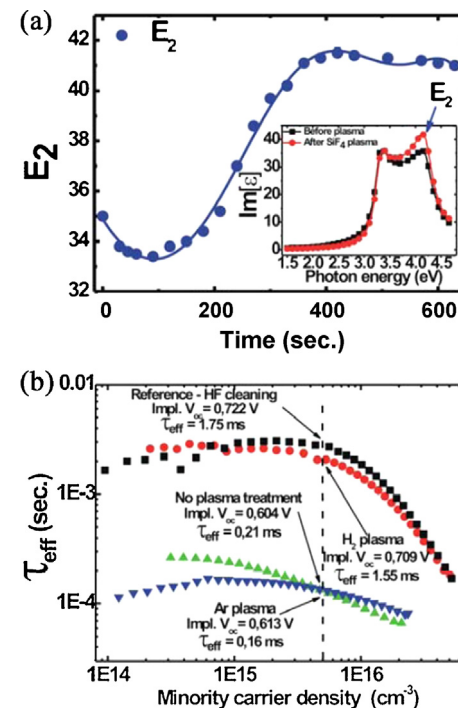


Fig. 14. (a) In situ real-time measurement of the evolution of the intensity of  $E_2$  peak of a c-Si surface exposed to a  $\text{SiF}_4$  plasma. (b) effective lifetime as a function of the carrier density of the samples cleaned by the plasma, compared with the reference sample cleaned by HF acid (after annealing at 200 °C for 30 min). Reproduced from Ref. [239].

plasma, with the different treatment (after annealing them at 200 °C for 30 min). A sample dip-cleaned by a standard HF acid solution and passivated with 40 nm of a-Si:H was used as a reference; this sample showed a high  $\tau_{\text{eff}}$  (around 1.75 ms at 1 Sun of illumination). In comparison, the sample that did not receive any plasma treatment after SiO<sub>2</sub> removal showed a very low  $\tau_{\text{eff}}$  (around 0.21 ms). The Ar plasma treatment did not produce any improvement; in fact the treated sample had a lower  $\tau_{\text{eff}}$  (0.16 ms) compared to the untreated sample. However, the sample treated with H<sub>2</sub> plasmas showed an outstanding improvement in  $\tau_{\text{eff}}$  (around 1.55 ms), which led to the high open-circuit voltage of 716 mV. These results suggest a strong potential of the plasma cleaning and hydrogen plasma treatment for surface passivation, which is applicable even for HIT or high-efficiency Si wafer-based solar cells.

#### 4.3. Plasma texturing

Plasma texturing of Si surfaces is of major interest for Si-based solar cells. Improving the surface texturing is one of the important factors required to increase the solar cell short-circuit current and hence the solar cell photo-conversion efficiency. At present, wet chemical treatments are routinely used by the PV industry for texturing as well as for cleaning the Si surface. Potassium hydroxide (KOH) [238,242], sodium hydroxide (NaOH) [243,244], and tetramethyl ammonium hydroxide ((CH<sub>3</sub>)<sub>4</sub>NOH) [245] are currently used to texture Si surfaces. Hydrofluoric acid (HF) combined with deionized (DI) water is a standard solution used to remove the native SiO<sub>2</sub> which is present on the Si wafers due to ambient oxidation [246].

A major limitation of the currently dominant Si wafer-based solar cells is the high cost per watt power of energy produced. Moreover, many hazardous and corrosive chemicals and gases are involved in the wet etching processes. This leads to adverse environmental impact and enormous cost of waste disposal. The plasma dry etching is promising in reducing the wafer consumption and the use of chemical etching (or cleaning) agents as well as eliminating handling of hazardous acids and solvents. The greatest advantage of dry plasma etching processing is the effective control over the process parameters which may ultimately lead to clean, fully automated, reliable, highly reproducible, in-line integrated, high-throughput processes where wafers are automatically transported through the production line.

In addition to the relative ease of automation, plasma dry etching can selectively enable isotropic or anisotropic etch profiles to perform directional etching without merely relying on the crystal orientation of silicon, which leads to a better process control and cleanliness. Furthermore, it is not merely a matter of industrial and environmental sustainability: thinner wafers (<180 μm) pose serious problems of yield, and require different and independent conditioning of the front (minimum reflectance) and rear (least surface damage) sides. The plasma dry etching offers a series of new avenues to overcome these bottlenecks and increase the flexibility of the process, namely: (i) high-yield processing on ultra-thin wafers; (ii) etching/texturing independent of the initial surface preparation; (iii) controllable degree of roughness; (iv) easily adjustable etching rates, suitable for μm-thick layers (e.g., epitaxial); (v) independent treatment and conditioning of the front and rear surface (single-side emitter removal, different front/rear structures).

##### 4.3.1. One-dimensional nanostructures

One way to achieve effective surface texturing is to produce large arrays of vertically aligned one-dimensional (1D) nanostructures (NSs), such as nanowires, nanorods, nanocones, nanotips (NTs), nanograss (NG) and others [247–256], which can be fabricated by a

maskless plasma etching process [40–42,257–259]. These surface textures can be used to create topographically enhanced light-trapping PV cells, similar to the black silicon solar cells [260–266]. The antireflection properties of these Si NSs result from changes in the refractive index caused by variations in the height of the Si NSs [267].

In a recent study [247], high-density aligned arrays made of silicon NSs, including nanocones, nanorods, and nanowires, are fabricated by the plasma etching in a hot-filament chemical vapor deposition system using the gas mixture of hydrogen, nitrogen and methane. The formation mechanism of aligned silicon NS arrays is likely due to the plasma etching combined with the redeposition of silicon radicals.

In 2004, Hsu et al. [250] proposed and reported a single-step, self-masked dry etching technique for fabricating uniform and high-density NT arrays over a large area in a cost-effective manner, using a high-density electron cyclotron resonance (ECR) plasma reactor. The SiC nanosized clusters formed from the SiH<sub>4</sub> + CH<sub>4</sub> plasmas [268] and the etching effect of Ar+H<sub>2</sub> plasmas are both responsible for the NT formation. On one hand, the SiC nanoclusters uniformly distributed over the substrate surface serve as nanomasks against etching because of their higher hardness and chemical inertness. On the other hand, the interspace between SiC nanoclusters can be etched by Ar + H<sub>2</sub> plasmas to form high-density and high-aspect-ratio NT arrays.

In the contribution by Yang et al. [251], the authors reported a well-aligned silicon NG fabricated on a silicon wafer through hydrogen plasma etching alone, i.e., without the use of a mask or a catalyst. A selective etching mechanism in which hydrogen ion flux was accelerated toward the substrate by the low-frequency bias and the partial native oxide was sputtered off, has been proposed.

In a recent work [257], pillar-shaped NSs were formed on the c-Si surface through a dry and lithography-free texturing process based on SF<sub>6</sub>/O<sub>2</sub> plasmas generated in an ICP source. The high-aspect-ratio vertically aligned Si NSs with a low reflectance have been obtained.

Likewise, Moreno et al. [258] have systematically investigated a dry and mask-free texturing process of crystalline silicon wafers using SF<sub>6</sub>/O<sub>2</sub> plasmas in a reactive ion etching (RIE) system. An average reflectance value as low as 6% was achieved by optimizing the process parameters. It is understood that two counteracting effects take place in the SF<sub>6</sub>/O<sub>2</sub> plasmas: an etching process due to reactive fluorine radicals that enable silicon etching, and a redeposition process because of residual SiO<sub>x</sub>F<sub>y</sub> radicals, which induce a masking effect [269]. These micro-masks enhance the texturing of the c-Si surface and thus reduce the light reflectance, as well as improve the light trapping.

**Fig. 15(a)** and (b) shows a typical comparison of the SEM images of poly-Si surfaces before and after the inductively coupled SF<sub>6</sub>/O<sub>2</sub> plasma etching. For the sample with no plasma treatment, no evident textured structures can be observed and thus the average surface reflectance in the wavelength region from 400 to 900 nm is still at a high value of ~34% (see **Fig. 15(c)**). The reflectance of acid-textured poly-Si surface is also presented as a reference with a moderate average value of ~15%. For the plasma-treated sample, however, pyramid NSs with features less than 200 nm width are formed in dense and regular patterns on a silicon surface.

Consequently, the average surface reflectance can reach a low value of 5%, as can be seen in **Fig. 15(c)**. The reflectivity can be further reduced by introducing Cl<sub>2</sub> to the SF<sub>6</sub>/O<sub>2</sub> plasma [270]. A representative example of large-area completely-black (with a reflectance as low as 2%) poly-Si substrates with a size of 15 cm × 15 cm fabricated by a reactive self-masking ion etching SF<sub>6</sub>/Cl<sub>2</sub>/O<sub>2</sub> plasma is shown in **Fig. 15(d)** [270]. **Fig. 15(e)** and (f) shows the external quantum efficiency (EQE) and the electrical characteristics, respectively, for the selective emitter poly-Si solar

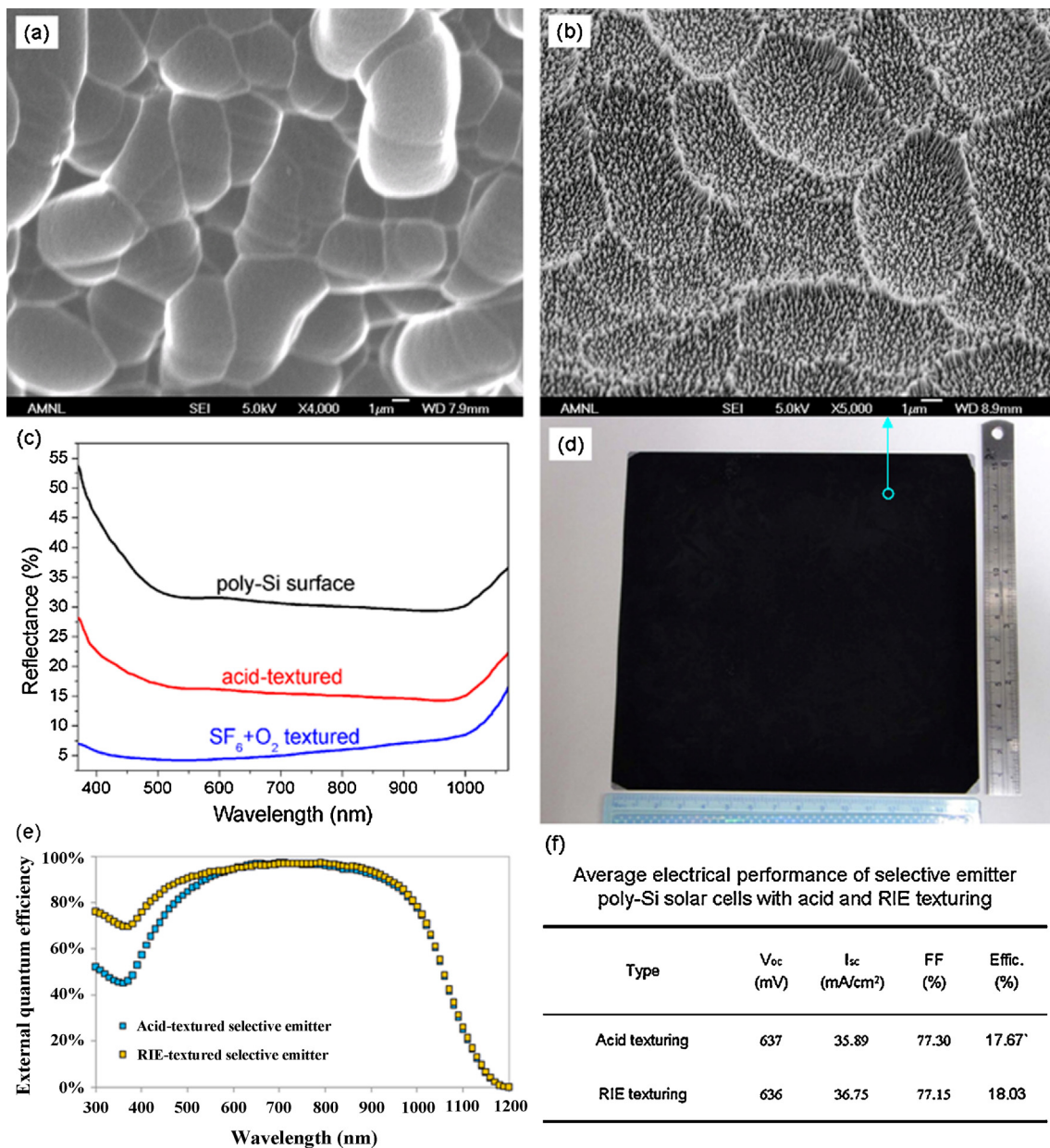


**Fig. 15.** The SEM images of poly-Si surfaces textured at PSAC before (a) and after (b) inductively coupled  $\text{SF}_6/\text{O}_2$  plasma etching; (c) typical reflectances of the original poly-Si surface, and the samples after acid texturing and inductively coupled  $\text{SF}_6/\text{O}_2$  plasma etching (original unpublished results by the authors of this review); (d) the large-area completely black poly-Si substrate with pyramid NSs (adapted from Ref. [270]); external quantum efficiency (EQE) (e) and average electrical performance (f) of selective emitter poly-Si solar cells with acid and RIE texturing.  
Adapted from Ref. [271].

cells fabricated using the acid and RIE texturing [271]. An absolute  $I_{sc}$  gain of above 200 mA and the corresponding efficiency gain of 0.4% were obtained for the poly-Si solar cells with RIE texturing. This improvement is due to the enhanced quantum efficiency for wavelengths below 600 nm compared with that of the acid-textured surface, as clearly shown in Fig. 15(e).

In another example, Yoo et al. [272] have fabricated a large-area (156 mm × 156 mm) polycrystalline silicon solar cell by maskless surface texturing using a  $\text{SF}_6/\text{O}_2$  reactive ion etching. They accomplished texturing by reducing silicon loss to approximately a half of the Si material loss in wet texturing process as well as achieved the photoconversion efficiency, open circuit voltage, short circuit current density, and fill factor as high as 16.1%, 619 mV, 33.5 mA/cm<sup>2</sup>, and 77.7%, respectively.

Almost at the same time, Lee et al. [273] have developed a damage-free RIE texturing for polycrystalline Si solar cells by using

$\text{SF}_6/\text{Cl}_2/\text{O}_2$  gas mixtures. This improved texturing process can produce a better surface with less surface recombination rates due to the removal of RIE-induced damage and effective control of nanocone shape. Applying this damage-free etching technique to polycrystalline Si solar cells, an increase in short-circuit current gain of ~1.3 mA/cm<sup>2</sup>, and a resultant increase in cell efficiency gain of 0.7% were achieved. Importantly, the feed gas ratio and the plasma power density were the key parameters to mitigate the plasma-induced-damage during the RIE processing while maintaining the reasonable values of the surface reflectance. This shows that the surface damage induced during the RIE processing can be removed by in situ processing, which means that there is no need for any additional wet chemistry based processing.

Many dry plasma etching techniques mentioned above commonly use quite toxic and corrosive gases such as  $\text{CF}_4$ ,  $\text{C}_2\text{F}_6$ ,  $\text{NF}_3$ , and  $\text{SF}_6$ . These gases are not environmentally friendly, and

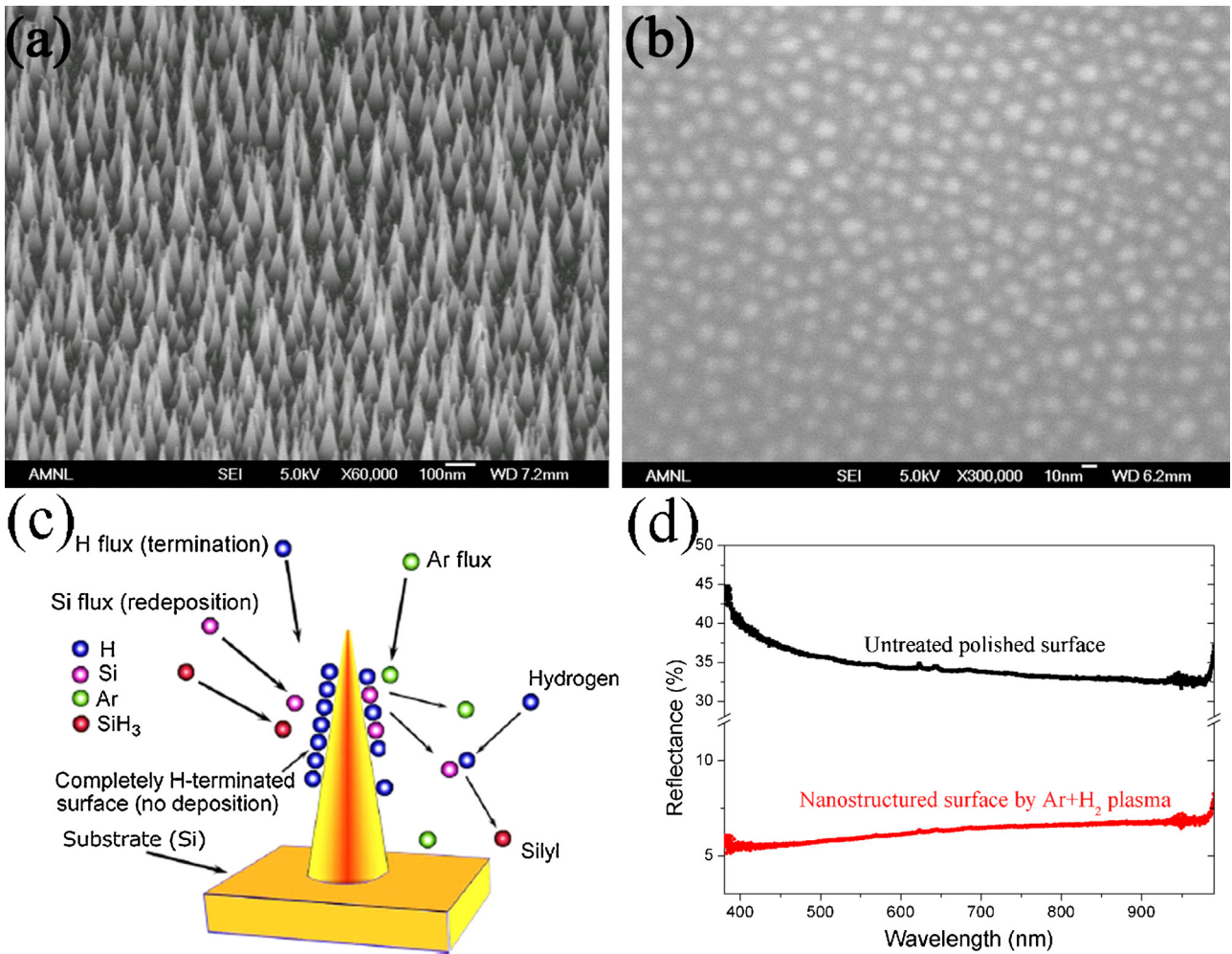


**Fig. 16.** (a) A typical image of large arrays of vertically aligned Si NSs (nanocones) fabricated at PSAC. (b) A typical photo of roundish nanodots (no NSs can be observed). (c) Schematic of the main elementary processes on a Si surface exposed to low-temperature Ar + H<sub>2</sub> plasma. H-termination impedes silicon material redeposition; concurrent Ar<sup>+</sup> ion bombardment improves conditions for Si attachment. Silyl radicals contribute to the growth through redeposition mediated by their interaction with the H-terminated surfaces (reproduced from Ref. [274]). (d) A typical comparison of the reflectance for the sample before and after the Ar + H<sub>2</sub> plasma etching (original unpublished results by the authors of this review).

cause a significant green house effect and also large amounts of chemical waste. In addition, these processes use relatively high temperature which influences the optical properties of the wafer surface. Several studies [274,275] reported on an effective and green technique for fabricating large arrays of vertically aligned Si NSs via 'self-organized' maskless etching in low-temperature Ar+H<sub>2</sub> plasmas. Two sharply contrasting typical images prepared at different experimental conditions are shown in Fig. 16(a) and (b), respectively. Vertical nanocones can be seen in Fig. 16(a), while roundish nanodots were only obtained in Fig. 16(b). The effect of a broad range of experimental parameters, such as the gas composition (the H<sub>2</sub>:Ar ratio), substrate temperature, etching time and discharge power on the formation of vertically aligned single-crystalline silicon NSs has been systematically investigated [275].

The H<sub>2</sub>:Ar ratio, substrate temperature and discharge power significantly influence the surface morphology [275]. When the H<sub>2</sub> content is either too low or too high, only semispherical nanodots can be produced on the surface. When the substrate temperature is too low (200 °C), the NT array is very non-uniform, with a large number of short NSs present on the surface. At the optimum temperature of 300 °C, the NT array of the highest mean aspect ratio (up to 4.0) can be formed, though with a high degree of non-uniformity. A further increase in the substrate temperature results in the formation of highly uniform arrays with lower mean aspect

ratios. The power below 1.0 kW is insufficient to produce the nanocones; on the contrary, a high-density nanodot array can be formed.

Based on these experimental results, a NS growth scenario that is consistent with the main observations was proposed [275]. In the case of Ar + H<sub>2</sub> as schematically shown in Fig. 16(c), argon serves as the sputtering agent. The intense flux of the energetic Ar<sup>+</sup> ions removes the hydrogen atoms from the surface and therefore helps maintaining the surface unterminated, while hydrogen terminates the surface (and hence reduces the surface energy) and acts as a reactant. The nanocone formation is driven by at least two competing physico-chemical processes, namely the etching of the surface with the reactive plasma accompanied by the simultaneous redeposition of Si radicals etched away from the surface. A combination of these processes with thermokinetically driven dynamic surface reconstruction eventually leads to the NS size, shape, as well as adjusting the array macro-characteristics such as NS density and size (aspect ratio). The detailed NS growth scenario and interpretation of these results can be found elsewhere [275].

Similar large arrays of quasi one-dimensional vertically aligned Si NSs significantly enhance the light absorption, which is often called the black silicon effect. As shown in Fig. 16(d), low reflectance can be achieved after hydrogen and argon plasma etching in the wavelength region from 400 to 1000 nm demonstrating the good

anti-reflection surface properties. Importantly, this technique is environment-friendly and only relies on environmentally clean gases.

The introduced fine surface texturing on the silicon substrate provides a better surface light trapping responsible for the short-circuit current improvement in the bulk silicon solar cell technology. Similarly, Dhamrin et al. [276] have also developed a new etching technique for crystalline silicon wafers based on remote hydrogen plasmas. A low surface reflectance below 2% is realized over the broad wavelength range of 500–900 nm. In addition, the technique is applied to chemically textured crystalline silicon wafers demonstrating the potential to further improve the already textured surfaces.

Besides the mask-free processes described above it is also possible to apply a plasma etching process to a Si surface which is locally masked. The masking can be implemented by using photolithography. After applying the mask, a plasma etching was performed in a single-wafer reactor applying a RIE process in the mixture of SF<sub>6</sub> and O<sub>2</sub> gases. After removing the mask, honeycomb-like structures were created [277]. Using such a front surface texturization process it was possible to manufacture the efficient solar cell on a poly-Si substrate [277].

#### 4.3.2. Hybrid nanostructures

Different from the nanostructures of Section 4.3.1, the hybrid NSs of this section consist of different structures and also feature graded refractive indexes. Recently, hybrid NSs including dual-diameter nanopillar structures [278] and nanoisland patterns on nanofrustum arrays [279], have demonstrated their superior performance in terms of the minimum reflectance and maximum absorption compared to the NSs involved taken separately. These hybrid nanopillar structures were fabricated based on vapor-liquid-solid growth utilizing lithography. As to the latter, the hybrid nanoisland-on-nanofrustum arrays were formed by using colloidal nanosphere lithography and RIE etching process. The RIE etching process based on inductively coupled SF<sub>6</sub> + C<sub>4</sub>F<sub>8</sub> + O<sub>2</sub> discharges can etch the substrates covered with a self-assembled monolayer of nanospheres as an etching mask to produce regular NS patterns. The antireflection property of such hybrid nanoisland-on-nanofrustum arrays was significantly enhanced compared to that of sharp-tipped nanocone structures, so that the average reflectance in the near-ultraviolet spectral range (300–400 nm) was as low as 3.8% [279].

A closer example related to hybrid NSs fabricated in the entirely plasma-based process can be found in the recent article [280]. It was demonstrated that unique hybrid two-layer NSs comprising amorphous silicon nanograss (a-Si NG) on top of monocrystalline silicon nanofrustums (c-Si NFs) behave as almost perfect optical absorbers. To form a-Si/c-Si hybrid NSs, an intrinsic a-Si thin film with a thickness of approximately 1 μm was first deposited on a p-type c-Si wafer (675 μm) using low-pressure PECVD. Then, a 13.56 MHz high-density inductively coupled hydrogen plasma with a high density of hydrogen radicals was used to etch the as-deposited substrate to form the two-layer NSs.

Tilt-view SEM images of such a-Si/c-Si two-layer hybrid NSs are presented in Fig. 17(a)–(e), showing that the average heights of the NSs increased upon increasing the etching time. The top-view SEM images of the sample etched for 90 min in Fig. 17(g) reveal that the density of the NSs was greater than ~10<sup>10</sup> cm<sup>-2</sup>. Vertically aligned a-Si NG/c-Si NF structures were clearly observed in the typical cross-sectional bright-field TEM image of the sample etched for 90 min [Fig. 17(f)]. A corresponding enlarged cross-sectional bright-field TEM image of the a-Si thin film sample etched for 90 min is shown in Fig. 17(g). The columnar NSs indicate that the etching proceeded through the a-Si thin film, reaching the a-Si/c-Si substrate interface, and continued to etch into the underlying c-Si

substrate to form the Si NFs. The presence of the a-Si structure on top of the NG layer was demonstrated from the diffuse ring of the selected area electron diffraction (SAED) pattern [inset of Fig. 17(h)].

Fig. 17(i) shows the measured specular and total reflectances as a function of the wavelength for a-Si NG/c-Si NF hybrid NSs at varied etching times (30–120 min) as well as for the a-Si thin film. The average specular and total reflectances of the a-Si thin film were 44.9 and 48.3%, respectively, over the wavelengths from 300 to 800 nm. In contrast, all of the hybrid nanostructured samples exhibited both specular and total reflectances that were much lower compared to the a-Si thin films over the entire spectral range, demonstrating their broadband antireflection characteristics. In particular, for the sample of a-Si NG/c-Si NF hybrid structures etched for 120 min, the average specular and total reflectances had the lowest values of 0.10 and 0.34%, respectively, over the spectral range from 300 to 800 nm.

The ultralow reflectance of these two-layer nanostructured samples was presumably related to the smooth transition of the effective refractive index throughout the NS [281,282]. The calculated refractive index profile of the 90 min-etched a-Si NG/c-Si NF hybrid NSs is shown in Fig. 17(j). The smooth transition of the refractive index, not only in the NG layer but also in the bottom NF layer, was the key to the ultralow reflectance, which was difficult to achieve for super-dark materials [283–285] or Si NSs as discussed above.

Such all-Si hybrid nanostructures with the further advantage of the ease of fabrication through simple and effective hydrogen plasma etching appear to be very efficient absorbers for the use in thin-film solar cells, which might lead to the development of low-cost, more flexible devices as the c-Si substrate may be replaced by other materials (e.g., poly-Si or glass). However, the design of the p-n junction utilizing such hybrid NSs as the absorbers requires further research.

#### 4.4. Plasma-induced p–n junction formation

The plasma etching can not only clean Si substrate surfaces and produce large arrays of vertically aligned Si NSs used for light trapping in solar cells but also lead to the creation of donor-like states, which implies the p-to-n type conductivity conversion (PNTCC), and simultaneously the formation of p–n junction. In practice, it is well known that the formation of a p–n junction is usually realized in solar cell industry through the high-temperature phosphorous diffusion process in c-Si or poly-Si materials. However, this technique usually involves energy-consuming thermal diffusion-based processes as well as toxic chemicals/gases. In recent years, various methods other than traditional diffusion have been utilized to realize PNTCC on p-type Si substrates. One technique is the use of high-energy (>100 eV) ion (Ar<sup>+</sup>, H<sup>+</sup>) bombardment and implantation [286–290]. Another one is the radio frequency [193–196] and direct current [197] hydrogen plasma treatment, followed by long time annealing at the temperature below 550 °C.

##### 4.4.1. Origin of plasma-induced p–n junction

The origin of PNTCC is still a matter of debates and the key to understand this phenomenon is in the origin of excess donors. There have so far been several accepted points of view on this issue. First, substitutional boron atoms (acceptors) can be transferred into the electrically inactive interstitial positions by the generated interstitial silicon atoms; this is known as the kick-out mechanism [291]. However, this can only account for the loss of an acceptor but cannot demonstrate the occurrence of a donor. Second, the weakly bonded interstitial hydrogen which reacts with the impurities, as described by Wolkenstein's theory, can also serve as

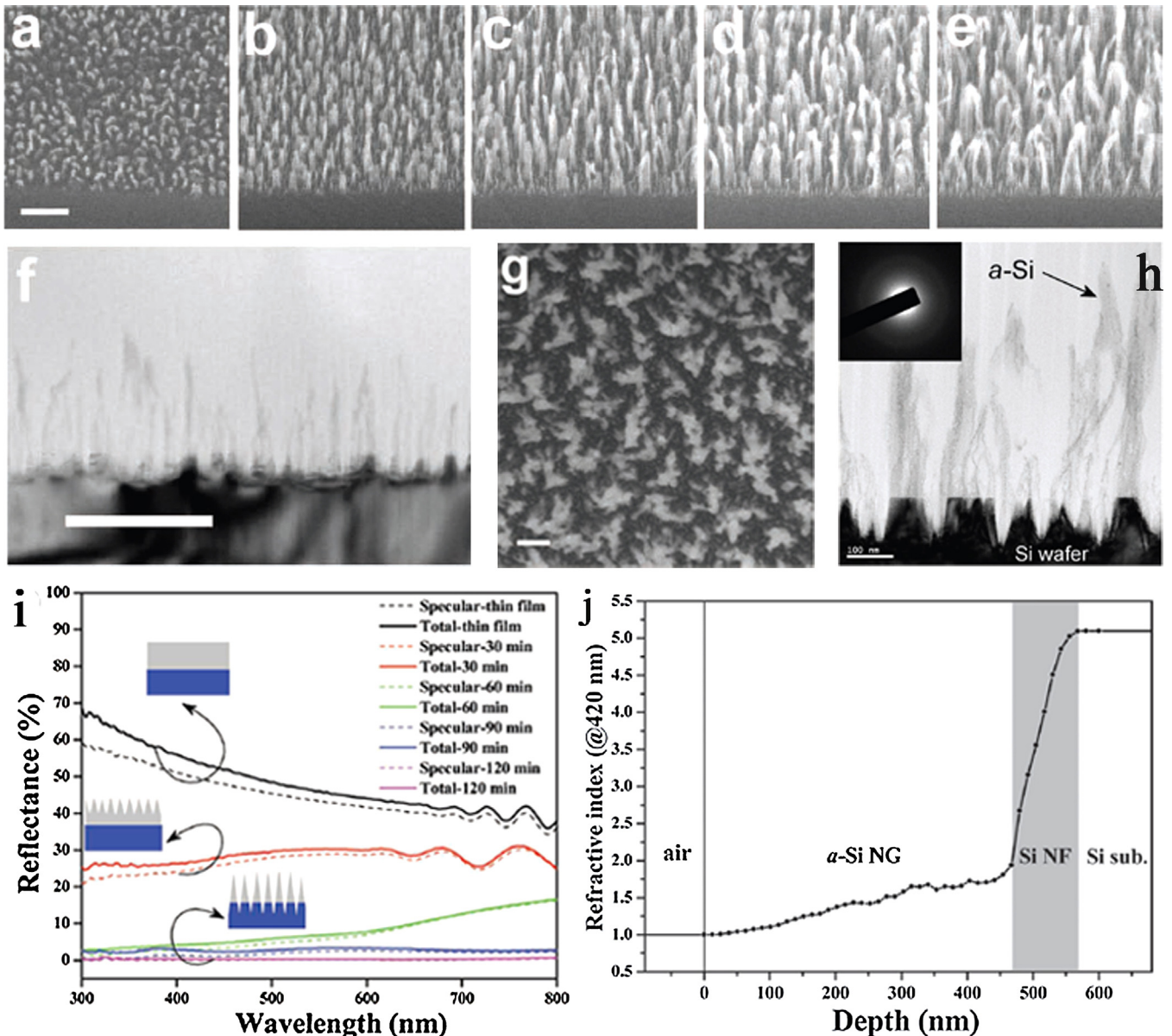


**Fig. 17.** (a)–(e) Tilt-view SEM images of a-Si/c-Si NSs etched for 10, 20, 30, 40, and 50 min, respectively (scale bar: 200 nm). (f) Cross-sectional TEM images of the nanostructured sample etched for 90 min (scale bar: 200 nm). (g) Top-view SEM image of the 90 min-etched sample. (h) Enlarged cross-sectional TEM images of the nanostructured sample etched for 90 min; inset is the selected area electron diffraction (SAED) pattern of the a-Si NG. (i) Measured specular (dashed lines) and total (thick lines) reflectances of a-Si/c-Si NSs; those of bare a-Si thin film (black curve) are also provided for comparison. (j) The calculated refractive index profile of the 90 min-etched a-Si NG/c-Si NF hybrid structure.

Adapted from Ref. [280].

a donor [292]. Third, helium-like double oxygen-related thermal donors (OTDs) in interstitial oxygen-rich ( $[O_i]$  density  $\sim 10^{18} \text{ cm}^{-3}$ ) silicon are attributed to the presence of larger oxygen clusters ( $O_2$ ,  $O_3$ , and  $O_4$ ) [293]. Fourth, the single shallow thermal donor (STD) [294] incorporates a hydrogen atom to form hydrogen related STD, i.e., STDH. In the case of OTD and STDH, hydrogen atoms are believed to play a crucial role.

At low temperatures, theoretical investigation [295] has revealed that an activation energy of 0.84 eV is required for hydrogen to diffuse into silicon, when all hydrogen atoms occupy the BC site (i.e., the bond-centered site between two adjacent silicon atoms) and nearly all hydrogen atoms are trapped. At high temperatures, however, some hydrogen atoms may occupy the AB site (antibonding site on the axis of two adjacent silicon atoms), and hydrogen diffusion occurs with a much lower activation energy of about 0.4 eV [295]. When hydrogen diffuses deeply into

the silicon wafer it reduces the potential barrier for the  $O_i$  migration, and then several  $O_i$  atoms migrate through the wafer until they reach an appropriate local site in the Si lattice where an OTD is produced. Therefore, hydrogen plays a catalytic role that promotes the formation of OTD. Indeed, it was found that at 450 °C the formation of OTD can be enhanced by a possible factor of 5–10 in the presence of hydrogen [296].

#### 4.4.2. Plasma-induced p–n junction solar cells

An example of one-step formation of a p–n junction by means of PNTCC on a p-type substrate exposed to Ar + H<sub>2</sub> plasmas in the low-frequency (460 kHz) ICP system has been demonstrated [193,297,298]. The heating and the plasma treatment are simultaneous without any additional annealing process. Interestingly, as the p-type surface is converted into the n-type, large arrays of vertically aligned Si NSs can also be formed on the surface

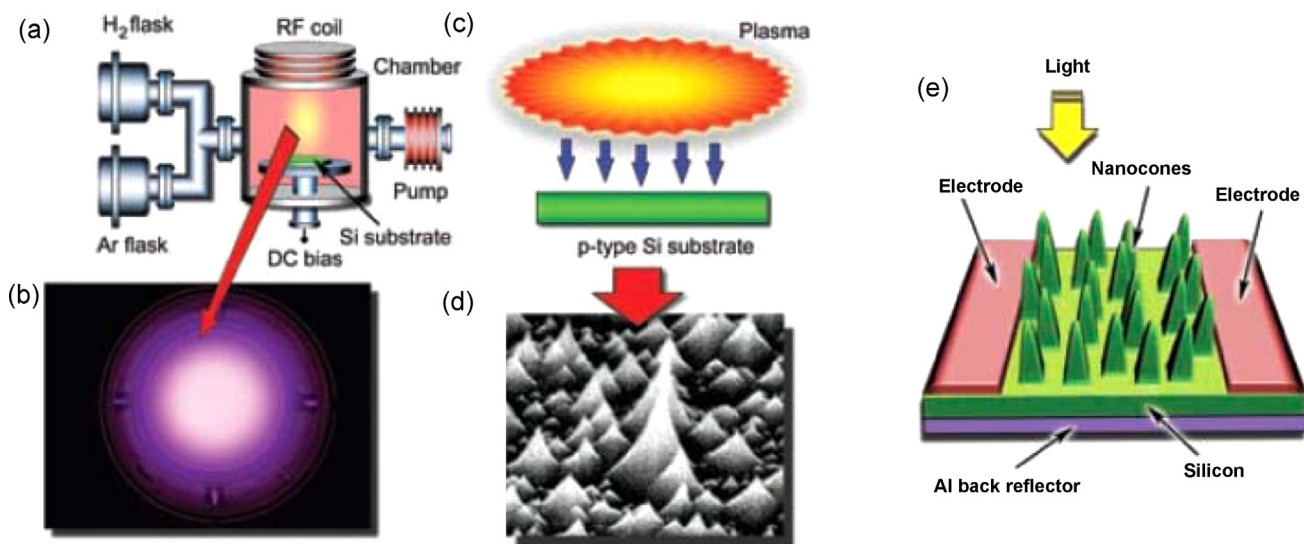


**Fig. 18.** (a) Schematic of the experimental setup at PSAC for one-step formation of a p-n junction by means of PNTCC; (b) photograph of the Ar + H<sub>2</sub> plasma discharge; (c) scheme of the PNTCC process; (d) representative SEM image of a Si NS array; and (e) schematic of the nanoarray-based solar cell. Reproduced from Ref. [297].

in the appropriate range of experimental conditions as discussed above.

A schematic of the experimental setup is shown in Fig. 18(a), and a representative photo of the discharge can be seen in Fig. 18(b). A scheme of the process and a representative SEM image of the Si NS arrays created on the surface of a boron-doped p-type Si wafer are shown in Fig. 18(c) and (d), respectively. A schematic of the nanoarray-based solar cell is shown in Fig. 18(e). This cell (typical size 2 cm × 2 cm, with an Al finger grid as a front electrode and Al metal pad as a back electrode) only required as-processed Si wafers with a nanostructured top surface, an Al back reflector and metal grid electrodes.

Let us discuss the details of the p-n junction formation during the direct plasma exposure. In this process, both hydrogen and argon play important yet different roles. During the plasma treatment, the flat wafer surface is intensively heated through electron, ion, and radical-related heating, and also sputtered by heavy argon ions impinging on the Si surface. Reactive hydrogen ions and radicals also roughen the Si surface by hydrogen-assisted etching through the formation of volatile Si-containing molecules (SiH<sub>n</sub>, n = 1, 2, 3) of various complexity. The process consists of two stages. At the stage of the NS formation, the hydrogen/argon ratio determines the resulting microscopic morphology of the surface. Hydrogen radicals provide very strong heating of the silicon surface due to the exothermic recombination [299,300]. Eventually, the hierarchical two-level array of NS is formed, and the surface is covered with very small and dense nanocones [274,275].

During the next stage, the p-n junction is formed under the nano-structured surface. The first process is the diffusion of boron atoms from the bulk silicon to the surface (heated up by the plasma-surface interactions), extraction of boron atoms from Si by atomic hydrogen, and their removal from the surface in the form of volatile boron-hydrides B<sub>x</sub>H<sub>y</sub>. The presence of B<sub>x</sub>H<sub>y</sub> was detected by quadrupole mass spectroscopy in the plasma diagnostic experiments [297]. As a result, a boron-depleted sub-surface layer is formed. Second, after partial removal of boron-related acceptor sites, an n-type layer is formed due to the hydrogen-assisted formation of oxygen-related thermal donors and shallow thermal donors (note that thermal donors are able to compensate the boron doping in Si [301]). Besides, Si-H-Si centers which act as donors can be formed in Si [302]. Moreover, reactive H radicals from the plasma can form positively charged bond-center sites; this in turn

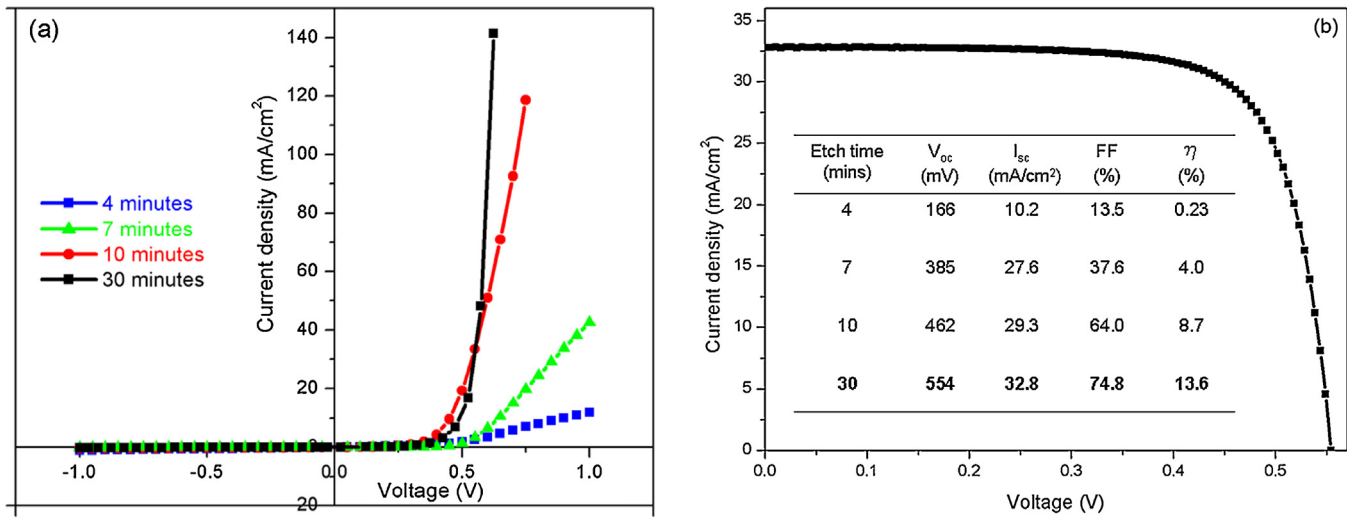
provides passivation of the shallow acceptors by annihilating the free holes by electrons from hydrogen atoms [303]. This eventually leads to the PNTCC, and an effective gradient p-n junction is formed.

Fig. 19(a) displays the dark I-V curves of the hydrogen plasma generated p-n junctions as a function of processing time. For the sample treated for 4 min, the generated OTDs are not enough to compensate for the original boron doping and thus lead to quite a weak response and a poor rectifying performance. As the treatment time increases, a clear trend to stronger rectifying diode action is seen. For the optimum treatment of 30 min, the dark I-V curve exhibits an excellent rectifying characteristic (rectifying ratio up to ~10<sup>3</sup>) comparable to the common p-n junction formed by thermal diffusion. It is worth noting that the optimum p-n junction passivated by silicon nitride features an open-circuit voltage ( $V_{oc}$ ) of 554 mV, a short-circuit current ( $I_{sc}$ ) of 32.8 mA/cm<sup>2</sup> and a photoconversion efficiency ( $\eta$ ) of 13.6% measured under one sun illumination, as shown in Fig. 19(b). Such a clear PV signal indicates that the resultant junction is of real potential to convert solar radiation into electrical energy for practical use.

Therefore, a simple and environment-friendly plasma treatment may indeed result in a simultaneous formation of the two essential features that enable the effective operation of the solar cell prototype. First, an effective p-n junction can be formed in the sub-surface region. Second, an effective light-trapping two-level hierarchical array of vertically aligned Si nanocones capable to effectively increase the light absorption of the wafer surface can also be produced in the same process. Such a fabrication technique would be a powerful candidate for low-cost PV applications due to low energy consumption, dry etching instead of wet chemical etching, and no usage of toxic gases such as phosphorus or boron as compared to the industrial energy-demanding diffusion-based manufacturing of bulk-silicon solar cells.

#### 4.5. PSG removal

In the standard industrial c-Si solar cell fabrication process, the phosphorus silicate glass (PSG) which is formed during the phosphorus diffusion at the Si surface is commonly removed by diluted hydrofluoric acid (HF). This process can also be replaced by a dry plasma etching process. Rentsch et al. [304] showed that the application of a low-frequency plasma source built into an



**Fig. 19.** (a) Four representative dark  $I$ - $V$  curves and (b) photo  $I$ - $V$  curve under the simulated AM 1.5 spectrum with the best cell performance of Si homojunction solar cells passivated by silicon nitride with a structure of Al/p-c-Si/n-c-Si/SiN/Al etched by hydrogen plasma for different times developed at PSAC. The inset table shows the key parameters of the above solar cells, including  $V_{oc}$ ,  $I_{sc}$ , FF and  $\eta$ .

Reproduced from Ref. [298].

inline industrial-type plasma tool is an effective means to selectively etch PSG. A selectivity of  $>10$  (etch rate of PSG/etch rate of Si) was achieved by a process gas mixture of  $CF_4$  and  $H_2$ , as shown in Fig. 20 [27].

Here we note that the PSG layer is a doped  $SiO_2$  layer. For the fast plasma etching of  $SiO_2$  typically high ion energies are required due to its relatively high chemical stability. To enable a selective process, a selective polymeric protection layer is required. This polymer layer ( $CH_x$ ) builds up mainly on top of the Si surface. The oxygen out of the PSG layer reacts with the  $CH_x$  to form  $CO_x$  and hydride species and hence prevents the formation of the polymer layer on the surface. The etching of the Si surface is thus mainly limited by the diffusion of etching species through the polymer layer. Highly energetic ions physically sputter the PSG layer at the same time [305–307].

## 5. Future prospects

One of the advantages of low-temperature plasmas in PV processing, especially in the field of Si-based solar cells is the reasonable degree of control of the plasma species generated by time-variable (e.g., RF and MW) electromagnetic fields and other

process parameters. This gives the possibility of isotropic or anisotropic etching of Si substrates, as well as precise and effective control of photonic and electronic properties of the materials by careful engineering of the thin-film composition and microstructure, which in turn can be achieved by the appropriate, in situ control of the plasma process parameters. One can evaluate the effects of the process variables on the performance and eventually optimize the growth process to meet the device requirements by combining the plasma diagnostics with the process and reactor modeling. This high degree of control is particularly desirable for the fabrication of large-area thin-film Si solar cells, and is also promising for applications in heterojunction structures and light emitting diodes.

The plasma-based synthesis of microcrystalline/amorphous silicon and related materials and their integration in solar cell prototypes has produced a strong impact on the development of the second-generation thin-film solar cells and has been widely adopted internationally. These low-temperature plasma processes have also attracted a significant interest from the established and emerging industries. Among the plasma-synthesized Si thin-film solar cells, the stacking solar cells including the ‘micromorph’ tandem and triple-junction solar cells will be the platform for novel PV devices which are low-cost substitutes of bulk crystalline silicon solar cells and thus will open new horizons for highly-efficient green power generation.

In addition, low-temperature plasmas offer many advantages in dry plasma processing, including the removal of PSG or parasitic emitters, wafer cleaning, masked or mask-free surface texturization, as well as the direct formation of p-n junction through PNTCC. With the sustainable development becoming a global trend, increasing chemical waste disposal costs, and environmental and water [308] concerns are presently given the key priority. Furthermore, the PV industry has been showing an increasing interest in dry etching processes as well because of the demand for integrated solutions in the process equipment.

One salient feature of dry plasma processing is the control over the process parameters which allows for good reliability and reproducibility, especially in industrial production [41,309]. For heterostructure devices such as HIT solar cells, one of the most important steps is the wafer cleaning before the deposition of amorphous Si layer in order to avoid the introduction of defects. To achieve this aim, different wet etching methods have been

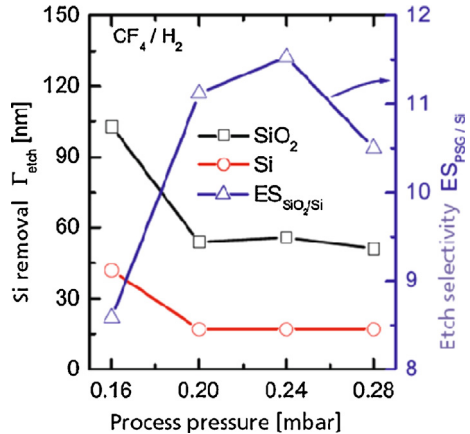


**Fig. 20.** Si removal and etch selectivity (PSG/Si) for the selective low-frequency plasma etching process.

Reproduced from Ref. [27].

proposed, but they are difficult to control and often produce hazardous and toxic residuals. In comparison, the plasma dry cleaning procedures may solve this problem and thus be more viable for the transfer to mass production.

For Si wafer based solar cells, the first commonly used step is wafer cleaning by using hazardous acids and solvents such as HF and HNO<sub>3</sub> followed by wet etching by using alkaline solutions with isopropyl alcohol (IPA) addition to achieve surface texturing. In contrast, the plasma dry etching processes can realize both wafer cleaning and surface texturization in one single step. As a result, the wet chemistry can be replaced by a dry etching process, where expensive chemical etching agents and chemical waste disposal become redundant. Also, the PSG which is formed during the phosphorus diffusion at the Si surface can be removed by the plasma dry etching.

Considering the plasma deposition process of silicon nitride films, a combination of the sequence of the plasma processes including surface cleaning and texturing, PSG removal as well as deposition of SiN can be combined in a plasma cluster tool. Furthermore, plasma processing allows for the processing of only the top surface of the substrate so that there is no more processing limitations for very thin wafers (<100 μm). Thus, low-temperature plasma processing becomes increasingly attractive for new highly efficient low-cost Si solar cells on thin substrates. For the synthesis of high-quality SiN films, the plasma atomized deposition technology is promising as a viable alternative to the existing standard processes and can be incorporated into the established production cycles.

Solar cell structures that allow for higher energy conversion efficiencies than the industrial standard can benefit from the plasma processes. A solar cell structure which is presently being commercialized is based on the “passivated emitter and rear cell” (PERC) concept [310,311]. The cell structure is sketched in Fig. 21 and shows a similar front design as required by the industrial standards of Si wafer-based solar cells with a few distinguishing features at the rear. Here, a passivation layer or a stack which covers more than 90% of the rear surface is applied. Periodic local rear contacts are formed for current transport. The preparation of a PERC-type structure involves several plasma processes, such as the rear emitter removal, the removal of the PSG on the front, surface cleaning on the front and rear sides as well as the deposition of a front ARC and a rear passivation stack of a-SiO<sub>x</sub>:H and a-SiN<sub>x</sub>:H [312]. If more than one plasma process is present within a solar cell manufacturing process line, it makes sense from a cost and energy-consumption point of view to cluster the plasma processes. This leads to a large plasma tool with one entering and one exiting load lock and vacuum processes in between. It was calculated that the manufacturing cost of a crystalline silicon solar cell would be slightly lower than the current industrial standard [312]. Aiming at

more advanced solar cell structures, more efficient process sequences, for example involving plasmas can be incorporated into the production workflow.

Silicon thin-film modules based on the plasma-synthesized a-Si:H and μc-Si:H tandem cells are among the promising future technologies for providing efficient and cost-effective PV electricity. The necessary prerequisites for a cost-effective mass production of these thin-film solar cells incorporating μc-Si films are the demonstration of high deposition rates and scalability to large areas. As discussed in Section 3.4, low-pressure, thermally non-equilibrium, high-density ICPs and MPs are effective and versatile process environments to resolve the presently persistent deposition rate issue. Nevertheless, how to simultaneously achieve high deposition rates and device-quality Si thin films still remains a significant challenge for both ICPs and MPs. Remote plasma configurations may provide solutions to some of the issues yet still require further improvement.

Another promising route to obtain high deposition rates for μc-Si:H is the use of VHF (>40 MHz) in combination with relatively high deposition pressures in PECVD reactors. However, problems concerning the process scaling up toward square meter size like standing waves, skin effect or voltage uniformity may impede homogeneous film growth in the VHF-regime [17,313]. Moreover, significant powder formation occurs and dust is often visible in the deposition chamber already after only a few runs under the high pressure and high power conditions applied for high-rate μc-Si:H deposition. An important and related solution is the development of plasma-etching-based cleaning processes that address this issue and shorten the maintenance cycle and thus increase the effective operation time of the plasma sources.

Large arrays of vertically aligned Si NSs in combination with PNTCC simultaneously produced by the plasma dry etching processes are of a major potential in PV applications. The principle of operation of solar cell with such NSs is quite similar to the third-generation photovoltaics. Semiconductor NSs exhibit quantization effects when the charge carriers (negative electrons and positive holes) are confined by potential barriers to the very small volumes. Quantum confinement of charge carriers in NSs gives rise to unique optical and electronic properties that have the potential to enhance the power conversion efficiency of solar cells for PV production at lower cost. These approaches and applications may help advancing the third-generation photovoltaic device development. A prominent opportunity is to enable generation of more than one electron-hole pair (called excitons in nanocrystals) by a single absorbed photon. This exciting yet challenging phenomenon is known as multiple exciton generation [314].

For silicon wafer-based solar cells, one of the primary cost factors is the starting silicon wafer, which requires extensive purification to maintain a reasonable performance [315–317]. Therefore, reducing the required silicon's quality and quantity will help drive large-scale and cost-effective implementation of Si PV electricity. Using solar cells with nanostructured p-n junctions (third-generation solar cells) may solve both of these problems simultaneously by orthogonalizing the direction of light absorption and charge separation while allowing for the improved light scattering and trapping [318]. Therefore, the plasma dry etching processes are expected to play an important role in the third-generation solar cells in the near future. Accordingly, the detailed understanding and control of the plasma-synthesized NSs as well as the technological applications of NSs for the third-generation PV cells need to be further advanced.

## 6. Conclusion

The interest in low-temperature plasmas for PV applications has gained much attention in the last decade. This review article

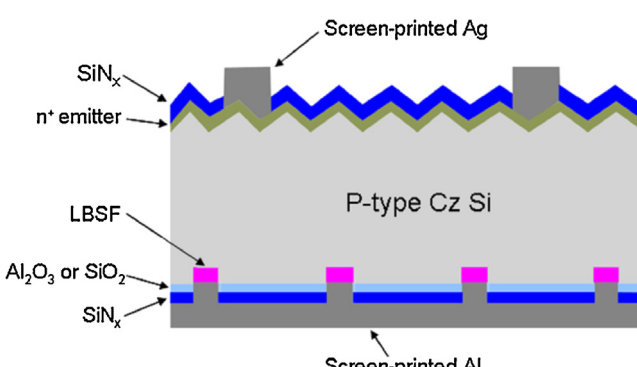


**Fig. 21.** A scheme of the PERC solar cells with screen-printed front and rear contacts with Al<sub>2</sub>O<sub>3</sub>/SiN<sub>x</sub> or SiO<sub>2</sub>/SiN<sub>x</sub> rear passivation stacks. LBSF denotes the local back surface field.

presented some typical examples of the rapid progress in the field. We emphasize that the low-temperature plasmas have been widely applied in Si-based solar cell manufacturing and this field is rapidly expanding. The applications of low-temperature plasmas are not limited to the most traditional synthesis of Si-based (including SiN) thin-films, Si-based thin-film solar cells and HIT solar cells, but also cover the plasma etching techniques such as the removal of phosphorus silicate glass or parasitic emitters, wafer cleaning, masked or mask-free surface texturization, as well as the direct formation of p-n junctions by means of PNTCC. The chemical and physical interactions in such plasmas of electrons, ions, radicals and neutral species as well as hydrogen plasma interactions with c-Si surface have been discussed systematically.

The quest for low-cost and high-efficiency solar cells is gaining momentum. Many high-quality researchers and engineers in academia, R&D, and industry sectors seek solutions to improve the cell efficiency and reduce the cost as well as the environmental impact of the fabrication processes. Finally, photovoltaic renewable energy technologies are expected to grow even more rapidly in the next decades, thus giving more and more opportunities for the integrated, versatile, low-cost, and environmentally friendly plasma-based technologies to contribute to the solution of the ever escalating global energy issues.

## Acknowledgements

The authors thank R. Steeman, Y. Xu, D. Y. Wei, H. P. Zhou, S. Y. Huang, L. X. Xu, Y. N. Guo, C. C. Sern, Y. Xu, J. D. Long, and M. Y. Yu for fruitful collaborations, discussions, and critical comments. All authors of original figures are greatly appreciated for their kind permission to reproduce them. This work was partially supported by the National Research Foundation (Singapore), the Agency for Science, Technology and Research (A\*STAR) of Singapore, CSIRO's OCE Science Leadership Program, the Australian Research Council, the Natural Science Foundation of Jiangsu Province, China under Grant BK2012110, and the Fundamental Research Funds for the Central Universities of China under Grant No. JUSR51323B.

## References

- [1] <http://www.worldenergyoutlook.org/media/weowebsite/2012/factsheets.pdf>.
- [2] F. Granek, Fraunhofer Institute for Solar Energy Systems (ISE), (Ph.D.Thesis), 2009.
- [3] D.M. Chapin, C.S. Fuller, G.L. Pearson, *Journal of Applied Physics* 25 (1954) 676.
- [4] M.A. Green, K. Emery, Y. Hishikawa, W. Warta, E.D. Dunlop, *Progress in Photovoltaics: Research and Applications* 21 (2013) 1.
- [5] J. Ma, J. Ni, J.J. Zhang, Z.H. Huang, G.F. Hou, X.L. Chen, X.D. Zhang, X.H. Geng, Y. Zhao, *Solar Energy Materials and Solar Cells* 114 (2013) 9.
- [6] D.E. Carlson, C.R. Wronski, *Applied Physics Letters* 28 (1976) 671.
- [7] M. Matsumoto, Y. Aya, A. Kuroda, H. Katayama, T. Kunii, K. Murata, M. Hishida, W. Shinohara, I. Yoshida, A. Kitahara, H. Yoneda, A. Terakawa, M. Iseki, M. Tanka, *IEEE Journal of Photovoltaics* 3 (2013) 35.
- [8] Y. Mai, S. Klein, R. Carius, H. Stiebig, X. Geng, F. Finger, *Applied Physics Letters* 87 (2005) 073503.
- [9] S.Q. Xiao, S. Xu, Critical reviews in solid state and materials sciences (2014) (in press).
- [10] J. Meier, E. Vallat-Sauvain, S. Dubail, U. Kroll, J. Dubail, S. Golay, L. Feitknecht, P. Torres, S. Fay, D. Fischer, A. Shah, *Solar Energy Materials and Solar Cells* 66 (2001) 73.
- [11] F.A. Shirland, P. Rai-Choudhury, *Reports on Progress in Physics* 41 (1978) 1839.
- [12] M. Taguchi, Y. Tsunomura, H. Inoue, S. Taira, T. Nakashima, T. Baba, H. Sakata, E. Maruyama, in: *Proceedings of the 24th European Photovoltaic Solar Energy Conference (Hamburg)*, WIP-Renewable Energies, 21–25 September, (2009), pp. 1690–1693.
- [13] <http://www.ise.fraunhofer.de/en/downloads-englisch/pdf-files-englisch/photovoltaics-report.pdf>.
- [14] K. Yamamoto, A. Nakajima, M. Yoshimi, T. Sawada, S. Fukuda, T. Suezaki, M. Ichikawa, Y. Koi, M. Goto, T. Meguro, T. Matsuda, M. Kondo, T. Sasaki, Y. Tawada, *Solar Energy* 77 (2004) 939.
- [15] K. Yamamoto, A. Nakajima, M. Yoshimi, T. Sawada, S. Fukuda, T. Suezaki, M. Ichikawa, Y. Koi, M. Goto, T. Meguro, T. Matsuda, M. Kondo, T. Sasaki, Y. Tawada, *Progress in Photovoltaics: Research and Applications* 13 (2005) 489.
- [16] J. Muller, O. Kluth, S. Wieder, H. Siekmann, G. Schope, W. Reetz, O. Vetterl, D. Lundszen, A. Lambertz, F. Finger, B. Rech, H. Wagner, *Solar Energy Materials and Solar Cells* 66 (2001) 275.
- [17] T. Roschek, T. Repmann, J. Muller, B. Rech, H. Wagner, *Journal of Vacuum Sciences and Technology A* 20 (2002) 492.
- [18] E.V. Johnson, P.A. Delattre, J.P. Booth, *Applied Physics Letters* 100 (2012) 133504.
- [19] O. Vetterl, F. Finger, R. Carius, P. Hapke, L. Houben, O. Kluth, A. Lambertz, A. Muck, B. Rech, H. Wagner, *Solar Energy Materials and Solar Cells* 62 (2000) 97.
- [20] J. Meier, H. Keppner, S. Dubail, U. Kroll, P. Torres, P. Pernet, Y. Ziegler, J.A.A. Selvan, J. Cuperus, D. Fischer, A. Shah, *Materials Research Society Symposium Proceedings* 507 (1998) 139.
- [21] S.Y. Myong, K. Sriprapha, Y. Yashiki, S. Miyajima, A. Yamada, M. Konagai, *Solar Energy Materials and Solar Cells* 92 (2008) 639.
- [22] H. Shirai, T. Arai, H. Ueyama, *Japanese Journal of Applied Physics* 37 (1998) L1078.
- [23] H. Inoue, K. Tanaka, Y. Sano, T. Nishimura, A. Teramoto, M. Hirayama, T. Ohmi, *Japanese Journal of Applied Physics* 50 (2011) 036502.
- [24] W.J. Soppe, C. Devilee, M. Geusebroek, J. Loffler, H.J. Muffler, *Thin Solid Films* 515 (2007) 7490.
- [25] H.J. Jia, J.K. Saha, N. Ohse, H. Shirai, *Journal of Physics D – Applied Physics* 39 (2006) 3844.
- [26] J.K. Saha, N. Ohse, K. Hamada, H. Matsui, T. Kobayashi, H.J. Jia, H. Shirai, *Solar Energy Materials and Solar Cells* 94 (2010) 524.
- [27] M. Höfmann, J. Rentsch, R. Preu, *European Physical Journal Applied Physics* 52 (2010) 11101.
- [28] J.W. Leem, Y.M. Song, Y.T. Lee, J.S. Yu, *Applied Physics B – Lasers and Optics* 100 (2010) 891.
- [29] I.O. Parm, K. Kim, D.G. Lim, J.H. Lee, J.H. Heo, J. Kim, D.S. Kim, S.H. Lee, J. Yi, *Solar Energy Materials and Solar Cells* 74 (2002) 97.
- [30] G. Federici, P. Andrew, P. Barabaschi, J. Brooks, R. Doerner, A. Geier, A. Herrmann, G. Janeschitz, K. Krieger, A. Kukushkin, A. Loarte, R. Neu, G. Saibene, M. Shimada, G. Strohmayer, M. Sugihara, *Journal of Nuclear Materials* 313 (2003) 11.
- [31] C. Leguijt, P. Lolgen, J.A. Eikelboom, A.W. Weeber, F.M. Schuurmans, W.C. Sinke, P.F.A. Alkemade, P.M. Sarro, C.H.M. Maree, L.A. Verhoef, *Solar Energy Materials and Solar Cells* 40 (1996) 297.
- [32] S. Duttagupta, F. Lin, K.D. Shetty, A.G. Aberle, B. Hoex, *Progress in Photovoltaics: Research and Applications* 21 (2013) 760–764.
- [33] M. Xu, S. Xu, J.W. Chai, J.D. Long, Y.C. Ee, *Applied Physics Letters* 89 (2006) 251904.
- [34] Z.R. Chowdhury, K. Cho, N.P. Kherani, *Applied Physics Letters* 101 (2012) 021601.
- [35] W.A. Nositschka, O. Voigt, A. Kenanoglu, D. Borchert, H. Kurz, *Progress in Photovoltaics: Research and Applications* 11 (2003) 445.
- [36] M. Tucci, E. Salurso, F. Roca, F. Palma, *Thin Solid Films* 403 (2002) 307.
- [37] C. Forster, P. Schnabel, P. Weih, T. Stauden, O. Ambacher, J. Pezoldt, *Thin Solid Films* 455 (2004) 695.
- [38] Y. Momono, K. Yokogawa, M. Izawa, *Journal of Vacuum Science and Technology B* 22 (2004) 268.
- [39] A. Strass, W. Hansch, P. Bieringer, A. Neubecker, F. Kaesen, A. Fischer, I. Eisele, *Surface and Coating Technology* 97 (1997) 158.
- [40] S.H. Zaidi, D.S. Ruby, J.M. Gee, *IEEE Transactions on Electron Devices* 48 (2001) 1200.
- [41] J. Yoo, K. Kim, M. Thamilselvan, N. Lakshminarayn, Y.K. Kim, J. Lee, K.J. Yoo, J. Yi, *Journal of Physics D – Applied Physics* 41 (2008) 125205.
- [42] H. Nagayoshi, K. Konno, S. Nishimura, K. Terashima, *Japanese Journal of Applied Physics* 44 (2005) 7839.
- [43] S.Q. Xiao, S. Xu, *Journal of Physics D – Applied Physics* 44 (2011) 174033.
- [44] A. Friedman, *Plasma Chemistry*, Cambridge University Press, Cambridge, 2009p. 224.
- [45] S. Xu, K.N. Ostrikov, Y. Li, E.L. Tsakadze, I.R. Jones, *Physics of Plasmas* 8 (2001) 2549.
- [46] K.N. Ostrikov, S. Xu, M.Y. Yu, *Journal of Applied Physics* 88 (2000) 2268.
- [47] Z.L. Tsakadze, L. Levchenko, K. Ostrikov, S. Xu, *Carbon* 45 (2007) 2022.
- [48] I.B. Denysenko, S. Xu, J.D. Long, P.P. Rutkevych, N.A. Azarenkov, K. Ostrikov, *Journal of Applied Physics* 95 (2004) 2713.
- [49] M.A. Lieberman, A.J. Lichtenberg, *Principles of Plasma Discharges and Materials Processing*, 2nd ed., Wiley, New York, 1994, 2005.
- [50] K. Ostrikov, *Reviews of Modern Physics* 77 (2005) 489.
- [51] E. Amanatides, D. Mataras, *Journal of Applied Physics* 89 (2001) 1556.
- [52] E. Abdel-Fattah, H. Sugai, *Japanese Journal of Applied Physics* 42 (2003) 6569.
- [53] A. Perret, P. Chabert, J. Jolly, J.-P. Booth, *Applied Physics Letters* 86 (2005) 021501.
- [54] T.V. Rakhimova, O.V. Braginsky, V.V. Ivanov, T.K. Kim, J.T. Kong, A.S. Kovalev, D.V. Lopaev, Yu.A. Manklevich, O.V. Proshina, A.N. Vasilieva, *IEEE Transactions on Plasma Science* 34 (2006) 867.
- [55] Z. Bi, Y. Liu, W. Jiang, X. Xu, Y. Wang, *Current Applied Physics* 11 (2011) S2.
- [56] M.A. Lieberman, J.P. Booth, P. Chabert, J.M. Rax, M.M. Turner, *Plasma Sources Science and Technology* 11 (2002) 283.
- [57] J. Asmussen, T.A. Grotjohn, P. Mak, M.A. Perrin, *IEEE Transactions on Plasma Science* 25 (1997) 1196.
- [58] T. Ohmi, M. Hirayama, A. Teramoto, *Journal of Physics D – Applied Physics* 39 (2006) R1.
- [59] A.E. Rider, K. Ostrikov, S.A. Furman, *European Physical Journal D* 66 (2012) 226.
- [60] T. Arai, H. Shirai, *Journal of Applied Physics* 80 (1996) 4976.
- [61] Y. Fukuda, Y. Sakuma, C. Fukai, Y. Fujimura, K. Azuma, H. Shirai, *Thin Solid Films* 386 (2001) 256.
- [62] C. Das, A. Dasgupta, S.C. Saha, S. Ray, *Journal of Applied Physics* 91 (2002) 9401.
- [63] C. Droz, E.V. Sauvain, J. Bailat, L. Feitknecht, J. Meier, A. Shah, *Solar Energy Materials and Solar Cells* 81 (2004) 61.
- [64] C. Niikura, M. Kondo, A. Matsuda, *Journal of Non-Crystalline Solids* 338 (2004) 42.

- [65] A.H.M. Smets, T. Matsui, M. Kondo, *Journal of Applied Physics* 104 (2008) 034508.
- [66] N. Kosku, S. Miyazaki, *Journal of Non-Crystalline Solids* 352 (2006) 911.
- [67] J. Li, J. Wang, M. Yin, P.Q. Gao, D.Y. He, Q. Chen, Y.L. Li, H. Shirai, *Journal of Applied Physics* 103 (2008) 043505.
- [68] Q.J. Cheng, S. Xu, S.Y. Huang, K. Ostrikov, *Crystal Growth and Design* 9 (2009) 2863.
- [69] S.Q. Xiao, S. Xu, D.Y. Wei, S.Y. Huang, H.P. Zhou, Y. Xu, *Journal of Applied Physics* 108 (2010) 113520.
- [70] T. Takeda, K. Tanaka, H. Inoue, M. Hirayama, T. Tsumori, H. Aharoni, T. Ohmi, *Japanese Journal of Applied Physics* 46 (2007) 2542.
- [71] P. Leempoel, P. Descamps, T. Kervyn de Meerendré, J. Charliac, P. Roca i Cabarrocas, P. Bulkin, D. Daineka, T.H. Dao, J.P. Kleider, M.E. Gueunier-Farret, C. Longeaud, *Thin Solid Films* 516 (2008) 6853.
- [72] A. Bogaerts, M. Eckert, M. Mao, E. Neyts, *Journal of Physics D – Applied Physics* 44 (2011) 174030.
- [73] T.J.M. Boyd, J.J. Sanderson, *The Physics of Plasmas*, Cambridge University Press, Cambridge, 2008.
- [74] P. Horvath, A. Gallagher, *Journal of Applied Physics* 105 (2009) 013304.
- [75] E. Amanatides, A. Hammad, E. Katsia, D. Mataras, *Journal of Applied Physics* 97 (2005) 073303.
- [76] S. Klein, F. Finger, R. Carius, M. Stutzmann, *Journal of Applied Physics* 98 (2005) 024905.
- [77] I.B. Denysenko, K. Ostrikov, S. Xu, M.Y. Yu, C.H. Diong, *Journal of Applied Physics* 94 (2003) 6097.
- [78] Amanur-Rehman, H.C. Kwon, W.T. Park, J.K. Lee, *Physics of Plasmas* 18 (2011) 093502.
- [79] A. Matsuda, T. Goto, *Materials Research Society Symposium Proceedings* 164 (1990) 3.
- [80] B.F. Gordiet, M.J. Inestrosa-Izurieta, A. Navarro, E. Bertran, *Journal of Applied Physics* 110 (2011) 103302.
- [81] J.R. Doyle, D.A. Doughty, A. Gallagher, *Journal of Applied Physics* 71 (1992) 4771.
- [82] P. Kae-Nune, J. Perrin, J. Guillon, J. Jolly, *Plasma Sources Science and Technology* 4 (1995) 250.
- [83] E. Krishnakumar, S.K. Srivastava, *Contributions to Plasma Physics* 35 (1995) 395.
- [84] Y. Hahn, *Reports on Progress in Physics* 60 (1997) 691–759.
- [85] A. Gallagher, A.A. Howling, Ch. Hollenstein, *Journal of Applied Physics* 91 (2002) 5571.
- [86] U.V. Bhandarkar, M.T. Swihart, S.L. Girshick, U.R. Kortshagen, *Journal of Physics D – Applied Physics* 33 (2000) 2731.
- [87] K. De Bleeker, A. Bogaerts, W.J. Goedheer, R. Gijbels, *IEEE Transactions on Plasma Science* 32 (2004) 691.
- [88] G.J. Nienhuis, W.J. Goedheer, E.A.G. Hamers, W.G.J.H.M. Van Sark, J. Bezemer, *Journal of Applied Physics* 82 (1997) 2060.
- [89] J. Perrin, Y. Takeda, N. Hirano, Y. Takeuchi, A. Matsuda, *Surface Science* 210 (1989) 114.
- [90] A. Matsuda, K. Nomoto, Y. Takeuchi, A. Suzuki, A. Yuuki, J. Perrin, *Surface Science* 227 (1990) 50.
- [91] S. Morisset, A. Allouche, *Journal of Chemical Physics* 129 (2008) 024509.
- [92] W.P. Leroy, S. Mahieu, R. Persoons, D. Depla, *Thin Solid Films* 518 (2009) 1527.
- [93] G. Kokkoris, A. Goodeyre, M. Cooke, E. Gogolides, *Journal of Physics D – Applied Physics* 41 (2008) 195211.
- [94] G. Ozaydin-Ince, A.M. Coclite, K.K. Gleason, *Reports on Progress in Physics* 75 (2012) 016501.
- [95] P.P. Rutkevych, K. Ostrikov, S. Xu, S.V. Vladimirov, *Journal of Applied Physics* 96 (2004) 4421.
- [96] I. Levchenko, A.E. Rider, K. Ostrikov, *Applied Physics Letters* 90 (2007) 193110.
- [97] Z.J. Han, B.K. Tay, C.M. Tan, M. Shakerzadeh, K. Ostrikov, *ACS Nano* 3 (2009) 3031.
- [98] K. Ostrikov, I. Levchenko, S. Xu, *Pure and Applied Chemistry* 80 (2008) 1909.
- [99] A.D. Arulsamy, K. Ostrikov, *Physics Letters A* 373 (2009) 2267.
- [100] K. Ostrikov, E.C. Neyts, M. Meyyappan, *Advances in Physics* 62 (2013) 113.
- [101] K.N. Ostrikov, S. Xu, A.B.M. Shaiful Azam, *Journal of Vacuum Science and Technology A* 20 (2002) 251.
- [102] A. Matsuda, K. Nakagawa, K. Tanaka, M. Matsumura, S. Yamasaki, H. Okushi, S. Iizima, *Journal of Non-Crystalline Solids* 35–36 (1980) 183.
- [103] L. Feitknecht, J. Meier, P. Torres, J. Zurcher, A. Shah, *Solar Energy Materials and Solar Cells* 74 (2002) 539.
- [104] Y.T. Gao, X.D. Zhang, Y. Zhao, Y. Zhao, H. Sun, Z. Feng, C.C. Wei, *Acta Physica Sinica* 55 (2006) 1497.
- [105] S. Kirner, O. Gabriel, B. Stannowski, B. Rech, R. Schlatmann, *Applied Physics Letters* 102 (2013) 051906.
- [106] M.N. van den Donker, B. Rech, W.M.M. Kessels, M.C.M. van de Sanden, *New Journal of Physics* 9 (2007) 280.
- [107] N. Itabashi, N. Nishiwaki, M. Magane, T. Goto, A. Matsuda, C. Yamada, E. Hirota, *Japanese Journal of Applied Physics* 29 (1990) 585.
- [108] A. Matsuda, *Plasma Physics and Controlled Fusion* 39 (1997) 431.
- [109] A. Kono, N. Koike, H. Nomura, T. Goto, *Japanese Journal of Applied Physics* 34 (1995) 307.
- [110] A.F.I. Morral, P.R.I. Cabarrocas, C. Clerc, *Physical Review B* 69 (2004) 125307.
- [111] R. Huang, X.Y. Lin, Y.P. Yu, X.K. Lin, Z.S. Zhu, J.H. Wei, K.J. Chen, *Journal of Physics D – Applied Physics* 39 (2006) 4423.
- [112] K.N. Ostrikov, I.B. Denysenko, E.L. Tsakadze, S. Xu, R.G. Storer, *Journal of Applied Physics* 92 (2002) 4935.
- [113] H.M. Mott-Smith, I. Langmuir, *Physical Review* 28 (1926) 727.
- [114] V.A. Godyak, R.B. Piejak, B.M. Alexandrovich, V.I. Kolobov, *Physics of Plasmas* 6 (1999) 1804.
- [115] A. Matsuda, *Journal of Non-Crystalline Solids* 338 (2004) 1.
- [116] A. Matsuda, *Journal of Non-Crystalline Solids* 59–60 (1983) 767.
- [117] J. Stangl, V. Holy, G. Bauer, *Reviews of Modern Physics* 76 (2004) 725.
- [118] V. Shchukin, N.N. Ledentsov, D. Bimberg, *Epitaxy of Nanostructures*, Springer, Berlin/Heidelberg, 2003.
- [119] C.C. Tsai, G.B. Anderson, R. Thompson, B. Wacker, *Journal of Non-Crystalline Solids* 114 (1989) 151.
- [120] K. Nakamura, K. Yoshida, S. Takeoka, I. Shimizu, *Japanese Journal of Applied Physics* 34 (1995) 442.
- [121] A. Matsuda, *Thin Solid Films* 337 (1999) 1.
- [122] S. Benagli, D. Borrello, E. Vallat-Sauvain, J. Meier, U. Kroll, J. Hötzler, J. Bailat, J. Steinhauser, M. Marmelo, G. Monteduro, L. Castens, in: *Proceedings of the 24th European Photovoltaic Solar Energy Conference*, Hamburg, Germany, (2009), pp. 2293–2298.
- [123] G. Bugnon, G. Parascandolo, T. Söderström, P. Guony, P. Cuony, M. Despeisse, S. Hänni, J. Holovsky, F. Meillaud, C. Ballif, *Advanced Functional Materials* 22 (2012) 3665.
- [124] J. Meier, J. Spitznagel, U. Kroll, C. Bucher, S. Fay, T. Moriarty, A. Shah, in: *Proceedings of 3rd World Conference on Photovoltaic Energy Conversion*, IEEE, Osaka, Japan, 2003, pp. 2801–2805.
- [125] D.L. Staebler, C.R. Wronski, *Applied Physics Letters* 31 (1977) 292.
- [126] A.V. Shah, J. Meier, E. Vallat-Sauvain, N. Wyrsch, U. Kroll, C. Droz, U. Graf, *Solar Energy Materials and Solar Cells* 78 (2003) 469.
- [127] H. Takatsuka, Y. Yamauchi, Y. Takeuchi, M. Fukagawa, K. Kawamura, S. Goya, A. Takano, *Proceedings of 4th World Conference on Photovoltaic Energy Conversion*, IEEE, HI, USA, 2006, pp. 2028–2033.
- [128] A.V. Shah, H. Schade, M. Vaneczek, J. Meier, E. Vallat-Sauvain, N. Wyrsch, U. Kroll, C. Droz, J. Bailat, *Progress in Photovoltaics: Research and Applications* 12 (2004) 113.
- [129] T. Matsui, H. Jia, M. Kondo, *Progress in Photovoltaics: Research and Applications* 18 (2010) 48.
- [130] M. Konagai, *Japanese Journal of Applied Physics* 50 (2011) 030001.
- [131] B. Yan, G. Yue, L. Sivec, J. Yang, S.C. Guha, S. Jiang, *Applied Physics Letters* 99 (2011) 113512.
- [132] F. Meillaud, A. Shah, C. Droz, E. Vallat-Sauvain, C. Mazzia, *Solar Energy Materials and Solar Cells* 90 (2006) 2952.
- [133] Y. Mai, S. Klein, R. Carius, J. Wolff, A. Lambertz, F. Finger, X. Geng, *Journal of Applied Physics* 97 (2005) 114913.
- [134] M. Kondo, M. Fukawa, L.H. Guo, A. Matsuda, *Journal of Non-Crystalline Solids* 266 (2000) 84.
- [135] B. Rech, T. Roschek, T. Repmann, J. Müller, R. Schmitz, W. Appenzeller, *Thin Solid Films* 427 (2003) 157.
- [136] M. Kondo, A. Matsuda, *Thin Solid Films* 457 (2004) 97.
- [137] Y. Mai, S. Klein, J. Wolff, A. Lambertz, X. Geng, F. Finger, in: *Proceedings of the 19th European Photovoltaic Solar Energy Conference*, WIP-Munich and ETAF-Fluence, Paris, France, 2004, p. 1399.
- [138] B. Rech, T. Repmann, M.N. Van den Donker, M. Berginski, T. Kilper, J. Hüpkens, S. Calnan, H. Stiebig, S. Wieder, *Thin Solid Films* 511 (2006) 548.
- [139] N. Kosku, S. Miyazaki, *Thin Solid Films* 511–512 (2006) 265.
- [140] N. Kosku, F. Kurisu, M. Takegoshi, H. Takahashi, S. Miyazaki, *Thin Solid Films* 435 (2003) 39.
- [141] Q.J. Cheng, S. Xu, K. Ostrikov, *Nanotechnology* 20 (2009) 215606.
- [142] Q.J. Cheng, S. Xu, K. Ostrikov, *Journal of Materials Chemistry* 19 (2009) 5134.
- [143] B.Y. Moon, J.H. Youn, S.H. Won, J. Jang, *Solar Energy Materials and Solar Cells* 69 (2001) 139.
- [144] M. Goto, H. Toyoda, M. Kitagawa, T. Hirao, H. Sugai, *Japanese Journal of Applied Physics* 35 (1996) L1009.
- [145] C.H. Shen, J.M. Shieh, J.Y. Huang, H.C. Kuo, C.W. Hsu, B.T. Dai, C.T. Lee, C.L. Pan, F.L. Yang, *Applied Physics Letters* 99 (2011) 033510.
- [146] J.Y. Huang, C.Y. Lin, C.H. Shen, J.M. Shieh, B.T. Dai, *Solar Energy Materials and Solar Cells* 98 (2012) 277.
- [147] J. Poortmans, V. Arkhipov, *Thin Film Solar Cell*, Wiley, England, 2006.
- [148] E. Bhattacharya, A.H. Mahan, *Applied Physics Letters* 52 (1988) 1587.
- [149] R. Biswas, Y.-P. Li, *Physical Review Letters* 82 (1999) 2512.
- [150] E. Amanatides, D. Mataras, D.E. Rapakoulias, *Journal of Applied Physics* 90 (2001) 5799.
- [151] L. Sanxonens, A.A. Howling, Ch. Hollenstein, *Plasma Sources Science and Technology* 7 (1998) 114.
- [152] B. Strahm, A.A. Howling, L. Sanxonens, Ch. Hollenstein, *Journal of Vacuum Science and Technology A* 25 (2007) 1198.
- [153] T. Lagarde, Y. Arnal, A. Lacoste, J. Pelletier, *Plasma Sources Science and Technology* 10 (2001) 181.
- [154] T. Mishima, M. Taguchi, H. Sakata, E. Maruyama, *Solar Energy Materials and Solar Cells* 95 (2011) 18.
- [155] M. Taguchi, A. Terakawa, E. Maruyama, M. Tanaka, *Progress in Photovoltaics: Research and Applications* 13 (2005) 481.
- [156] M. Taguchi, K. Kawamoto, S. Tsuge, T. Baba, H. Sakata, M. Morizane, K. Uchihashi, N. Nakamura, S. Kiyama, O. Oota, *Progress in Photovoltaics: Research and Applications* 8 (2000) 503.
- [157] A. Descoeuilles, L. Barraud, S. De Wolf, B. Strahm, D. Lachenal, C. Guerin, Z.C. Holman, F. Zicarelli, B. Demaurex, J. Seif, J. Holovsky, C. Ballif, *Applied Physics Letters* 99 (2011) 123506.
- [158] P. Mahtani, K.R. Leong, B. Jovet, D. Yeghikyan, N.P. Kherani, *Journal of Non-Crystalline Solids* 358 (2012) 3396.
- [159] J. Govaerts, S.N. Granata, T. Bearda, F. Dross, C. Boulord, G. Beaucarne, F. Korso, K. Baert, I. Gordon, J. Poortmans, *Solar Energy Materials and Solar Cells* 113 (2013) 52.

- [160] C.S. Liu, C.Y. Wu, I.W. Chen, H.C. Lee, L.S. Hong, Progress in Photovoltaics: Research and Applications 21 (2013) 326.
- [161] <http://eu-solar.panasonic.net/fr/presse/news-article/article/panasonic-hitR-solar-cell-achieves-worlds-highest-conversion-efficiency-of-24.7-at-research-level-4/>.
- [162] J. Pankove, M. Tarn, Applied Physics Letters 34 (1979) 156.
- [163] J. Damon-Lacoste, P. Roca i Cabarrocas, Journal of Applied Physics 105 (2009) 063712.
- [164] H. Fujiwara, M. Kondo, Applied Physics Letters 90 (2007) 013503.
- [165] Y.L. Qin, H.Q. Yan, F. Li, L. Qiao, Q.M. Liu, D.Y. He, Applied Surface Science 257 (2010) 817.
- [166] H.P. Zhou, D.Y. Wei, S. Xu, S.Q. Xiao, L.X. Xu, S.Y. Huang, Y.N. Guo, Y.S. Yan, M. Xu, Journal of Applied Physics 100 (2011) 023517.
- [167] L. Korte, A. Laades, M. Schmidt, Journal of Non-Crystalline Solids 352 (2006) 1217.
- [168] C. Jeong, Y.B. Kim, S.H. Lee, J.H. Kim, Journal of Nanoscience and Nanotechnology 10 (2010) 3321.
- [169] S.Q. Xiao, S. Xu, H.P. Zhou, D.Y. Wei, S.Y. Huang, L.X. Xu, C.C. Sern, Y.N. Guo, S. Khan, Applied Physics Letters 100 (2012) 233902.
- [170] W.J. Soppe, B.G. Duivelaar, S.E.A. Schiermeier, in: Proceedings of 16th European Photovoltaic Solar Energy Conference, James & James (Science Publishers) Ltd., Glasgow, UK, 2000, pp. 1420–1423.
- [171] F. Duerinckx, J. Szlufcik, Solar Energy Materials and Solar Cells 72 (2002) 231.
- [172] M.J.J. Kerr, A. Cuevas, J.H. Bultman, Journal of Applied Physics 89 (2001) 3821.
- [173] M.J.J. Kerr, A. Cuevas, Semiconductor Science and Technology 17 (2002) 166.
- [174] J. Schmidt, A.G. Aberle, Journal of Applied Physics 81 (1997) 6186.
- [175] H. Mackel, R. Ludemann, Journal of Applied Physics 92 (2002) 2602.
- [176] J.D. Moschner, J. Henze, J. Schmidt, R. Hezel, Progress in Photovoltaics: Research and Applications 12 (2004) 21.
- [177] H.O. Pierson, Handbook of Refractory Carbides and Nitrides, Noyes Publications, Westwood, NJ, 1996p. 290 (Chapter 15).
- [178] A. Luque, S. Hegedus, Handbook of Photovoltaic Science and Engineering, Wiley, New York, 2003p. 284 (Chapter 7).
- [179] C.Q. Sun, Progress in Materials Sciences 54 (2009) 179.
- [180] M. Molinari, H. Rinnert, M. Vergnat, Physica E 16 (2003) 445.
- [181] Y. Park, S.W. Rhee, Journal of Materials Science: Materials in Electronics 12 (2001) 515.
- [182] S.M. Myers, M.I. Baskes, H.K. Birnbaum, J.W. Corbett, G.G. Deleo, S.K. Estreicher, E.E. Haller, P. Jena, N.M. Johnson, R. Kirchheim, S.J. Pearton, M.J. Stavola, Reviews of Modern Physics 64 (1992) 559.
- [183] S. Sriramam, S. Agarwal, E.S. Aydin, D. Maroudas, Nature 418 (2002) 62.
- [184] O. Vetterl, P. Hapke, L. Houben, F. Finger, R. Carius, H. Wagner, Journal of Applied Physics 85 (1999) 2991.
- [185] J.J. Boland, Advances in Physics 42 (1993) 129.
- [186] K. Oura, V.G. Lifshits, A.A. Saranin, A.V. Zotov, M. Katayama, Surface Science Reports 35 (1999) 1.
- [187] A. Dinger, C. Lutterloh, J. Kuppers, Journal of Chemical Physics 114 (2001) 5338.
- [188] M. Niwano, M. Terashi, J. Kuge, Surface Science 420 (1999) 6.
- [189] Z. Suet, D.J. Paul, J. Zhang, S.G. Turner, Applied Physics Letters 90 (2007) 203501.
- [190] P. Chen, S.S. Lau, P.K. Chu, K. Henttinen, T. Suni, I. Suni, N.D. Theodore, T.L. Alford, J.W. Mayer, L. Shao, M. Nastasi, Applied Physics Letters 87 (2005) 111910.
- [191] L. Shao, Y. Lin, J.K. Lee, Q.X. Jia, Y.Q. Wang, M. Nastasi, P.E. Thompson, N.D. Theodore, P.K. Chu, T.L. Alford, J.W. Mayer, P. Chen, S.S. Lau, Applied Physics Letters 87 (2005) 091902.
- [192] A. Vengurlekar, S. Ashok, C.E. Kalnas, N.D. Theodore, Applied Physics Letters 85 (2004) 4052.
- [193] H.P. Zhou, L.X. Xu, S. Xu, S.Y. Huang, D.Y. Wei, S.Q. Xiao, W.S. Yan, M. Xu, Journal of Physics D – Applied Physics 43 (2010) 505402.
- [194] E. Simoen, Y.L. Huang, Y. Ma, J. Lauwaert, P. Clauws, J.M. Rafi, A. Ulyashin, C. Claeyns, Journal of the Electrochemical Society 156 (2009) H434.
- [195] Y.L. Huang, Y. Ma, R. Job, A.G. Ulyashin, Journal of Applied Physics 96 (2004) 7080.
- [196] E. Simoen, C. Claeyns, J.M. Raff, A.G. Ulyashin, Materials Science and Engineering B 134 (2006) 189.
- [197] A.G. Ulyashin, Y.A. Bunmay, R. Job, W.R. Fahrner, Applied Physics A – Materials Science and Processing 66 (1998) 399.
- [198] L. Shao, Z.F. Di, Y. Lin, Q.X. Jia, Y.Q. Wang, M. Nastasi, P.E. Thompson, N.D. Theodore, P.K. Chu, Applied Physics Letters 93 (2008) 041909.
- [199] P. Chen, P.K. Chu, T. Hochbauer, J.K. Lee, M. Nastasi, D. Buca, S. Mantti, R. Loo, M. Caymax, T. Alford, J.W. Mayer, N.D. Theodore, M. Cai, B. Schmidt, S.S. Lau, Applied Physics Letters 86 (2005) 031904.
- [200] C.M. Chiang, S.M. Gates, S.S. Lee, M. Kong, S.F. Bent, Journal of Physical Chemistry B 101 (1997) 9537.
- [201] G. Schulze, M. Henzler, Surface Science 124 (1983) 336.
- [202] J.I. Pankove, C.W. Magee, R.O. Wance, Applied Physics Letters 47 (1985) 748.
- [203] N.H. Nickel, G.B. Anderson, N.M. Johnson, J. Walker, Physica B – Condensed Matter 273–274 (1999) 212.
- [204] N.H. Nickel, W.B. Jackson, J. Walker, Physical Review B 53 (1996) 7750.
- [205] S. Veprek, F.A. Sarott, Plasma Chemistry and Plasma Processing 2 (1982) 233.
- [206] Y.J. Chabal, K. Raghavachari, Physical Review Letters 54 (1985) 1055.
- [207] M.K. Weldon, V.E. Marsico, Y.J. Chabal, A. Agarwal, D.J. Eaglesham, J. Sapjeta, W.L. Brown, D.C. Jacobson, Y. Caudano, S.B. Christman, E.E. Chaban, Journal of Vacuum Science and Technology B 15 (1997) 1065.
- [208] S.S. Lee, M. Kong, S.F. Bent, C.M. Chiang, S.M. Gates, Journal of Physical Chemistry 100 (1996) 20015.
- [209] J.J. Boland, Surface Science 261 (1992) 17.
- [210] W. Widdra, S.I. Yi, R. Maboudian, G.A.D. Briggs, W.H. Weinberg, Physical Review Letters 74 (1995) 2074.
- [211] K. Sinniah, M.G. Sherman, L.B. Lewis, W.H. Weinberg, J.T. Yates, K.C. Janda, Journal of Chemical Physics 92 (1990) 5700.
- [212] S.M. Gates, R.R. Kunz, C.M. Greenlieff, Surface Science 207 (1989) 364.
- [213] H.N. Waltenburg, J.T. Yates, Chemical Reviews 95 (1995) 1589.
- [214] K.W. Kolasinski, International Journal of Modern Physics B 9 (1995) 2753.
- [215] A.A. Langford, M.L. Fleet, B.P. Nelson, W.A. Lanford, N. Maley, Physical Review B 45 (1992) 13367.
- [216] J.C. Knights, G. Lucovsky, R.J. Nemanich, Journal of Non-Crystalline Solids 32 (1979) 393.
- [217] U. Kroll, J. Meier, A. Shah, S. Mikhailov, J. Weber, Journal of Applied Physics 80 (1996) 4971.
- [218] P. Roca i Cabarrocas, Journal of Non-Crystalline Solids 266–269 (2000) 31.
- [219] S. De Wolf, S. Olibet, C. Ballif, Applied Physics Letters 93 (2008) 032101.
- [220] T.F. Schulze, H.N. Beushausen, C. Leendertz, A. Dobrich, B. Rech, L. Korte, Applied Physics Letters 96 (2010) 252102.
- [221] M. Mews, T.F. Schulze, N. Mingirulli, L. Korte, Applied Physics Letters 102 (2013) 122106.
- [222] A.H.M. Smets, M.C.M. van de Sanden, Physical Review B 76 (2007) 073202.
- [223] M.J. Powell, S.C. Deane, Physical Review B 48 (1993) 10815.
- [224] S.J. Lee, S.H. Kim, D.W. Kim, K.H. Kim, B.K. Kim, J. Jang, Solar Energy Materials and Solar Cells 95 (2011) 81.
- [225] T.J. Donahue, R. Reif, Journal of Applied Physics 57 (1985) 2757.
- [226] H.W. Kim, Z.H. Zhou, R. Reif, Thin Solid Films 302 (1997) 169.
- [227] H.S. Tae, S.J. Park, S.H. Hwang, K.H. Hwang, E. Yoon, K.W. Whang, S.A. Song, Journal of Vacuum Science and Technology B 13 (1995) 908.
- [228] K. Choi, S. Ghosh, J. Lim, C.M. Lee, Applied Surface Science 206 (2003) 355.
- [229] B. Anthony, T. Hsu, L. Breaux, R. Qian, S. Banerjee, A. Tasch, Journal of Electronic Materials 19 (1990) 1027.
- [230] E.S. Aydin, R.A. Gottscho, Y.J. Chabal, Pure and Applied Chemistry 66 (1994) 1381.
- [231] Z.H. Zhou, E.S. Aydin, R.A. Gottscho, Y.J. Chabal, R. Reif, Journal of the Electrochemical Society 140 (1993) 3316.
- [232] R.J. Carter, T.P. Schneider, J.S. Montgomery, R.J. Nemanich, Journal of the Electrochemical Society 141 (1994) 3136.
- [233] J.S. Montgomery, T.P. Schneider, R.J. Carter, J.P. Barnak, Y.L. Chen, J.R. Hauser, R.J. Nemanich, Applied Physics Letters 67 (1995) 2194.
- [234] K.H. Hwang, E. Yoon, K.W. Whang, J.Y. Lee, Applied Physics Letters 67 (1995) 3590.
- [235] M. Shinohara, T. Kuwano, Y. Akama, Y. Kimura, M. Niwano, H. Ishida, R. Hatakeyama, Journal of Vacuum Science and Technology A 21 (2003) 25.
- [236] T.R. Yew, R. Rief, Journal of Applied Physics 68 (1990) 4681.
- [237] F. Walter, M. Hofmann, J. Rentsch, in: Proceedings of 23rd European Photovoltaic Solar Energy Conference and Exhibition, WIP-Munich, Valencia, Spain, 2008, p. 1789.
- [238] D.L. King, M.E. Buck, in: Proceedings of the 22nd IEEE Photovoltaic Specialist Conference, IEEE, Las Vegas, USA, 1991, pp. 303–308.
- [239] M. Moreno, D. Daineka, P. Roca i Cabarrocas, Physica Status Solidi C 7 (2010) 1112.
- [240] N. Layadi, P. Roca i Cabarrocas, B. Dréillon, Physical Review B 52 (1995) 5136.
- [241] E.A. Irene, Thin Solid Films 233 (1993) 96.
- [242] J.M. Kim, Y.K. Kim, Solar Energy Materials and Solar Cells 81 (2004) 239.
- [243] E. Vazsonyi, K. De Clercq, R. Einhaus, E. Van Kerschaver, K. Said, J. Poortmans, J. Szlućik, J. Nijs, Solar Energy Materials and Solar Cells 57 (1999) 179.
- [244] M. Edwards, S. Bowden, U. Das, M. Burrows, Solar Energy Materials and Solar Cells 92 (2008) 1373.
- [245] D. Lencinella, E. Centurioni, R. Rizzoli, F. Zignani, Solar Energy Materials and Solar Cells 87 (2005) 725.
- [246] G.W. Trucks, K. Raghavachari, G.S. Higashi, Y.J. Chabal, Physical Review Letters 65 (1990) 504.
- [247] X.D. Bai, Z. Xu, S. Liu, E.G. Wang, Science and Technology of Advanced Materials 6 (2005) 804.
- [248] K. Seeger, R.E. Palmer, Applied Physics Letters 74 (1999) 1627.
- [249] T. Tada, T. Kanayama, K. Koga, P. Weibel, S.J. Carroll, K. Seeger, R.E. Palmer, Journal of Physics D – Applied Physics 31 (1998) L21.
- [250] C.H. Hsu, H.C. Lo, C.F. Chen, C.T. Wu, J.S. Hwang, D. Das, J. Tsai, L.C. Chen, K.H. Chen, Nano Letters 4 (2004) 471.
- [251] M.C. Yang, J. Shieh, C.C. Hsu, T.C. Cheng, Electrochemical and Solid State Letters 8 (2005) C131.
- [252] K. Ostríkova, S. Xu, Plasma-Aided Nanofabrication: From Plasma Sources to Nanoassembly, Wiley-VCH, Weinheim, 2007, ISBN: 978-3-527-40633-3.
- [253] U. Cvelbar, K. Ostríkova, M. Mozeć, Nanotechnology 19 (2008) 405605.
- [254] S. Chattopadhyay, Y.F. Huang, Y.J. Jen, A. Ganguly, K.H. Chen, L.C. Chen, Materials Science and Engineering R – Reports 69 (2010) 1.
- [255] J.C. She, S.Z. Deng, N.S. Xu, R.H. Yao, J. Chen, Applied Physics Letters 88 (2006) 013112.
- [256] J. Shieh, C.H. Lin, M.C. Yang, Journal of Physics D – Applied Physics 40 (2007) 2242.
- [257] S.H. Ryu, C. Yang, W.J. Yoo, D.H. Kim, T. Kim, Journal of the Korean Physical Society 54 (2009) 1016.
- [258] M. Moreno, D. Daineka, P.R.I. Cabarrocas, Solar Energy Materials and Solar Cells 94 (2010) 733.
- [259] J. Shieh, F.J. Hou, Y.C. Chen, H.M. Chen, S.P. Yang, C.C. Cheng, H.L. Chen, Advanced Materials 22 (2010) 597.
- [260] J.S. Yoo, I.O. Parm, U. Gangopadhyay, K. Kim, S.K. Dhungel, D. Mangalaraj, J.S. Yi, Solar Energy Materials and Solar Cells 90 (2006) 3085.
- [261] L.L. Ma, Y.C. Zhou, N. Jiang, X. Lu, J. Shao, W. Lu, J. Ge, X.M. Ding, X.Y. Hou, Applied Physics Letters 88 (2006) 171907.

- [262] S. Koynov, M.S. Brandt, M. Stutzmann, *Applied Physics Letters* 88 (2006) 203107.
- [263] Y. Jia, J.Q. Wei, K.L. Wang, A.Y. Cao, Q.K. Shu, X.C. Gui, Y.Q. Zhu, D.M. Zhuang, G. Zhang, B.B. Ma, L.D. Wang, W.J. Liu, Z.C. Wang, J.B. Luo, D. Wu, *Advanced Materials* 20 (2008) 4594.
- [264] H.C. Yuan, V.E. Yost, M.R. Page, P. Stradins, D.L. Meier, H.M. Branz, *Applied Physics Letters* 95 (2009) 123501.
- [265] E. Garnett, P. Yang, *Nano Letters* 10 (2010) 1082.
- [266] D. Mariotti, S. Mitra, V. Srivastava, *Nanoscale* 5 (2013) 1385.
- [267] Y.F. Huang, S. Chattopadhyay, Y.J. Jen, C.Y. Peng, T.A. Liu, Y.K. Hsu, C.L. Pan, H.C. Lo, C.H. Hsu, Y.H. Chang, C.S. Lee, K.H. Chen, L.C. Chen, *Nature Nanotechnology* 2 (2007) 770.
- [268] W.H. Lee, J.C. Lin, C. Lee, H.C. Cheng, T.R. Yew, *Diamond and Related Materials* 10 (2001) 2075.
- [269] H. Jansen, M. De Boer, H. Wensink, B. Kloek, M. Elwenspoek, *Microelectronics Journal* 32 (2001) 769.
- [270] H.H. Lin, W.H. Chen, C.J. Wang, F.C.N. Hong, *Thin Solid Films* 529 (2013) 138.
- [271] J.M. Shim, H.W. Lee, K.Y. Cho, E.J. Lee, J.S. Kim, J.H. Kong, S.J. Jo, J.S. Kim, H.S. Lee, *Japanese Journal of Applied Physics* 51 (2012) 10NA14.
- [272] J. Yoo, G. Yu, J. Yi, *Solar Energy Materials and Solar Cells* 95 (2011) 2.
- [273] K.S. Lee, M.H. Ha, J.H. Kim, J.W. Jeong, *Solar Energy Materials and Solar Cells* 95 (2011) 66.
- [274] S. Xu, I. Levchenko, S.Y. Huang, K. Ostrikov, *Applied Physics Letters* 95 (2009) 111505.
- [275] I. Levchenko, S.Y. Huang, K. Ostrikov, S. Xu, *Nanotechnology* 21 (2010) 025605.
- [276] M. Dhamrin, N.H. Ghazali, M.S. Jeon, T. Saitoh, K. Kamisako, Conference Record of the 2006 IEEE 4th World Conference on Photovoltaic Energy Conversion, IEEE, HI, USA, 2006, pp. 1395–1398.
- [277] O. Schultz, University Konstanz, 2005 (Ph.D. Thesis).
- [278] Z. Fan, R. Kapadia, P.W. Leu, X. Zhang, Y.L. Chueh, K. Takei, K. Yu, A. Jamshidi, A.A. Rathore, D.J. Ruebusch, M. Wu, A. Javey, *Nano Letters* 10 (2010) 3823.
- [279] H. Park, D. Shin, G. Kang, S. Baek, K. Kim, W.J. Padilla, *Advanced Materials* 23 (2011) 5796.
- [280] S. Ravipati, J. Shieh, F.H. Ko, C.C. Yu, H.L. Chen, *Advanced Materials* 25 (2013) 1724.
- [281] C. Lee, S.Y. Bae, S. Mobasser, H. Manohara, *Nano Letters* 5 (2005) 2438.
- [282] J.A. Dobrowolski, D. Poitras, P. Ma, H. Vakil, M. Acree, *Applied Optics* 41 (2002) 3075.
- [283] R.J.C. Brown, P.J. Brewer, M.J.T. Milton, *Journal of Materials Chemistry* 12 (2002) 2749.
- [284] Z.P. Yang, L. Ci, J.A. Bur, S.Y. Lin, P.M. Ajayan, *Nano Letters* 8 (2008) 446.
- [285] N.P. Dasgupta, S.C. Xu, H.J. Jung, A. Lancu, R. Fasching, R. Sinclair, F.B. Prinz, *Advanced Functional Materials* 22 (2012) 3650.
- [286] O. Zinchuk, N. Drozdov, A. Fedotov, A. Mazanik, N. Krekotsen, V. Ukhov, J. Partyka, P. Wegierek, T. Koltunowicz, *Vacuum* 83 (2009) s99.
- [287] V.P. Popov, I.E. Tyschenko, L.N. Safronov, O.V. Naumova, I.V. Antonova, A.K. Gutakovskiy, A.B. Talochkin, *Thin Solid Films* 403 (2002) 500.
- [288] D. Barakel, A. Ulyashin, I. Perichaud, S. Martinuzzi, *Solar Energy Materials and Solar Cells* 72 (2002) 285.
- [289] T. Yamaguchi, S.J. Taylor, S. Watanabe, K. Ando, M. Yamaguchi, T. Hisamatsu, S. Matsuda, *Applied Physics Letters* 72 (1998) 1226.
- [290] P.K. Chu, S. Qin, C. Chan, N.W. Cheung, L.A. Larson, *Materials Science and Engineering R – Reports* 17 (1996) 207.
- [291] A. Buzynin, A. Luk'yanov, V. Osiko, V.V. Voronkov, *Nuclear Instruments and Methods in Physics Research Section B* 186 (2002) 366.
- [292] T. Wolkenstein, *Physico-Chimie de la Surface des Semiconducteurs*, MIR, Moscow, 1973.
- [293] W. Götz, G. Pensl, W. Zulehner, *Physical Review B* 46 (1992) 4312.
- [294] R.C. Newman, M.J. Ashwin, R.E. Pritchard, J.H. Tucker, *Physica Status Solidi B* 210 (1998) 519.
- [295] P. Deak, L.C. Snyder, J.L. Lindstrom, J.W. Corbett, S.J. Pearton, A.J. Tavendale, *Physics Letters A* 126 (1988) 427.
- [296] R.C. Newman, J.H. Tucker, A.R. Brown, S.A. McQuaid, *Journal of Applied Physics* 70 (1991) 3061.
- [297] S. Xu, S.Y. Huang, I. Levchenko, H.P. Zhou, D.Y. Wei, S.Q. Xiao, L.X. Xu, W.S. Yan, K. Ostrikov, *Advanced Energy Materials* 1 (2011) 373.
- [298] S.Q. Xiao, S. Xu, H.P. Zhou, D.Y. Wei, S.Y. Huang, L.X. Xu, C.C. Sern, Y.N. Guo, Y. Xu, *Journal of Physics D – Applied Physics* 46 (2013) 105103.
- [299] M. Wolter, I. Levchenko, H. Kersten, K. Ostrikov, *Applied Physics Letters* 96 (2010) 133105.
- [300] H.R. Maurer, H. Kersten, *Journal of Physics D – Applied Physics* 44 (2011) 174029.
- [301] M. Bruzzi, D. Menichelli, M. Scaringella, J. Harkonen, E. Tuovinen, Z. Li, *Journal of Applied Physics* 99 (2006) 093706.
- [302] A. Janotti, C.G. Van de Walle, *Nature* 46 (2007) 44.
- [303] C.G. Van de Walle, P.J.H. Denteneer, Y. Bar-Yam, S.T. Pantelides, *Physical Review B* 39 (1989) 10791.
- [304] J. Rentsch, F. Binaie, C. Schetter, R. Preu, H. Schlemm, K. Roth, D. Theirich, in: *Proceedings of 19th European Photovoltaic Solar Energy Conference*, WIP-Munich and ETA-Florence, Paris, France, 2004, p. 891.
- [305] G.S. Oehrlein, H.L. Williams, *Journal of Applied Physics* 62 (1987) 662.
- [306] N.R. Rueger, J.J. Beulens, M. Schaepkens, M.F. Doemling, J.M. Mirza, T.E.F.M. Standaert, G.S. Oehrlein, *Journal of Vacuum Science and Technology A* 15 (1997) 1881.
- [307] T.E.F.M. Standaert, M. Schaepkens, N.R. Rueger, P.G.M. Sebel, G.S. Oehrlein, J.M. Cook, *Journal of Vacuum Science and Technology A* 16 (1998) 239.
- [308] G. Agostinelli, H.F.W. Dekkers, S. de Wolf, G. Beaucarne, in: *Proceedings of the 19th European Photovoltaic Solar Energy Conference*, WIP-Munich and ETA-Fluence, Paris, France, 2004, p. 132.
- [309] B.T. Chan, E. Kunnen, K.D. Xu, W. Boullart, J. Poortmans, *IEEE Journal of Photovoltaics* 3 (2013) 152.
- [310] A.W. Blakers, A. Wang, A.M. Milne, J.H. Zhao, M.A. Green, *Applied Physics Letters* 55 (1989) 1363.
- [311] L. Gautero, M. Hofmann, J. Rentsch, A. Lemke, S. Mack, J. Seiffe, J. Nekarda, D. Biro, A. Wolf, B. Bitnar, J.M. Salles, R. Preu, in: *Proceedings of 34th IEEE Photovoltaic Specialist Conference*, IEEE, Philadelphia, USA, 2009, pp. 1982–1987.
- [312] J. Rentsch, J. Seiffe, F. Walter, M. Hofmann, L. Weiss, L. Gautero, D. Decker, H. Schlemm, R. Preu, in: *Proceedings of 23rd European Photovoltaic Solar Energy Conference*, WIP, Valencia, Spain, 2008, pp. 1188–1192.
- [313] B. Rech, T. Roschek, T. Repmann, J. Muller, R. Schmitz, W. Appenzeller, *Thin Solid Films* 427 (2003) 157.
- [314] A.J. Nozik, *Nano Letters* 10 (2010) 2735.
- [315] M. Fawer-Wassner, Solar energy-sunny days ahead? Current status and outlook for photovoltaic and solar thermal power, Sarasin Sustainable Investment Report, 2004.
- [316] M.A. Green, *Solar Energy* 76 (2004) 3.
- [317] E.A. Alsema, *Progress in Photovoltaics: Research and Applications* 8 (2000) 17.
- [318] B.M. Kayes, H.A. Atwater, N.S. Lewis, *Journal of Applied Physics* 97 (2005) 114302.